THE DESIGN AND EVALUATION OF COLLIMATORS FOR THE MEASUREMENT OF RADIOACTIVE ISOTOPE DISTRIBUTION 'IN VIVO'

by

Pamela Mary Kibby

A thesis submitted for the degree of Ph. D.
of the University of London

March 1969

ABSTRACT

This thesis is concerned with the design and evaluation of multihole focusing collimators for radioisotope scanning, and the design of multichannel collimators with cylindrical holes for radioisotope camera systems.

The performance of focusing collimators has been evaluated theoretically by calculating the variation with depth in tissue of resolution, efficiency and a factor proportional to the probability of detection of regions of increased or decreased concentration. The influence of altering different parameters of the collimator has been examined and it has been shown that very large crystals, collimators with large numbers of holes and collimators with very long focal lengths are unsuitable for many scanning applications.

An improved procedure for the design of focusing collimators has been developed, and the factors which determine the most suitable design have been discussed with particular reference to scanning a large organ with single and double headed detector systems equipped with 3" and 5" diameter crystals.

Theoretical efficiencies have been compared with

experimental measurements in air and indicate that radiation scattered from the collimator walls may significantly increase the counting rate at small source to collimator distances. The effects of radiation scattered from tissue have been investigated theoretically and experimentally and the factors by which theoretical probabilities of detection should be reduced to allow for tissue scattering have been given for the radioactive isotopes ^{197}Hg, ^{99m}Tc and ^{203}Hg. The settings of the analyser window for which scattering from tissue has the smallest effect have been obtained for the detector used in the experimental work.

The designs of multichannel collimators for camera systems which give the highest point source efficiency for a specified resolution have been calculated theoretically for gamma-ray energies from 0.025 to 0.5 MeV, using a more accurate approach than previously available.

I N D E X

Notation

Symbols:

B'	collimator figure of merit (equations 4.9 and 4.10)
C	count rate
D	diameter of smallest circular detector covered by all the collimator holes, often equal to the crystal diameter
E	sensitivity
K	shape factor
N	number of holes in collimator
P	penetration fraction (equation 2.2)
Q	quantity of radioactivity
R	radius of the field of view
S	scatter fraction (equations 2.2 and 2.4)
T	time
V	volume
d	distance of source from external collimator face
f	focal length
h	distance of centre of hole from collimator axis
q	fraction of disintegrations which give rise to detectable radiation

r	radius of collimator holes at crystal face
r'	radius of collimator holes at external face
s	septum thickness at crystal face of collimator
s'	septum thickness at external face of collimator
t	collimator length
ϵ	collimator efficiency
$\epsilon(g)$	collimator geometrical efficiency
η	crystal efficiency
λ	linear absorption coefficient of lead
ρ	concentration of activity
τ	transmission ratio
μ	linear absorption coefficient of water

Subscripts:

f	focal plane
NT	non-target
pl	plane source
T	target

CHAPTER 1

THE MEASUREMENT OF RADIOACTIVE ISOTOPE DISTRIBUTION 'IN VIVO'

1.1 Introduction

Radioactive isotopes are widely used in medicine for diagnosis, therapy and research. Of the many uses, those diagnostic and research applications in which a quantity of a radioisotope is administered to a patient are referred to as 'in vivo' procedures. This thesis is concerned with those 'in vivo' procedures in which the distribution of radioactivity in the body is measured externally using a radiation detector.

The aim of external measurements of isotope distribution may be to determine either the size, shape, position or function of a particular organ, or any impairment of function due to lesions or other causes. For most measurements it is necessary to restrict the size of the region of the body from which the detector can receive radiation and hence a collimating device is employed. Measurements of organ uptake may be carried out using a stationary scintillation crystal and some simple form of collimation, but when

knowledge of the distribution of an isotope within an organ or region of the body is required, scanning or camera systems are needed which utilise more complex collimators. The subject of this thesis is the design and evaluation of collimators for the latter systems.

1.2 Scanning systems

The earliest method of scanning consisted of moving a Geiger counter manually from point to point, recording the counting rate at corresponding positions on graph paper (Marvin and Moore, 1948). In scanners now available commercially, collimated scintillation counters are moved automatically over the region of interest and counting rates are recorded continuously. Some scanners have one detector and others have two, one above and one below the body. The latter systems are usually used with the detector outputs summed, but may also be used for coincidence counting of a positron emitter (Brownell and Sweet, 1953). Scanners incorporating more than two detectors have also been described (Beck, Charleston, Eidelberg and Harper, 1967; Hindel and Gilson, 1967).

Collimators for scanners should be designed so that the resolution is small enough to enable a relatively small

change in concentration of activity to be detected, and yet not so small that the sensitivity is low and the counting statistics poor. The resolution is related to the radius of the field of view of the collimator, which is defined as the radius of the area from which the detector may receive radiation travelling in straight lines. Scanners usually require collimators with a field of view of a few cm. in diamter, remaining reasonably constant with depth.

The single hole cylindrical and tapered collimators used for uptake measurements are unsuitable for scanning because they usually give a wide variation of field of view with depth. The variation may be reduced by increasing the collimator length but this also leads to a reduction in counting rate owing to the inverse square law. Griffith, Goland and Chamberlain (1950) designed a collimator with a smaller variation of the field of view, which consisted of two lead cylinders, the smaller of which was fixed inside the larger with plexiglass. More commonly, the variation is reduced by using multi-hole focusing collimators of the type introduced by Newell, Saunders and Miller (1952). These are made from lead or some other highly absorbing material and contain a number of holes which come to an imaginary focus at some distance from the external face of

the collimator (fig. 1.1). With this type of design and the correct choice of collimator parameters, it is possible to maintain a reasonably uniform field of view with depth with reasonably high sensitivity.

Scanners which utilise different arrangements of detectors and different forms of collimation have also been developed (Anger, 1966a; Davis and Martone, 1966; West, 1966; Kuhl, 1964; Cassen, 1964). The designs of collimators used with these instruments are not discussed in this thesis but many of the general conclusions reached also apply to them.

1.3 Camera systems

The distribution of an isotope within an organ may be measured with camera systems which visualise the whole area of interest at one time. The pin-hole camera of Anger (1958) uses a small hole in lead shielding material to form an inverted image of the subject on a large scintillation crystal. The position of the incident radiation on the crystal is determined by the distribution of light between an array of photomultipliers with which the crystal is viewed. The pin-hole camera is most suitable for small, thin organs such as the thyroid, which can be positioned close to the pin-hole. Larger subjects must be placed some distance from the

collimator in order to lie within the field of view and this results in a loss of sensitivity.

Larger subjects can be visualised with greater sensitivity using a multichannel rather than a pin-hole collimator (Anger, 1964). Multichannel collimators consist of lead or some other highly absorbing material, containing a large number of parallel cylindrical or hexagonal holes. The length of the collimator and the diameter of the holes determine the sensitivity and the variation of field of view with depth.

Anger has also described a camera system suitable for positron emitting isotopes. A large crystal is placed close to the patient and a second, smaller crystal is placed some distance away. Coincident scintillations in the detectors are recorded. A multichannel collimator can be used with the larger crystal to reduce random coincidences.

Camera systems which use different methods of detecting the positions of incident photons have also been described. Instruments incorporating X-ray image intensifiers (Ter-Pogossian and Eichlung, 1964; Ter-Pogossian, Niklas, Bell and Eichlung, 1966) and spark chambers (Kellershohn, Desgrez, and Lansiart, 1964; Horwitz, Lofstrom and Forsaith, 1965) use the same type of multichannel collimators. The

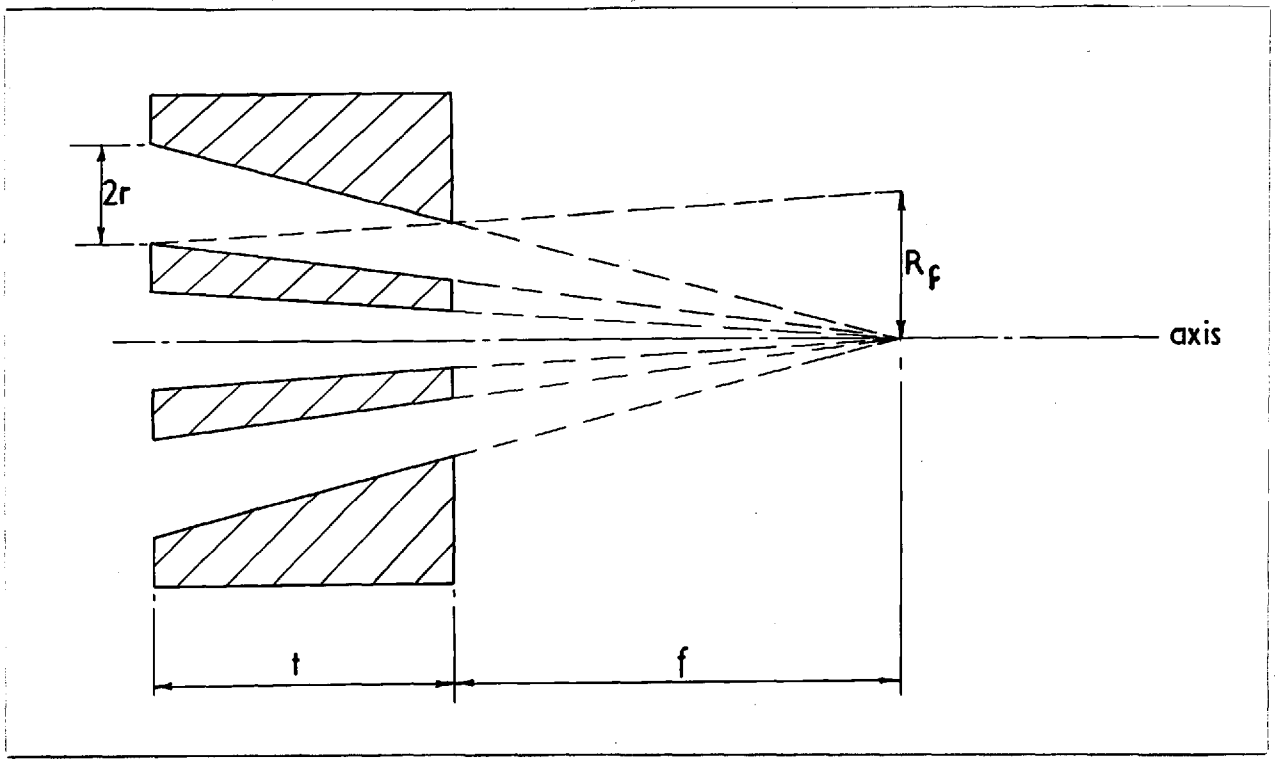

Fig. 1.1 A 7-hole focusing collimator in cross-section through a line of holes. The geometrical radius of the field of view in the focal plane (R_f) is defined by the maximum distance from the collimator axis from which radiation is directly incident on the crystal.

autofluorescope developed by Bender and Blau (1962) uses a multichannel collimator with holes focusing in a plane.

1.4 Aims of thesis

The study of focusing collimators used with scanners forms the major part of this thesis. The aims of the study were; firstly, to advance the understanding of the effects of collimator parameters on collimator performance; secondly, to devise methods of collimator design based on a complete analysis of the collimator response; and thirdly, to investigate the effects of penetration and scattering on collimator performance, particularly that of scattered radiation from the subject.

The design of multichannel collimators used with cameras has also been studied. This work is presented in the paper 'The design of multichannel collimators for radioisotope cameras' (Kibby, 1969) which is bound in the thesis. The results are summarised and discussed in the final chapter.

C H A P T E R 2

THE DESIGN AND EVALUATION OF COLLIMATORS

2.1 The evaluation of focusing collimators

The performance of scanning systems can be assessed in terms of sensitivity ($cps / \mu Ci$), resolution and the probability of detection of lesions. These quantities depend on the properties of the collimator under specified experimental conditions.

Sensitivity

In air, the sensitivity (E') is determined by (a) the fraction of disintegrations which give rise to detectable radiation, q, (b) the efficiency of the collimator, ϵ , defined as the fraction of the radiation emitted from the source which is incident on the detector, and (c) the crystal efficiency, η , i.e.,

$$E' = q\epsilon\eta \qquad (2.1)$$

A further factor should be included when the analyser window is set to include only a fraction of the photopeak counts.

The efficiency of the collimator is mainly determined by radiation which reaches the detector directly, the geometrical component $\epsilon(g)$. Radiation which reaches the detector after penetration of septa or side shielding and after scattering from the collimator walls also contributes to the total efficiency. Beck (1964a) has expressed the efficiency as :

$$\epsilon = \epsilon(g) [1 + P + S_1] \qquad (2.2)$$

where P and S_1 are the penetration and collimator scatter fractions.

When the source is placed in tissue, the sensitivity is decreased owing to absorption. Some of the absorption occurs as the result of Compton interactions which give rise to scattered photons which may subsequently be detected. Although scattered photons increase the sensitivity they can be detected when the source lies outside the geometrical field of view of the collimator and hence scattered radiation decreases the collimator resolution. For a source at depth x in tissue, the sensitivity can be expressed as :

$$E' = \beta \eta \epsilon a \qquad (2.3)$$

where α is the tissue attenuation factor and

$$\epsilon \alpha = \epsilon(g) [1 + P + S_1] e^{-\mu x} [1 + S_2] \qquad (2.4)$$

where μ is the linear absorption coefficient for tissue and S_2 is the tissue scatter fraction. It has been assumed that the penetration and collimator scatter fractions (P and S_1) are affected by attentuation and radiation scatter from tissue in the same way as the geometrical efficiency.

Resolution

The resolution of a scanning system is determined mainly by the resolution of the collimator and this depends on the collimator dimensions. Collimator resolution is also affected by penetration and scattering. The resolution can be defined as the full-width at half maximum (FWHM) of the curve obtained by moving a source across the collimator field of view. Line sources give slightly larger values of the FWHM than point sources (Gopala Rao and Wagner, 1968) in the focal plane.

Another estimate of resolution can be obtained from modulation transfer functions. The modulation transfer function is a measure of the ability of the system to resolve

equally spaced sources. It has the value one for infinite separation and falls to zero as the sources become closer together. A graph of MTF against source separation for a given distance from the collimator indicates the resolution at this distance. These graphs can be calculated from the resolution curves for line sources (Cradduck, Fedoruk and Reid, 1966; Cradduck, 1968). They can also be obtained from measurements on a Sieman's star phantom (Beck, 1964a).

Vetter (1967a,b) has suggested the half-flux index as a measure of resolution. Consider a uniform plane source of radioactivity perpendicular to the collimator axis; the half-flux index is the diameter of the circle centred on the axis, which circumscribes the area contributing half of the total plane source count rate. As it is a measure of area response, Vetter suggests that it is more closely related to ease of visualisation on a scan than the FWHM, which is a measure of linear response. The half-flux index at different distances from the collimator can be calculated from the collimator dimensions.

Discussion

The main disadvantage of the FWHM as a measure of resolution is that it does not give sufficient indication of the influence of penetration and scattering. These effects

produce the greatest increases in the width of the resolution curves at small percentages of the maximum response (Harris et al., 1962). Two further disadvantages are that the FWHM may have the same value for resolution curves of entirely different shapes, and that using simple methods it may be calculated theoretically only in the focal plane. The half-flux index can be calculated reasonably simply for all distances from the collimator and does take into account the shape of the resolution curve. If however, it is calculated from the geometrical properties of the collimator it does not take into account the effects of penetration and scattering.

The variation of MTF with source separation gives a complete description of collimator resolution. Since however, a considerable error is introduced in radioactive measurements by statistical fluctuations, it is doubtful whether such a detailed description is necessary. An adequate assessment of collimator resolution can probably be obtained from the FWHM together with the shape of the experimental resolution curve.

Probabilities of detection

The optimum scanning system and collimator for a

specific application should give a high probability for the detection of localised variations in activity and should have fine resolution. Since improving the resolution results in a loss of sensitivity, some method of formulating the combined effects of sensitivity and resolution is required in order to find the optimum collimator design.

The problem has been discussed by Dewey and Sinclair (1961) following earlier work by Newell, Saunders and Miller (1952) and Brownell (1958). Dewey and Sinclair postulated that as the collimator moves directly over the target area, the change in count rate must be a factor ℓ times the standard error of the difference in the count rate in order to be statistically significant. Let C_T and C_{NT} be the target and non-target count rates and let T be the time in which counts accumulate. Then,

$$C_T - C_{NT} = \ell \sqrt{\frac{C_T + C_{NT}}{T}} \qquad (2.5)$$

Dewey and Sinclair assumed the value three for ℓ and this has been verified experimentally (Haybittle, 1966; Mallard and Wilks, 1968; Matthews and Kibby, 1968).

By expressing the counting rates in terms of concen-

trations and sensitivities, Dewey and Sinclair have shown that collimators for the same application can be compared using the factor E_{NT}/E_T^2 where E_{NT} and E_T are the non-target and target sensitivities.

Matthews (1965) has developed the work of Dewey and Sinclair for isotopes which are distributed in the extracellular fluid, and has shown that the factor ℓ which determines the probability of detecting a tumour of volume V_T may be expressed as :

$$\ell = 126\sqrt{TF}\,\frac{ABV_T}{\sqrt{V_{NT}}} \qquad (2.6)$$

where F is the ratio of the concentration of the isotope in the tumour to the concentration of the isotope in the surrounding tissues and V_{NT} is the non-target volume. A depends on the biological and physical properties of the isotope and B depends on the collimating system and the physical properties of the isotope. Equation (2.6) is based on the assumption that the difference in concentration of the target and non-target regions is relatively small. The factor B can be used to compare collimators for the same application and is given by the expression :

$$B = \sqrt{\frac{\eta \epsilon_T^2 a_T^2}{\epsilon_{NT} a_{NT}}} \qquad (2.7)$$

where the subscripts T and NT refer to the target and non-target volumes. The factor B is inversely proportional to the square root of the collimator figure of merit E_{NT}/E_T^2 used by Dewey and Sinclair.

Beck (1966) has used a collimator figure of merit which is proportional to the sensitivity and the square of the modulation transfer function. This is based on the same statistical test (equation 2.5)(Beck, 1961).

Discussion

The factors described for comparing collimators all refer to the ability to detect changes in concentration of activity. As Matthews (1968) has pointed out in a discussion of the results of Simons and Bailey (1967), it is not appropriate to apply them when the probability for detection is very high. Under these conditions, the scan detail can be improved by making the collimator resolution finer. This results in a loss in sensitivity but does not lead to a loss in detection provided the factor ℓ is still greater than about three.

In the work presented here, a modified form of the expression for B (equation 2.7) has been used as the collimator figure of merit (section 4.5).

2.2 The calculation of focusing collimator performance

Focusing collimator performance can be assessed from calculated geometrical efficiencies if it is assumed that the effects of penetration and scattering are small. The limitations of this approach are discussed in the next section.

Geometrical efficiency

Garrett (1954) has pointed out that the accurate calculation of geometrical efficiency is similar to the calculation of mutual inductances of coils and solenoids. Existing tables of mutual inductance can however be applied only to collimators of simple geometries such as those with a single cylindrical hole.

Brownell (1958) has used the approximate method of approach of Does de Bye (1956) to calculate the geometrical efficiencies for a point source at positions on and off the axis of a cylindrical collimator, and single and multi-hole focusing collimators. The results for multi-hole collimators

are however confined to those cases in which the collimator length equals the focal length. Brownell (1958) has also calculated point source efficiencies for two cylindrically collimated detectors used in coincidence. Doust and Simons (1961) have applied a small correction to the values obtained by Brownell, in order to allow for the variation of crystal efficiency with position of the source.

Myhill (1961) has calculated the point source efficiencies for multi-hole focusing collimators but gives no details of his method. Pěrinová and Hušák (1967) have derived an approximate equation for one hole of a multi-hole focusing collimator, but since they assume that the source is in the same plane as that containing the axis of the hole and the collimator axis, their results cannot easily be used to calculate the efficiency of all the holes. Popovic and Hallard (1968) give an approximate expression for the point source efficiency of a multi-hole focusing collimator along the axis. They have also calculated the efficiencies for a point source located at any position in the focal plane.

Beck (1964a,b) has shown how the geometrical efficiency for a plane source may be calculated very simply, using the fact that in air the efficiency is approximately independent of distance. Beck (1961) has also shown how the plane source

response may be used to obtain the response to a volume source.

Discussion

A completely general expression for the geometrical point source efficiency of a multi-hole focusing collimator has been derived in this work. This has been used to calculate efficiencies both on and off the collimator axis. The latter calculations have enabled theoretical point source resolution curves to be drawn. Collimator figures of merit have been calculated by combining point source efficiencies with Beck's equation for the response to a volume source. The results of the calculations have been used to evaluate the influence of collimator parameters on performance and to form a basis for a method of collimator design.

Collimator performance and design

The early focusing collimators were designed rather arbitrarily with the collimator length equal to the focal length. Myers and Mallard (1964) have pointed out that this leads to a large variation of axial response and low sensitivity at great depths. They suggested that this may be overcome by using collimators with focal lengths twice the collimator length. Ephraim (1962, 1964) attempted to

gain a more uniform response by designing a collimator with holes focusing at different depths. Concannon and Bolhius (1957) suggested that two opposing detectors may lead to a more uniform response as has been demonstrated by Kakehi (1959) and Popovic and Fowler (1968).

Libby (1964) and Popovic and Fowler (1968) have demonstrated how collimator performance is influenced by the size of the air gap between the collimator and patient.

The relationships between collimator parameters and the importance of these relationships in collimator design has been clarified by the work of Beck (1964a,b). He has shown that the correct choice of collimator parameters can give a collimator with the maximum plane source efficiency under specified conditions. Matthews (1967) has described a similar method of collimator design for which the point source efficiency at the focus is maximised. Matthews has also shown how the collimator figures of merit may be calculated theoretically.

Beck (1964a,b) has stressed the importance of maintaining a reasonably constant resolution with depth. McAfee et al. (1966) found difficulty in obtaining constant resolution when designing a collimator for an 8" crystal and Popovic and Fowler (1968) have shown theoretically that although increasing the crystal diameter results in increased

sensitivity, there is also an increase in the variation of resolution.

Harris et al. (1962) have pointed out the importance of restricting penetration when designing a collimator. They have considered the relative merits of lead, tungsten and gold as shielding materials and describe a collimator made from gold with tungsten shielding (Francis, Harris and Bell, 1962). Both Harris et al. (1964) and Love and Smith (1966) have noted that long collimators limit penetration more effectively than short ones. Beck (1964a) has shown how penetration may be considered in collimator design.

Discussion

In general, conclusions on the effects of collimator parameters on collimator performance have been based on maintaining different parameters constant and are therefore difficult to interpret. For example, increasing the number of holes of a collimator has a different effect depending on whether the collimator and focal lengths are kept constant, or whether the field of view in the focal plane is kept constant. These effects have therefore been examined in detail on a theoretical basis.

Focusing collimator design has been greatly simplified by the work of Beck and of Matthews. The methods which they

suggest are based on maximising the plane source efficiency, or the point source efficiency in the focal plane. They assume that the optimum focal length for a given application is known. The method of collimator design suggested here is based on consideration of the collimator figures of merit as well as efficiencies. The relative merits of collimators of different focal lengths are assessed by calculating efficiencies and figures of merit throughout the region of interest. The proposed method of collimator design also includes practical considerations such as the probable size of the air gap between the collimator and patient, and the probable size of the patient.

2.3 The effects of penetration and scattering

In air, in addition to the geometrical efficiency, the factors which affect collimator performance are penetration of side shielding and septa, and scattering from the collimator walls. Penetration of side shielding can usually be reduced to a very low level by using a sufficient thickness of absorbing material to surround the detector.

Penetration

Penetration may also occur either by transmission

through one or more septa or by transmission through the top and bottom corners of the lead surrounding the holes. Mather (1957) has shown that, for a single cylindrical hole collimator, penetration of the top and bottom corners may be allowed for by effectively shortening the collimator length by two mean free paths at the specified energy. Simons (1962) has extended this theory to single-hole focusing collimators and has shown that they limit septum penetration more effectively then cylindrical collimators. Bell and Johnston (1968) have pointed out that the calculations of Mather and of Simons are only applicable when the distance of the source from the collimator is large compared with the size of the aperture. They have evaluated the expressions of Simons more accurately using a digital computer. Rotenberg and Johns (1965) using a different approach also come to the conclusion that penetration of corners is equivalent to a reduction in collimator length. They suggest that this type of penetration, which only leads to a small widening of the resolution curves, should be limited to less than 20 per cent of the geometrical efficiency.

Myhill (1961) has investigated radiation penetrating one or more septa and has derived an expression for the penetration length, that is, the length of lead transversed

by radiation travelling at a specified angle to the focal plane. Myers and Mallard (1964) have suggested that the smallest penetration length should equal seven half-value layers of lead. Rotenberg and Johns (1965) have calculated the minimum path length travelled through lead by radiation from the volume of interest and suggest that this should be equal to at least four mean free paths at the specified energy.

Beck (1961, 1964a,b) has derived two expressions for the penetration fraction for an extended source (equation 2.2). He has suggested that when designing a collimator the penetration fraction should be set to a low level so that errors in the approximations used in deriving the expressions have an insignificant effect on collimator response. Kuhl (1965) has investigated the performance of collimators designed using Beck's estimate of penetration and has shown that penetration is small at the energy for which they were designed.

Scattering from the collimator walls

Mather (1957) has calculated the effects of scattering from the walls of a particular cylindrical hole collimator and found that although Rayleigh scattering was small,

Compton scattering had a significant effect.

Discussion

Reasonable agreement between experimental measurements and theoretical calculations of geometrical efficiency (Myhill, 1961; Popovic and Mallard, 1968) have been obtained for axial sources in air under some particular experimental conditions, suggesting that the effects of penetration and scattering from the collimator walls are small. In the work presented here, these effects have been investigated for a range of collimators and gamma ray energies.

Scattering from tissue

In tissue, collimator performance is affected by attenuation and scattering. As described above, this results in an increasing loss of sensitivity with depth and a coarsening of resolution. Attenuation can be allowed for in theoretical calculations, but the amount of scattered radiation which is detected is difficult to calculate. As the energy of the primary radiation is decreased, radiation can be scattered with smaller losses in energy and is more difficult to eliminate by pulse-height discrimination without significantly reducing the photopeak counts. The effect of scattered radiation in reducing detection probability

has been demonstrated experimentally by Matthews and Kibby (1968) in a simulated scanning situation. This is due to the contribution of scattered radiation to the non-target count rate.

Little quantitative work has been published on the magnitude and effects of scattered radiation, mainly due to the difficulties in separating this component from unscattered radiation. Ter-Pogossian, Niklas and Bell (1966) have shown spectra of radiation scattered from a large volume, using a single-hole focusing collimator. Unscattered radiation was eliminated by using a non-radioactive cone which filled the geometric field of view at all depths. Beck (1964a, 1968) has used theoretical calculations of scattered spectra to obtain values for the increase in response due to scattering. He found little difference in the scatter fractions (equation 2.4) for large volume sources, using different collimators and crystal sizes. A decrease in scattering with increase in primary energy was however observed. From his results, Beck has calculated the settings of the lower level of the analyser window which give the highest values of the figure of merit.

In the work described here, the effects of radiation scattered from tissue have been investigated both theoretically

and experimentally.

2.4 Multichannel collimators for cameras

The performance of camera systems, like that of scanning systems, can be assessed in terms of sensitivity, resolution and the probability of detection of localised changes in activity. The resolution of a camera system is however determined both by the intrinsic resolution of the image converter and the resolution of the collimator. Brownell (1959) has defined the collimator resolution as the distance apart of two point sources which give touching image circles on the detector but it is difficult to apply this definition in practice. Mallard and Myers (1963) include the intrinsic resolution of the detector and define the overall resolution as the distance apart of two point sources which give touching image circles on the display. Westerman and Glass (1968) also consider the overall resolution which they define as the full-width at half maximum of the camera response to full photopeak radiation emitted from a line source placed with its longitudinal axis along a major axis of the crystal. Although the overall resolution is preferred for practical measurements, for simplicity the collimator resolution alone has been used in the paper

presented here.

By assuming a camera system in which a multichannel collimator moves in a manner similar to that of a Potter-Bucky filter, Anger (1964) has derived approximate theoretical expressions for the collimator resolution and for the efficiency for a point source. He has also shown how the minimum path length through one complete septum of a multichannel collimator may be calculated and suggests that this should be greater than three mean free paths through the collimator material at the specified energy. Keller (1968) has used the equations derived by Anger as a basis for a method of multichannel collimator design in which the point source efficiency is maximised.

Although the validity of the equations of Anger was confirmed experimentally in a few instances (Anger, 1964), since they were derived using a rather arbitrary assumption it was felt that further investigation would be of value.

CHAPTER 3

THEORETICAL CALCULATIONS OF GEOMETRICAL EFFICIENCIES OF FOCUSING COLLIMATORS

3.1 Introduction

Since it is unlikely that a collimator would be used at energies for which penetration is significant, and since any scattering from the collimator walls is probably small, in many cases the response of a collimator to a source in air can be adequately described by its geometrical efficiency. A completely general expression for the efficiency of a multi-hole focusing collimator has been derived in this work. Some of the simpler parts of the work have been described by other authors to whom reference is made.

The efficiencies of a number of multi-hole focusing collimators have been calculated by computer and used to form some general conclusions about collimator performance.

Assumptions

It has been assumed that the collimator holes are circular in cross-section. Although hexagonal holes increase the crystal area which is exposed by about 10% and therefore

give higher efficiencies, they are used less often than circular holes because of difficulties in construction. The use of hexagonal holes probably does not significantly alter the variation in efficiency with position of the source. Holes of other cross-sectional shapes (Höfer and Roszuczky, 1964) have not been considered.

It has been assumed that the arrangement of holes in a multi-hole collimator is hexagonal. This arrangement enables the largest number of holes of a given cross-section to be packed into a given area and it is therefore preferable to circular or other arrays.

3.2 Efficiencies of individual holes

Point source efficiency

Consider one hole of a focusing collimator (fig. 3.1). Let the hole have radius r at the crystal face of the collimator, and radius r' at the external face and then :

$$r' = \frac{r}{\left(1 + \frac{t}{f}\right)}$$

where t is the collimator length and f is the focal length. Let the base of the hole be a distance h from the collimator axis. Then the centre of the external face of the hole is

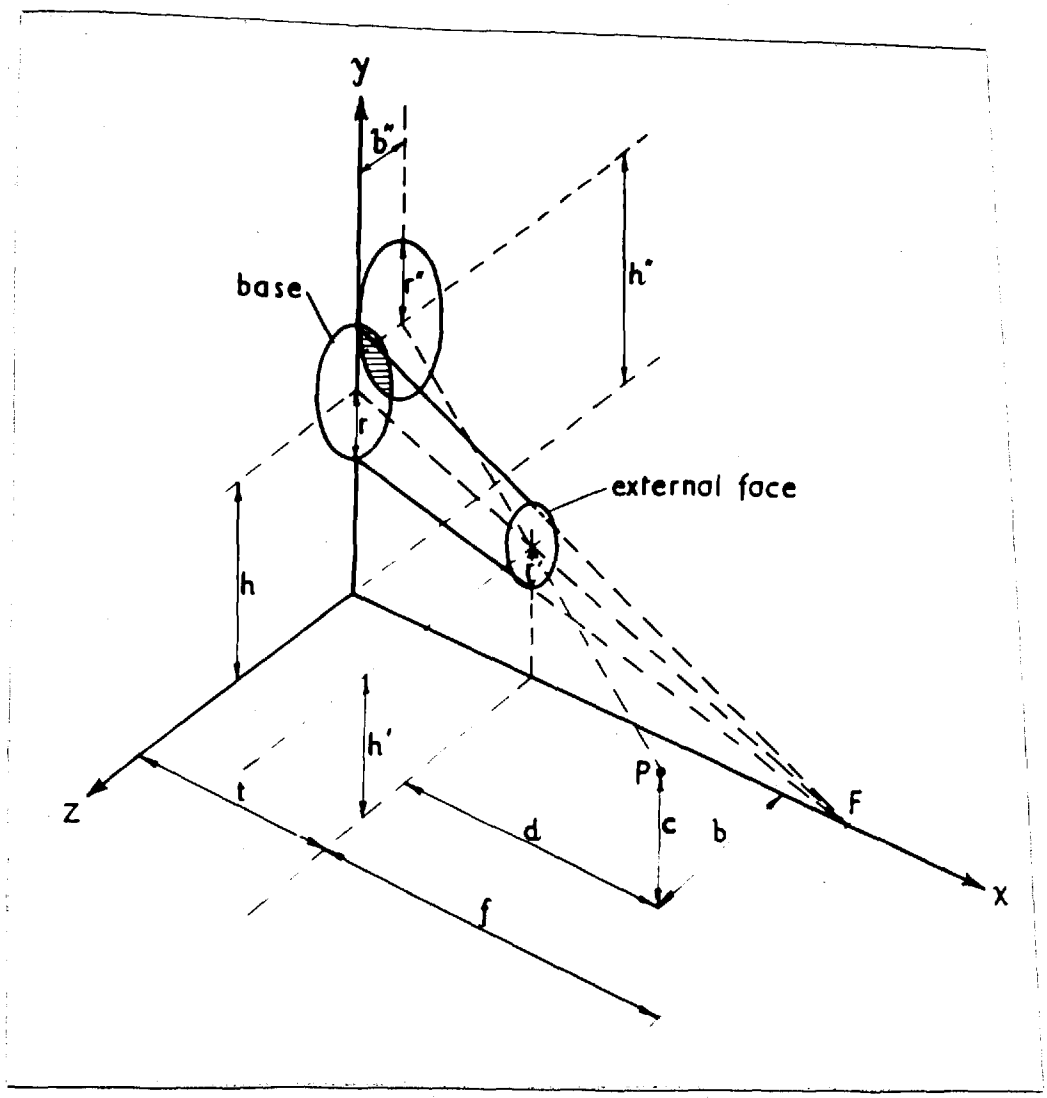

Fig. 3.1 One hole of a collimator with focus at F. A point source of radiation is situated at P.

a distance h' from the collimator axis, where

$$h' = \frac{h}{\left(1 + \frac{t}{r}\right)}$$

Take co-ordinate axes x, y and z as shown and consider a point source of radiation at point P with co-ordinates (t+d), c, b. Radiation is incident on the detector over the area of intersection of the base of the hole with the projection of the external hole face on the base plane. The accurate calculation of the solid angle subtended by the area at P requires integration over each element of area, involving the numerical evaluation of incomplete elliptic integrals. Only the approximate solution is considered here. This is based on the assumption that the dimensions of the area of intersection are small compared with the distance of the area from the source. This assumption, which is generally true, allows the area to be considered as a whole in the calculation of solid angles.

Let the centre of the circle obtained by projecting the external face of the hole onto the base plane have co-ordinates (0, h", b") and let the projected circle have radius r". It can be shown that :

$$r'' = kr \qquad (3.1)$$

where $$k = (1 + \frac{t}{d}) \,/\, (1 + \frac{t}{f}) \qquad (3.2)$$

$$h'' = kh - ct/d \qquad (3.3)$$

and $$b'' = -\frac{bt}{d} \qquad (3.4)$$

The distance between the centre of the projected circle and the centre of the base of the hole is given by :

$$\sqrt{(h'' - h)^2 + b''^2}$$

The area of intersection of the circles (A) may then be calculated, giving :

$$A = r^2 \cos^{-1}\left[\frac{(b''^2+(h''-h)^2) - r^2(k^2-1)}{2r\sqrt{b''^2 + (h''-h)^2}}\right]$$

$$+ k^2 r^2 \cos^{-1}\left[\frac{(b''^2+(h''-h)^2) + r^2(k^2-1)}{2kr\sqrt{b''^2 + (h''-h)^2}}\right]$$

$$- \frac{1}{2}\sqrt{2r^2(1+k^2)(b''^2+(h''-h)^2) - r^4(k^2-1)^2 - (b''^2+(h''-h)^2)^2} \qquad (3.5)$$

When the source lies in the xy plane (i.e., b = 0

$b'' = 0$), the expression reduces to that derived by Pěrinová and Hušák (1967). When the source lies in the focal plane, $d = f$, $k = 1$, $h''-h = -\frac{ct}{f}$ and $b'' = -\frac{bt}{f}$, giving:

$$A = 2r^2 \cos^{-1}\left[\frac{(\frac{t}{f})\sqrt{b^2+c^2}}{2r}\right] - \frac{(\frac{t}{f})(b^2+c^2)}{2} \times \sqrt{4r^2 - (\frac{t}{f})^2 (b^2+c^2)}$$

This expression has been derived by Popovic and Mallard (1968). They have also derived an expression for the area, when the source is situated on the collimator axis. Then $b'' = 0$ and $h'' = kh$ giving :

$$A = r^2 \cos^{-1}\left[\frac{h^2(k-1)-r^2(k+1)}{2rh}\right] + k^2r^2\cos^{-1}\left[\frac{h^2(k-1) + r^2(k+1)}{2krh}\right] - \frac{1}{2}\sqrt{(k-1)^2\,[2r^2h^2(1+k^2) - r^4(k+1)^2 - h^4(k-1)^2]} \qquad (3.6)$$

The area of intersection of the circles becomes imaginary when :

$$(h'' - h)^2 + b''^2 \geqslant r^2 (1 + k)^2$$

i.e., when the circles lie outside each other, and also when :

$$(h'' - h)^2 + b''^2 \leqslant r^2 (k - 1)^2$$

i.e., when one circle lies completely within the other. In this latter case, the area over which radiation is incident is given by :

$$A = \pi k^2 r^2 \quad \text{when} \quad k < 1$$

and $$A = \pi r^2 \quad \text{when} \quad k > 1.$$

The centre of the area of intersection lies along the line joining the centres of the circles. The calculation of the mid-point of the area of intersection is complex for the general case, and it was therefore assumed that the centre of the area of intersection lay at the centre of the base of the hole. The error in this approximation increases when radiation is incident over only a small fraction of the base area of the hole. However, for multi-hole collimators, the contribution of these holes to the total efficiency is small and hence there is only small error in the final result.

Since the centre of the base of the hole is a distance $\sqrt{(h-c)^2 + b^2 + (t+d)^2}$ from the source P, the point source efficiency may be calculated from the expression :

$$\epsilon_T (g) = \frac{A(t+d)}{4\pi[(h-c)^2 + b^2 + (t+d)^2]^{3/2}} \qquad (3.7)$$

The expressions derived here may also be used to calculate point source efficiencies for collimators of the type used with the autofluoroscope (Bender and Blau, 1962; 1964). The holes of these collimators focus in a plane at equally spaced points, corresponding to the centres of the bases of the holes. Let a point source be situated a distance v from the axis of one hole, at a distance d from such a collimator. Then, since h = 0, $v = \sqrt{b^2+c^2} = \frac{d}{t}\sqrt{b''^2 + h''^2}$ (equations 3.3 and 3.4) and equation (3.5) gives :

$$A = r^2 \cos^{-1}\left[\frac{v^2(\frac{t}{d})^2 - r^2(k^2-1)}{2vr(\frac{t}{d})}\right] + k^2 r^2 \cos^{-1}\left[\frac{v^2(\frac{t}{d})^2 + r^2(k^2-1)}{2vkr(\frac{t}{d})}\right] - \frac{1}{2}\sqrt{2r^2v^2(1+k^2)(\frac{t}{d})^2 - r^4(k^2-1)^2 - v^4(\frac{t}{d})^4} \qquad (3.8)$$

The centre of the area of intersection lies along the line of centres of the circles at a distance $[(r-r') + v(\frac{t}{d})]/2$ from the axis of the hole. The point source efficiency is therefore given by the expression :

$$\epsilon_T \ (g) = \frac{A(t+d)}{4\pi \left[(t+d)^2 + \frac{[(r-r') + v(\frac{t}{d})]^2}{4}\right]^{3/2}} \qquad (3.9)$$

Plane source efficiency

The efficiency for a source placed next to the external face of a hole has been calculated by Beck (1964b), i.e.,

$$\epsilon_{pL} = \frac{\pi r^4}{4t^2(1 + \frac{t}{f})^2} \qquad (3.10)$$

Since the response of a focusing collimator to an infinite plane source perpendicular to the axis is reasonably independent of source position, equation (3.10) represents the efficiency in air at all distances from the collimator.

3.3 Summation of efficiencies for holes in hexagonal array

The expressions derived in section 3.2 may be used

directly to calculate the point and plane source geometrical efficiencies for single hole focusing collimators. In order to calculate the total point source efficiencies of multi-hole collimators it is necessary to sum the contributions of individual holes.

Hexagonal arrays

Consider a hexagonal array of round holes. Let one hole in the array be designated by $g = 0$, then the surrounding hexagon of six holes may be designated $g = 1$, the next hexagon of twelve holes by $g = 2$, etc.. When $g = 0$ there is one hole at a distance $h = 0$ from the reference hole. For each surrounding hexagon of holes ($g=1, 2, 3 \ldots$) there are six holes at distances $h = g(2r+s)$ where r is the hole radius and s is the septum thickness, i.e., the minimum distance between holes. In addition, when g is an even integer, there are six holes at distances

$$h = g(2r+s)\ \frac{\sqrt{3}}{2}$$

and twelve holes at distances $h = (2r+s)\sqrt{\frac{3g^2}{4} + i^2}$ for each value of i given by 1, 2, 3.... for which $i \leq (\frac{g}{2} - 1)$. When g is an odd integer, there are, in addition to the six holes noted above, twelve holes at distances

$h = \frac{(2r+s)}{2} \sqrt{3g^2+j^2}$ for each value of j given by 1, 3, 5.... for which $j \leq (g-2)$.

Total point source efficiency

Summation of the point source efficiencies of the holes of a multi-hole focusing collimator is relatively simple when the source is situated on the collimator axis. Values of h for the holes which contribute to the response can be used to calculate the efficiencies from equations (3.6) and (3.7). When the source is situated off the axis the procedure is considerably more complex. Assuming as before (fig. 3.1) that the axis of the collimator is the x-axis and that one hole lies along the y-axis, one requires values of b and c for that hole for some specified position of the source. Let the source be a perpendicular distance m from the x-axis and let the line joining the source to this axis make an angle θ, measured in a clockwise direction, with the y-axis. Then, for the hole lying on the y-axis,

$$b = m \sin \theta$$

and

$$c = m \cos \theta$$

The specified hole has others corresponding to it in each segment of the hexagonal array and the distances b and c

for each set of six holes are given by :

$$b = m \sin (q\frac{\pi}{3} + \theta)$$

$$\text{and} \qquad c = m \cos (q\frac{\pi}{3} + \theta)$$

where $q = 0, 1, 2, \ldots 5$. Some holes in the array will be displaced from the y-axis, and from lines at some multiple of $\frac{\pi}{3}$ with the axis. Let the angular displacement of these holes be ϕ, measured in a clockwise direction. Then the distances b and c are given by :

$$b = m \sin (q\frac{\pi}{3} + \theta - \phi)$$

$$\text{and} \qquad c = m \cos (q\frac{\pi}{3} + \theta - \phi)$$

where $q = 0, 1, 2, \ldots 5$. Values of ϕ may be calculated for any hole from the corresponding values of h. Thus, values of b, c and h may be used to calculate the efficiencies of individual holes in the array using equations (3.5) and (3.7).

Total plane source efficiency

The total plane source efficiencies of multi-hole collimators may be calculated by multiplying the efficiency of one hole by the number of holes in the array.

3.4 The calculation of the point source efficiencies of some multi-hole focusing collimators

Calculations have been carried out in an attempt to relate the variations in resolution of different collimators to the collimator dimensions.

Computer program

A computer program was written in Algol for the Elliott 4100 computer to calculate the total point source efficiencies of focusing collimators from the expressions presented in sections 3.2 and 3.3. For each collimator efficiencies were computed for a source position at different distances along and perpendicular to the collimator axis. The latter calculations could be carried out for the source along a diagonal of the hexagon of holes or at some angle to the diagonal. Further details of the program can be found in Appendix 1.

Resolution curves

The results of calculations on many collimators were plotted in a manner suggested by Hine (1967). The response along a line perpendicular to the collimator axis is shown as a three-dimensional function of distance from the collimator. A typical set of resolution curves obtained

in this manner are given in fig. 3.2. In the focal plane the curve is approximately triangular in shape although the sides show a slight concavity. Beyond the focal plane, the curves are Gaussian in shape and become flatter at greater distances, as the field of view increases and the sensitivity decreases. In front of the focal plane the curves are also Gaussian but tend to develop a flat top at small distances from the collimator. The undulations at very small distances from the collimator face are due to the contributions of individual holes and therefore depend on the number of holes. The effect becomes prominent at distances at which radiation from the source enters only a few holes in the array. In this example the peaks occur between the holes because the septa are thin and the sum of partial contributions from two holes is greater than that from one alone. For a collimator with thicker septa, the reverse effect can occur. The shape of the resolution curves depends on whether they are plotted for a source along a diagonal of the hexagon of holes or at some angle to a diagonal. In general the differences are small, decreasing as the source collimator distance increases and becoming negligible beyond the focus. They have been ignored in the following sections.

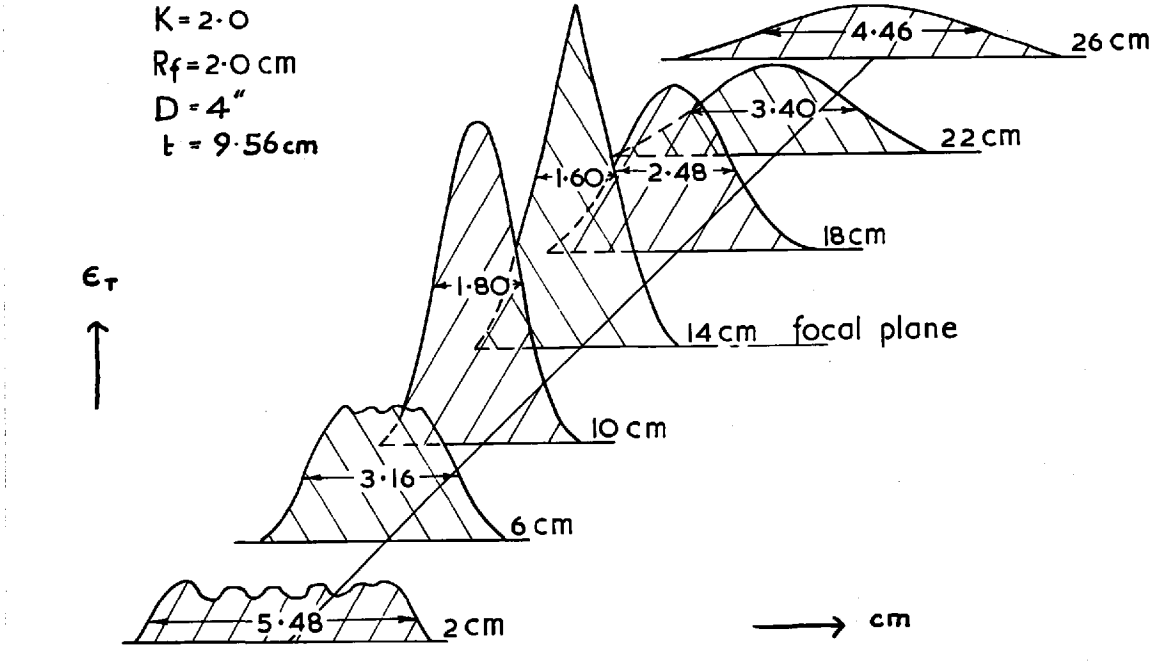

Fig. 3.2 Theoretical point source resolution curves for a 37-hole collimator with radius of field of view 2 cm in the focal plane, 14 cm from the collimator face.

Shape factor

The full-widths at half maximum are indicated on the resolution curves shown in fig. 3.2. When undulations were present, the FWHM was defined as the width of the curve at half the axial efficiency. It is apparent that for this collimator the FWHM increases rapidly on each side of the focal plane.

For most applications a reasonably uniform resolution is required over a range of distances and the FWHM should also be reasonably constant. In an attempt to introduce a parameter which describes the variation of resolution with distance, Beck (1964b) has introduced a quantity called the shape factor. The shape factor is defined as the area of the field of view at the collimator face divided by the area of the field of view in the focal plane (fig 1.1). For round holes in a hexagonal array it is given by the expression :

$$K = \frac{3\sqrt{3}}{8\pi} \cdot \frac{D^2}{(R_f + 2r)^2} \qquad (3.11)$$

where D is the diameter of the smallest crystal covered by all the holes and R_f is the radius of the field of view in the focal plane (fig. 1.1). The description of variations in resolution by variations in either the field of view or

the FWHM is not entirely satisfactory, but since the shape factor can be calculated very simply, the possibility of its use as an overall measure of variation in resolution was investigated. This was done by comparing the shape factors and the variation of the FWHM with distance for different collimators.

Collimators with the same shape factors but with different focal lengths, numbers of holes and radii of field of view in the focal plane all showed a similar variation of FWHM with distance. Some differences were observed beyond the focal plane but these were small compared with those between collimators of different shape factors.

The variation of FWHM for collimators of different shape factors is shown in fig. 3.3. The FWHM denoted by R is expressed as a fraction of the radius of the field of view in the focal plane and plotted against the distance from the collimator face as a fraction of the focal length. This presentation allows the same curves to be applied to other collimators of the same shape factors. The results show that a large shape factor indicates a large variation in the FWHM with distance and even those collimators with shape factors close to one show some variation. In the focal plane ($\frac{d}{f} = 1$), the FWHM is less than the radius of

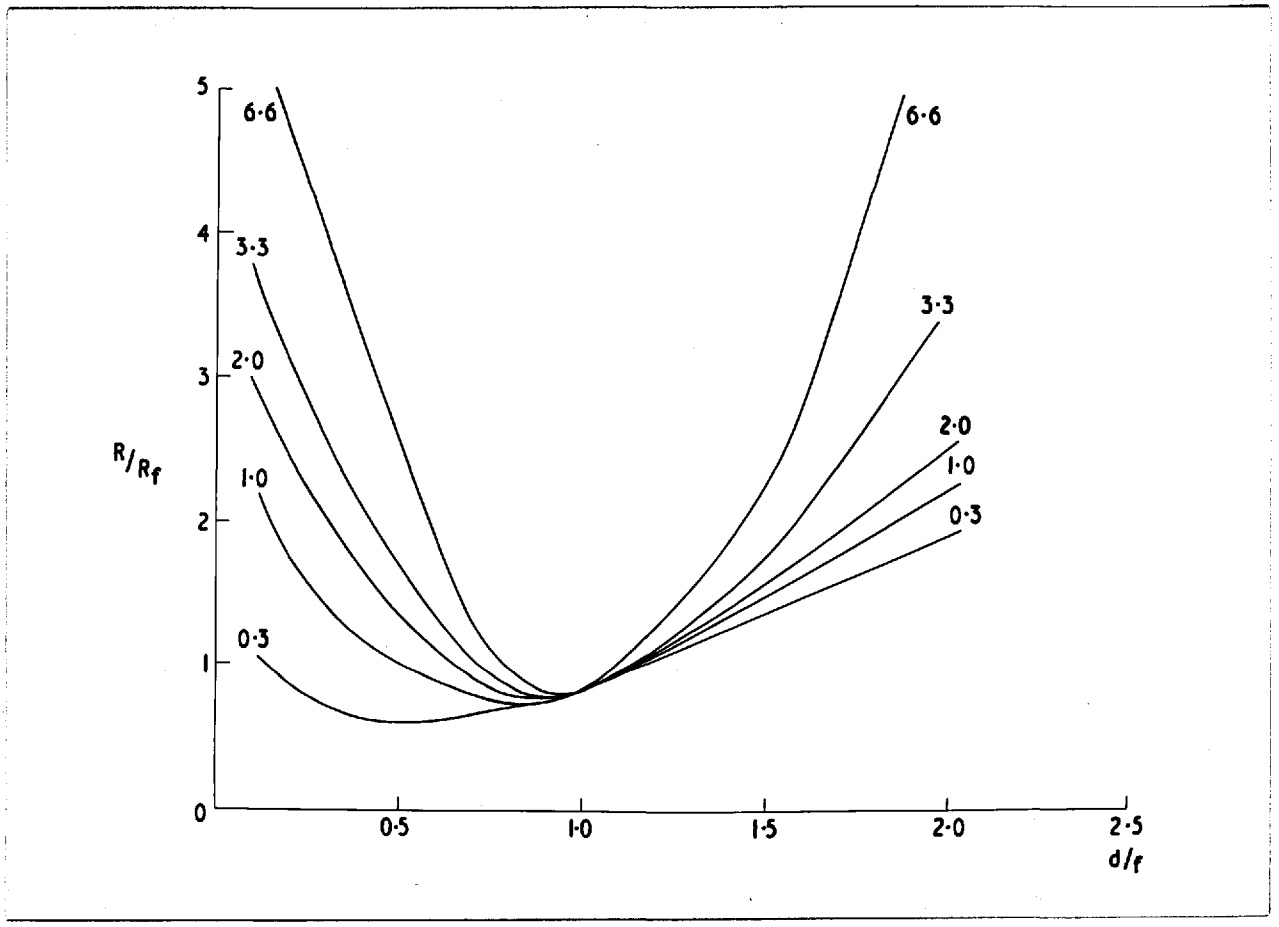

Fig. 3.3 The FWHM as a fraction of the radius of field of view in the focal plane plotted against distance from the collimator face as a fraction of the focal distance. Curves are shown for collimators with different shape factors.

the field of view due to the concavity of the resolution curve. Collimators with small shape factors show the smallest FWHM in front of the focal plane.

Figure 3.4 shows the same results with the fractional distances at which the FWHM increases by more than 25 per cent and 50 per cent of the radius of the field of view in the focal plane, plotted against the shape factor. This graph enables the limits between which a collimator shows reasonably uniform resolution to be determined. For example, a collimator with a shape factor of one has a FWHM not greater than 25 per cent of the radius of the field of view in the focal plane between distances of 0.46 and 1.33 of the focal length. All collimators show a significant increase in the FWHM at distances greater than 1.5 times the focal length. A collimator with a shape factor of 0.5 has a reasonably uniform resolution up to a distance 1.4 times the focal length.

Axial efficiencies

The total point source geometrical efficiencies along the axes of different collimators were plotted against distance from the collimator face. Examples of such curves will be given in Chapter 4. In general they show an increase in efficiency as the distance is increased, followed by a

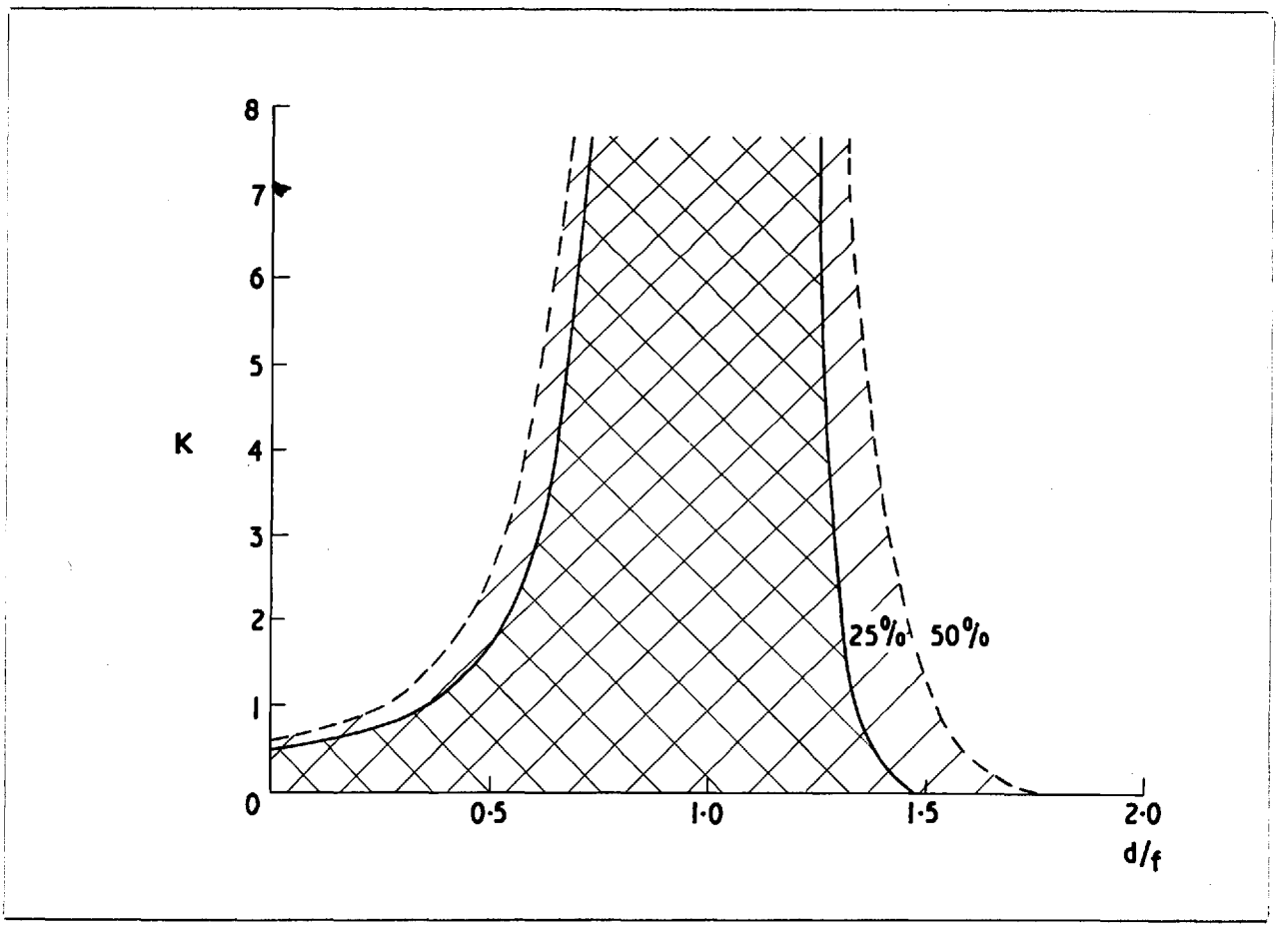

Fig. 3.4 The shape factor plotted against the fraction of the focal length at which the FWHM is 25% and 50% greater than the radius of the field of view in the focal plane.

decrease in efficiency. The maximum efficiency in air in many cases occurs at some distance in front of the focus. In fig. 3.5 the distance at which the efficiency in air is a maximum has been expressed as a fraction of the focal distance and plotted against the shape factor. Points are shown for collimators with different numbers of holes and radii of field of view in the focal plane. This curve shows that there is a tendency for the point of maximum response to move closer to the collimator as the shape factor is decreased.

Graphs of axial efficiency plotted against distance also showed that there was a tendency for collimators with small shape factors to show a more uniform variation of efficiency with distance. The efficiencies of collimators with large shape factors tend to decrease rapidly on either side of the focal plane.

Discussion

The variation of axial efficiency with distance is the result of two opposing effects. Close to the collimator, radiation from a point source is incident on the detector only at the base of the central hole. As the source is moved away from the collimator, radiation is also incident

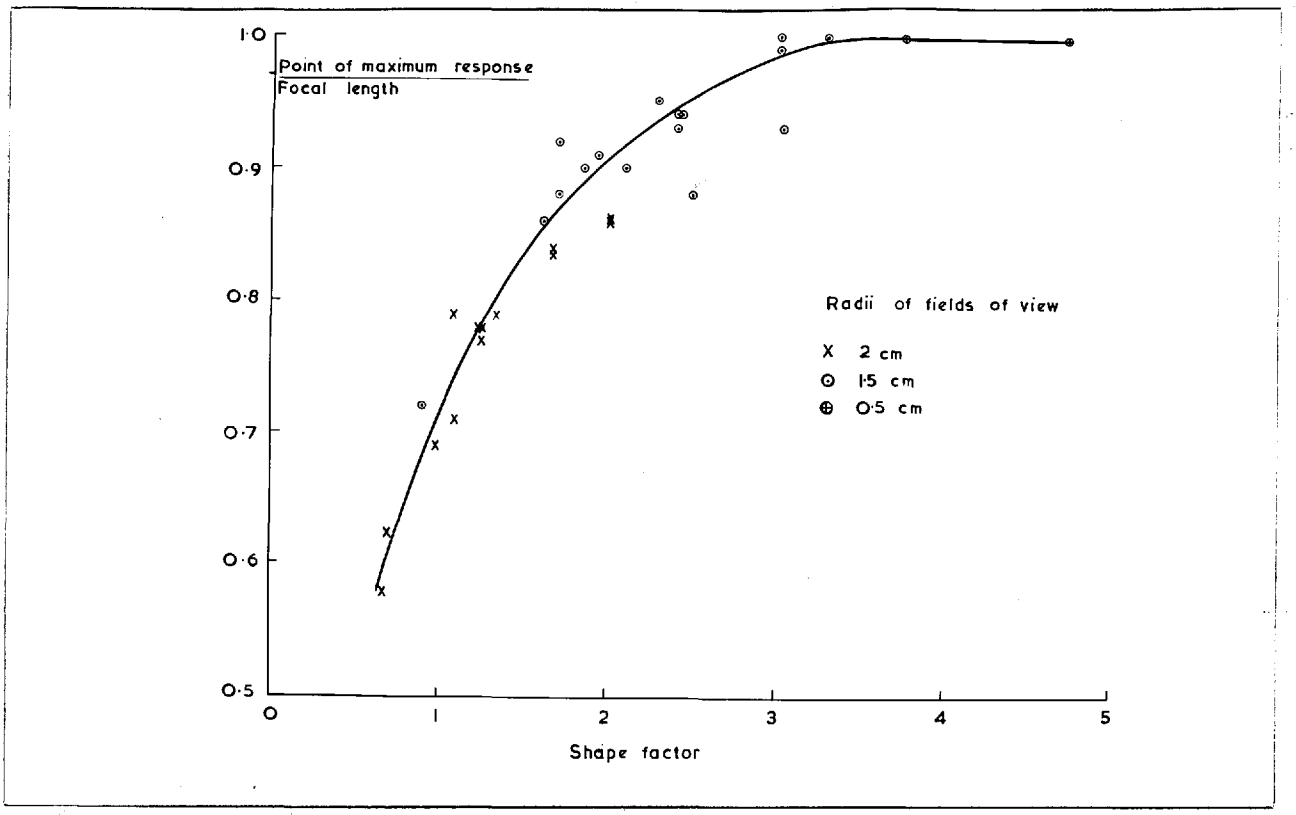

Fig. 3.5 The distance of the point of maximum response from the collimator, as a fraction of the focal length, plotted against shape factor. Points are shown for collimators with different radii of the field of view in the focal plane.

on the detector at the base of neighbouring holes. The contribution of other holes increases as the source is moved towards the focal plane and a greater detector area becomes exposed to radiation. At the same time however, there is a decrease in efficiency due to the inverse square law. With a small number of large holes, that is, a small shape factor (equation (3.11)), the latter effect rapidly becomes more important than the former, giving a maximum well in front of the focal plane.

When two collimated detectors are used with the outputs summed, the resolution of the system can be determined from the sum of the resolution curves at the distances of the source plane from each collimator. If the foci of the collimators coincide, the FWHM in the focal plane is the same as that for each individual collimator. In other planes, the FWHM of the total resolution curve is dependent on the relative magnitudes of the individual curves as well as their shapes. The shape factor for one collimator therefore gives a less accurate assessment of variation in resolution for a double headed system than for a single headed system.

The results of this chapter have been obtained for point sources in air. The axial efficiencies are affected by attenuation and scattering from tissue as discussed in

Chapter 6. Attenuation has a relatively small effect on the shape of the resolution curves for a single collimator but scattering has a greater effect. Since the total resolution curve of a double headed system is dependent on the magnitude of the individual resolution curves for each collimator, both attenuation and scattering affect the resolution of a double headed system.

These investigations have shown how the shape factor, which is very simple to calculate, can be used to assess collimator performance. Figure 3.4 gives the depths over which a reasonably constant resolution is obtained and fig. 3.5 indicates the distance of the point of maximum response in air from the collimator. These details are often sufficient to obtain a rough assessment of the suitability of a collimator for some specific application. This is particularly advantageous in collimator design as the calculation of resolution curves of the many possible designs takes a considerable time even using a computer.

CHAPTER 4

THE DESIGN OF MULTI-HOLE FOCUSING COLLIMATORS FOR SCANNING

4.1 Method of design of focusing collimators

For most scanning applications, a collimator is required which has fine resolution, high sensitivity and a high probability for the detection of a lesion, throughout the region of interest. In the method of design of collimators suggested here, calculations are carried out on a number of possible designs. The collimator which has the most suitable shape factor and gives the most suitable variation in efficiency and figure of merit with distance, is then selected.

Basic relationships between collimator parameters

The following equations relating collimator parameters have been derived by Beck (1964b) :

$$D = 2rn + s(n-1) \qquad (4.1)$$

where n is related to the number of holes (N) in the collimator, which are assumed to be arranged in a hexagonal array:

$$N = \frac{3n^2 + 1}{4} \qquad (4.2)$$

where $n = 3, 5, 7 \ldots$.

$$s = s' \left(1 + \frac{t}{f}\right) \qquad (4.3)$$

where s' is the septum thickness at the external face of the collimator.

$$\frac{2r}{R_f} = \frac{t}{f} \qquad (4.4)$$

Eliminating s and $(\frac{t}{f})$ from equations (4.1), (4.3) and (4.4):

$$r = \frac{R_f \left[D - s'(n-1)\right]}{2 \left[nR_f + s'(n-1)\right]} \qquad (4.5)$$

Therefore, if it is assumed that s' equals the minimum possible thickness of septum which it is possible to cast or drill (s_m), the hole radius may be calculated for known values of D, R_f and n. The other collimator parameters may then be calculated assuming a value for f.

At energies for which penetration of even a small thickness of lead is insignificant, collimators designed with $s' = s_m$ (s_m = 0.05 - 0.10 cm.) would probably not show

significant penetration effects. At higher energies this will not be the case. Beck (1964a) has derived the following expression for the penetration fraction (equation 2.2) for an extended plane source :

$$P = \frac{6N}{\lambda^3 t^3 (2+\tau)(1-\tau)^2 \tau^2} \qquad (4.6)$$

where λ is the linear absorption coefficient of the collimator material at the specified energy and τ is the transmission ratio. The transmission ratio is defined as the fraction of the detector area not covered by septa and is given by the expression :

$$\tau = \frac{4Nr^2}{D^2} \qquad (4.7)$$

If it is assumed that D, f, R_f and n are constant, differentiation of equation (4.6) shows that the penetration fraction P is a minimum when $\tau = 0.653$. The corresponding minimum penetration fraction may be greater or less than the set maximum tolerable level P_m. In the former case it is impossible to design a collimator with the set of values of D, f, R_f and n which sufficiently reduces penetration. In

the latter case there may be two possible collimators fulfilling the requirements. The collimator with the larger transmission ratio may however be extremely long, with septa which are thinner than the minimum possible. Beck (1964b) has stated that equation (4.6) may only be approximate and therefore suggests that the maximum tolerable penetration should be set to a low level ($P_m = 0.01$) so that errors in design will be small.

Practical considerations

The equations given above show that at any energy it is possible to design a collimator for known values of D, f, R_f, n and s. Collimators are usually required for an existing scanner and therefore the value of the crystal diameter D has been determined. The radius of the field of view in the focal plane R_f can be set from the required resolution since in the focal plane $R_f \triangleq$ FWHM. The minimum septum thickness s_m is set by manufacturing techniques.

Since the maximum response is not necessarily obtained at the focus as described in section 3.4, the value of the focal length which gives the most suitable variation in sensitivity throughout the region of interest is unknown. A range of possible focal lengths is therefore considered.

Collimators are also designed for a range of values of n.

Collimator performance is assessed both in air and in water representing tissue. Efficiencies are corrected for attenuation using the total linear absorption coefficients, allowing for an air gap between the collimator face and the body or phantom surface. The effects of scattered radiation are not included in the design procedure. They are discussed in Chapters 6 and 7.

Figure of merit

The relative probabilities of detection of lesions using different collimators are determined by calculating collimator figures of merit. The figure of merit used in this work was obtained from equation (2.5). For a region of increased activity, the target counting rate can be expressed as :

$$C_T = \rho_T E_T + \rho_{NT} (E_{NT} - E_T)$$

where ρ is the concentration of activity (μCi/ml) and E is the sensitivity in cps/(μCi/ml). The non-target counting rate can be expressed as :

$$C_{NT} = \rho_{NT} E_{NT}$$

Therefore, from equation (2.5):

$$\ell = \frac{\sqrt{T\rho_{NT}}\,(\rho_T/\rho_{NT} - 1)\,E_T}{\sqrt{2E_{NT} + E_T(\rho_T/\rho_{NT} - 1)}}$$

Under conditions when the figure of merit is applied,

$$2\,E_{NT} \gg E_T\,(\rho_T/\rho_{NT} - 1)$$

Therefore,

$$\ell = \sqrt{T\rho_{NT}}\,(\rho_T/\rho_{NT} - 1)\,\frac{E_T}{\sqrt{2E_{NT}}}$$

and from equation (2.3), since $E = E'V$ where V is the volume, and E' and E'' are the sensitivities in cps/μCi and cps/(μCi/ml):

$$\ell = \sqrt{\frac{T\rho_{NT}q\eta}{2}}\,(\rho_T/\rho_{NT}-1)\,\frac{\epsilon_T a_T V_T}{\sqrt{\epsilon_{NT} a_{NT} V_{NT}}}$$

Thus the collimator figure of merit $\epsilon_T a_T / \sqrt{\epsilon_{NT} a_{NT} V_{NT}}$ is proportional to the factor ℓ which determines the probability of detection. It is similar to the factor B of Matthews (1967)(equation 2.7) and can be used to compare collimators for the same application, isotope and scan time.

For regions of zero activity, the target and non-target

counting rates can be expressed as :

$$C_T = \rho_{NT} (E_{NT} - E_T)$$

and $$C_{NT} = \rho_{NT} E_{NT}$$

Equation (2.5) then gives :

$$\ell = \sqrt{\frac{T\rho_{NT}q\eta}{2}} \frac{\epsilon_T a_T V_T}{\sqrt{\epsilon_{NT} a_{NT} V_{NT}}}$$

Thus the collimator figure of merit may also be applied to the detection of 'cold' regions.

Computer program

A program was written in Algol for the Elliott 4100 computer to calculate axial efficiencies and figures of merit for the possible collimators suitable for a specific application. A simplified version of the flow diagram is given in fig. 4.1, and further details of the program can be found in Appendix 2. The program may also be used to calculate the axial response of existing collimators.

The input data is read in and if the design procedure is required, the number of collimator holes and the focal length are set to the minima of the desired ranges. The

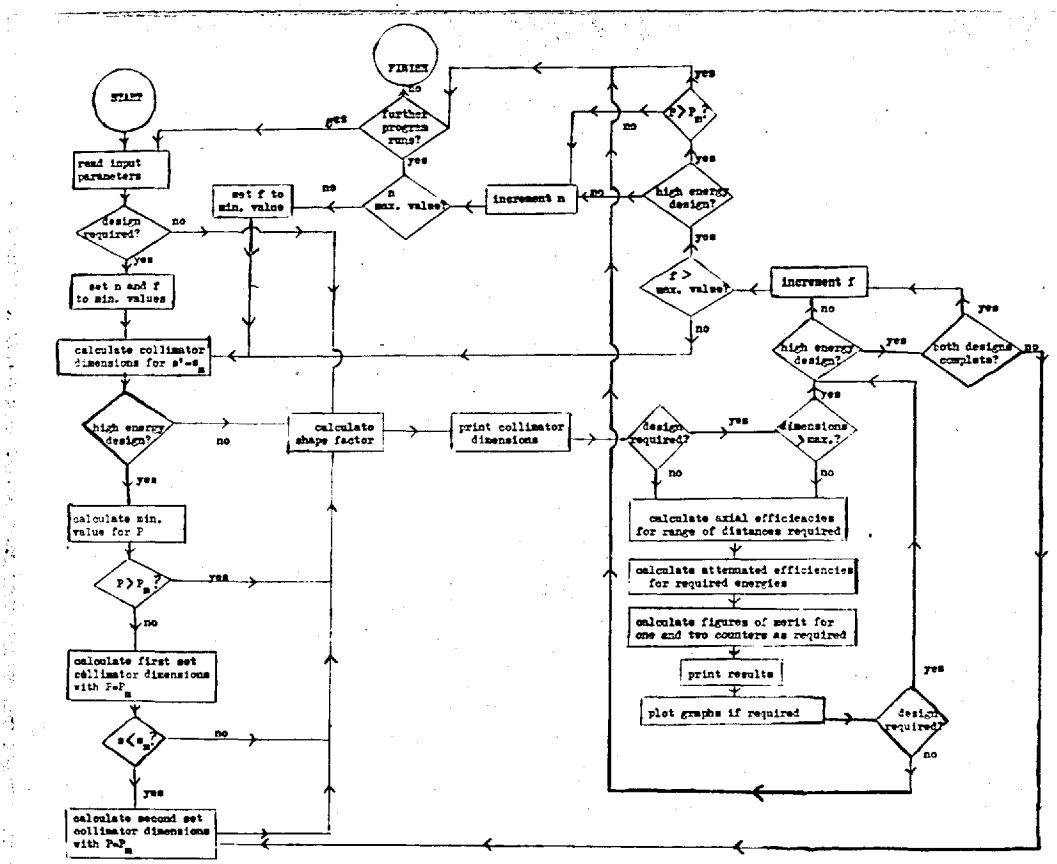

Fig. 4.1 Flow diagram for the computer program for the design of multihole focusing collimators.

remaining collimator dimensions are then calculated, assuming that the septum thickness at the external collimator face equals the minimum possible thickness. If the energy for which the collimator is being designed may lead to significant penetration effects, the program calculates the minimum possible value for the penetration fraction assuming that $\tau = 0.653$. Provided this is less than the maximum tolerable level, one set of dimensions for which $P = P_m$ are calculated. This is performed by making progressively smaller increments or decrements in the hole radii as the required condition is approached. The reiterative procedure is repeated ten times. If this leads to a collimator with septa greater than the minimum possible, the shape factor is calculated and the dimensions are pointed out. These steps are omitted when the program is run for an existing collimator or if penetration effects are likely to be small.

The shape factor, collimator length and the penetration fraction are tested to see whether they are greater than the maximum tolerable levels, in which case the program omits the next steps. The axial efficiencies are calculated for a point source in air at the distances specified in the data. Then, allowing for the air gap, the efficiencies are

corrected for attenuation in water, according to depth. This calculation of attenuated efficiencies may be carried out for several energies. The plane source efficiency is calculated from equation (3.10) multiplied by the number of holes in the collimator, and this is used to obtain an expression for the attenuated efficiency of a volume source, i.e.,

$$\epsilon_{NT} a_{NT} V_{NT} = \epsilon_{pl} \frac{(1 - e^{-\mu H})}{\mu} \qquad (4.8)$$

where H is the phantom thickness and μ is the linear absorption coefficient in water at the specified energy. The collimator figure of merit for a point source is then calculated. For a single detector this is given by :

$$B' = \sqrt{\frac{(\epsilon_T a_T)^2}{\epsilon_{NT} a_{NT} V_{NT}}} \qquad (4.9)$$

and for two opposing detectors by :

$$B' = \sqrt{\frac{(\epsilon_{T_1} a_{T_1} + \epsilon_{T_2} a_{T_2})^2}{2 \epsilon_{NT} a_{NT} V_{NT}}} \qquad (4.10)$$

The calculations of point source efficiencies and figures of merit may be carried out for two opposing detectors if

required. Calculations are carried out for all required axial distances and then the results are printed out. They may also be plotted in graphical form.

If penetration effects are being considered, the program then calculates the second possible set of dimensions with $P = P_m$ and returns to the calculations of efficiency and figures of merit. Following these calculations, the focal length is increased and the procedures described above are repeated. When calculations have been carried out for the required values of focal length, the number of holes of the collimator is increased. If the penetration fraction is greater than the maximum tolerable level, collimators with greater numbers of holes are not considered as they will have even greater penetration. When the program has completed designs for the required range of values of n and f, it returns to the start and can be re-run with a new set of data. When it is used to calculate efficiencies and figures of merit for an existing collimator, it returns directly to this point when the calculations are complete.

4.2 The influence of collimator parameters on performance

The results obtained with this program were used to assess the effects of altering different collimator parameters,

while maintaining the relationships of equations (4.1), (4.3) and (4.5). All the collimators considered in this section have been designed for low energies, assuming that penetration is insignificant. The minimum possible septum thickness was 0.1 cm.

Influence of the number of holes

Figure 4.2 shows diagrams of three collimators designed for a 3½" diameter crystal with focal lengths of 9 cm. and a radius of the field of view in the focal plane of 2 cm. As the number of holes is increased, the collimator length can be decreased and this results in higher efficiency. The shorter collimators have larger shape factors however, and this means that there is a greater variation in resolution with distance.

The increase in axial efficiency in air obtained by increasing the number of holes is shown in fig. 4.3 for collimators with a focal length of 14 cm. The relative gain in maximum efficiency becomes smaller as the number of holes is increased, suggesting a limit to the possible gain which can be obtained by increasing the number of holes. Figure 4.4 shows the figures of merit for the same collimators assuming that the point source consists of Tc-99m and is

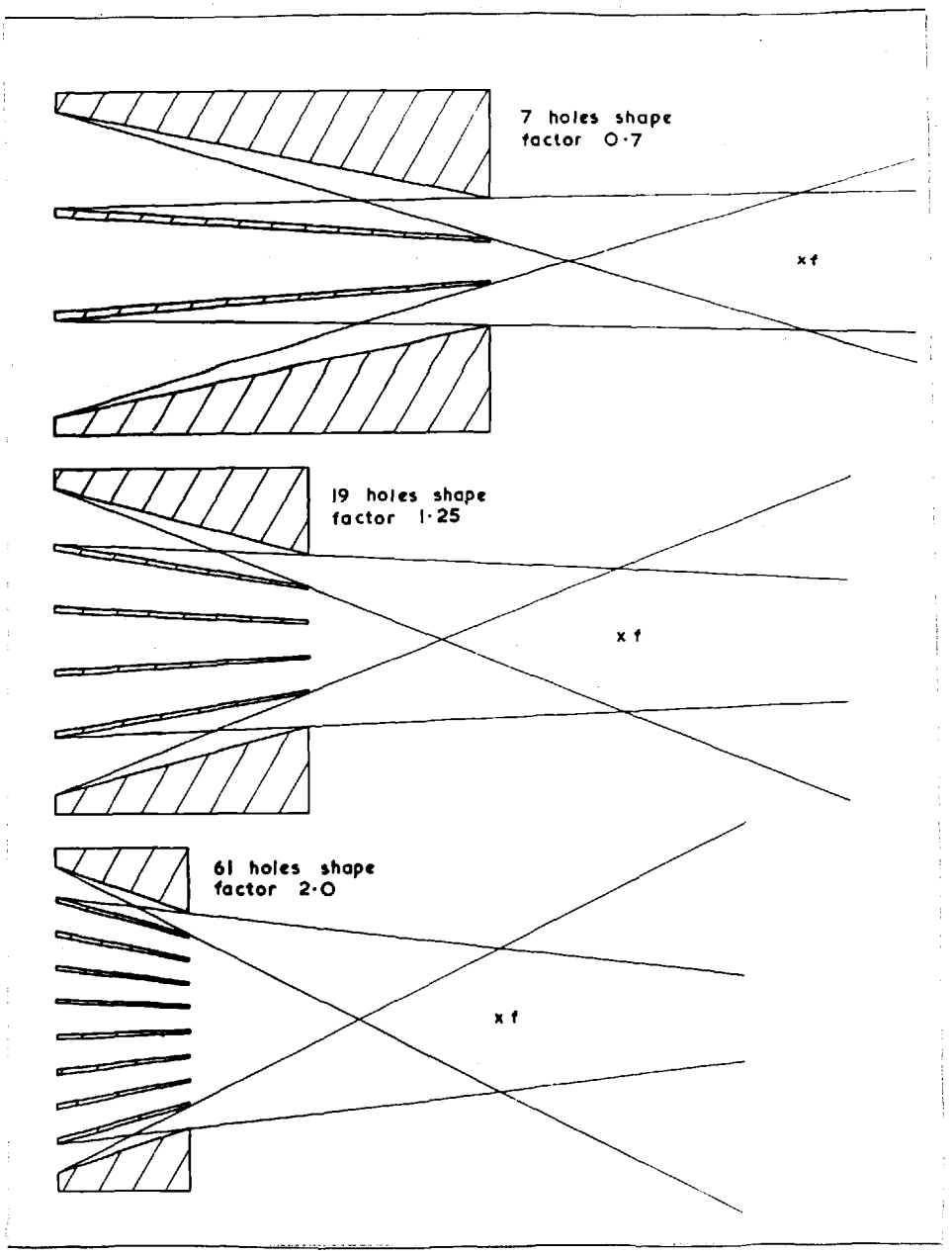

Fig. 4.2 Designs of collimators with focal lengths of 9 cm and radii of the field of view in the focal plane of 2 cm.

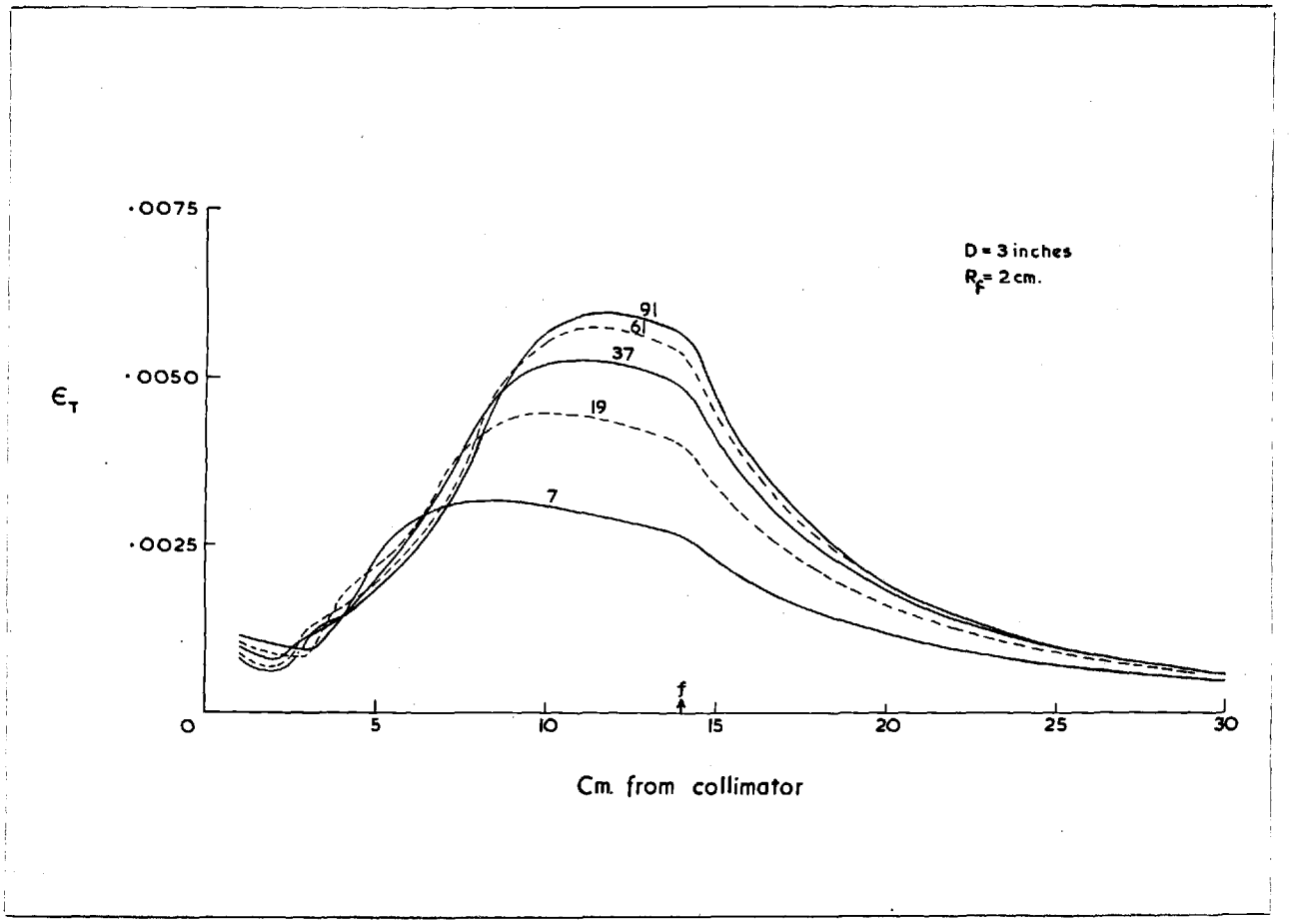

Fig. 4.3 The axial efficiencies in air of collimators with the same focal lengths and radii of the field of view in the focal plane, but with different numbers of holes.

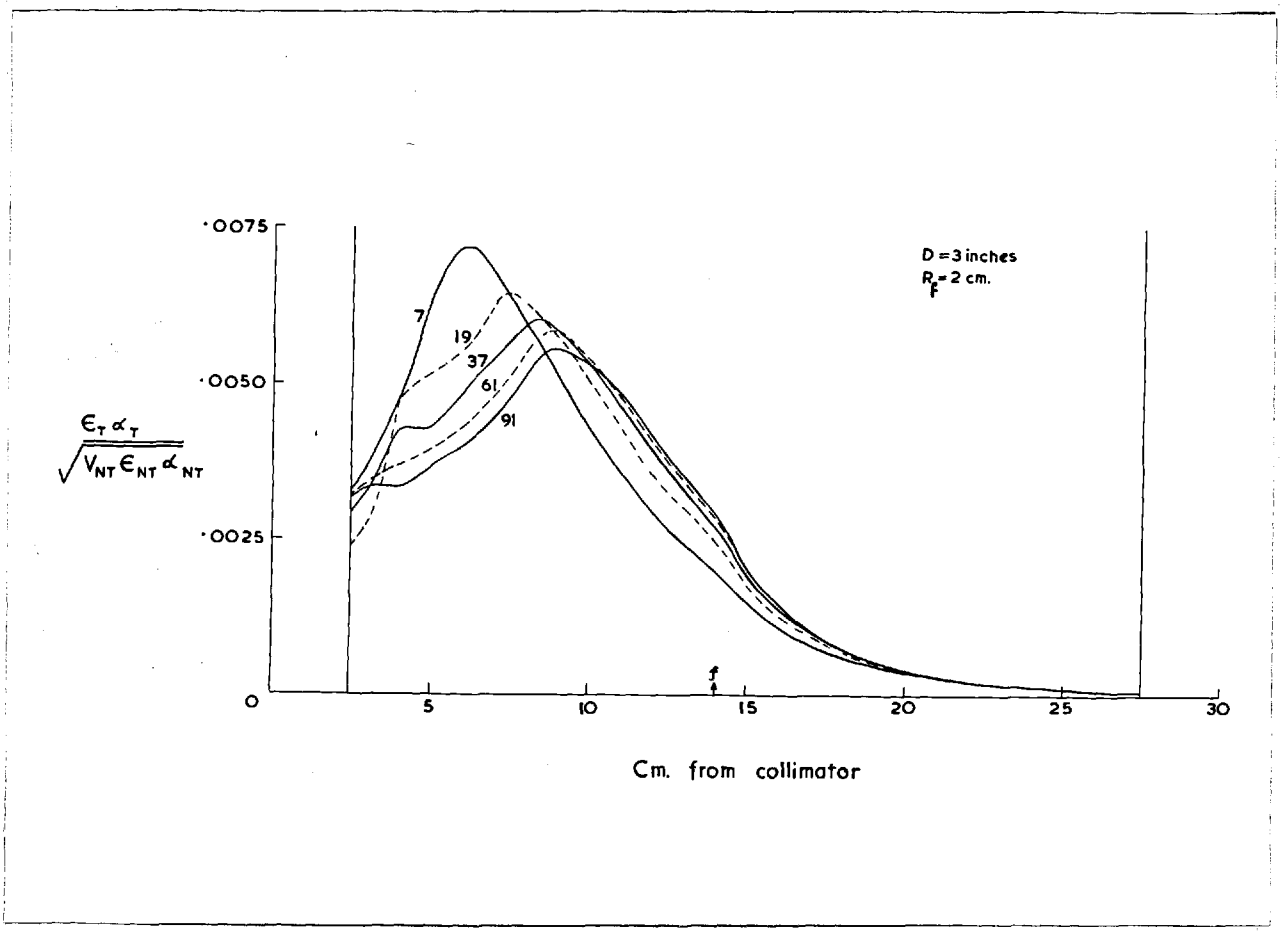

Fig. 4.4 The axial figures of merit for a point source of Tc-99m placed in a tank of water 25 cm wide at a distance 2.5 cm from the faces of the collimators of fig. 4.3.

placed in a tank of water, 25 cm wide, situated 2.5 cm from the end of the collimator. In this example, the figures of merit for small depths show a tendency to decrease as the number of holes is increased although they are similar at greater depths. In most cases the figures of merit of collimators with different numbers of holes are similar but sometimes an increase in figure of merit can be obtained by increasing the number of holes. The improvement is however accompanied by an increase in shape factor resulting in a wider variation in resolution. In this example the shape factor increased from 0.63 for the 7-hole collimator to 1.82 for the 91-hole collimator. Larger increases in shape factor are encountered with smaller resolutions or larger crystal diameters.

Influence of focal length

Figure 4.5 shows the axial efficiencies in air plotted against distance from the collimator face for collimators with different focal lengths. The collimator length increases as the focal length increases (equation 4.4) but the other parameters are constant. Increasing the focal length results in a large drop in efficiency at distances less than the focal length and only a relatively small increase in

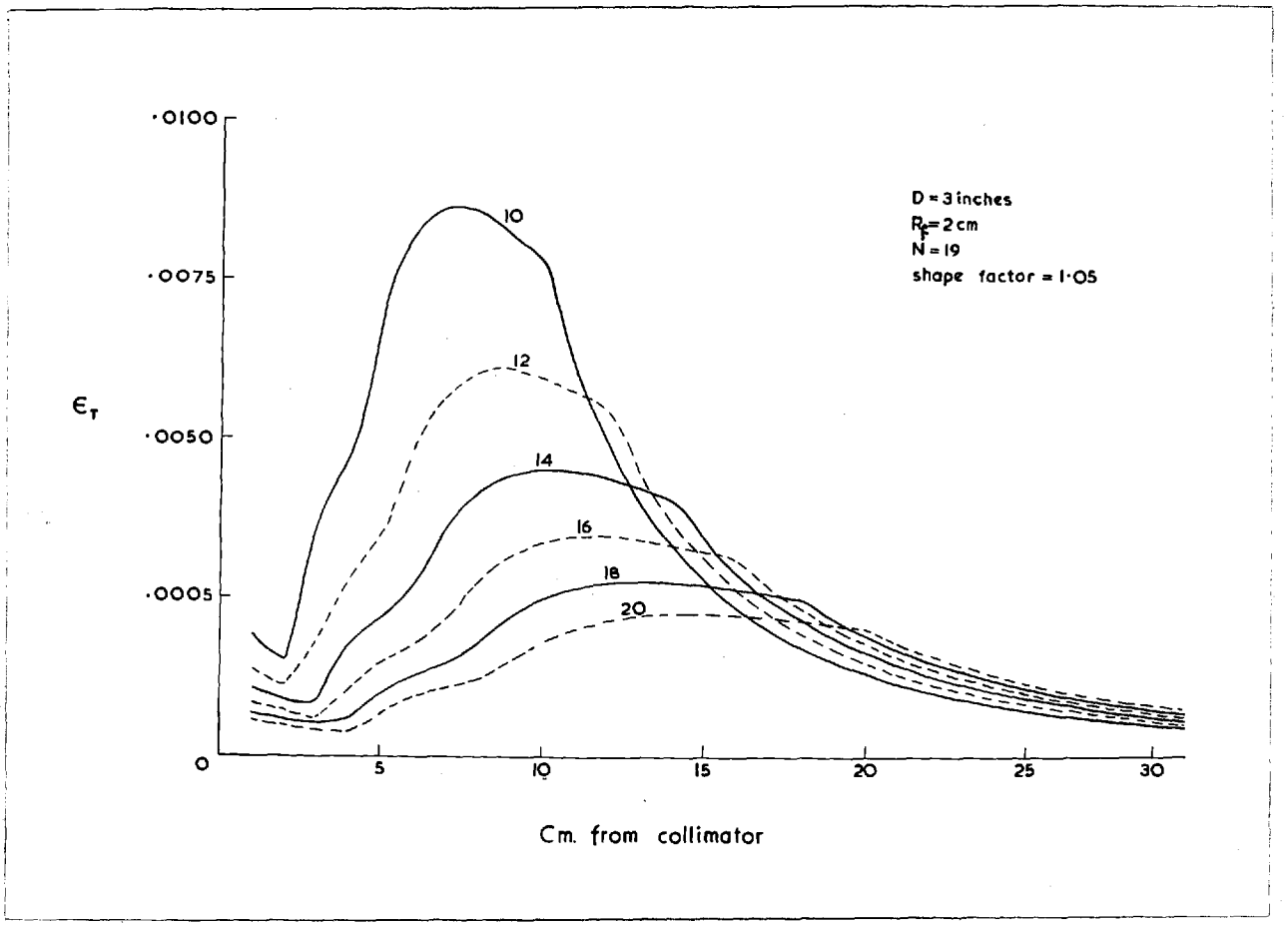

Fig. 4.5 The axial efficiencies in air of collimators with different focal lengths but the same radii of the field of view in the focal plane.

efficiency at greater distances. Figure 4.6 shows the axial figures of merit for the same collimators assuming the same isotope, air gap and phantom size as before. The differences between the figures of merit are similar to those between the efficiencies of different collimators. Only a small improvement appears to be gained at large distances by increasing the focal length and no significant advantage is gained in this example by increasing the focal length beyond about 16 cm. These curves illustrate one of the problems in collimator design; increasing the focal length may result in a three-fold loss in the probability of detection of superficial lesions while only producing a 50 per cent increase in the probability of mid-line lesions.

Influence of crystal diameter

Figure 4.7 shows the axial efficiencies in air plotted against distance from the collimator face for collimators designed for different diameter crystals. The collimator length varies between collimators but the other parameters are constant. As the crystal diameter is increased there is a large increase in efficiency, but at the same time there is a large increase in shape factor resulting in a wider variation in resolution. In this example the shape factor

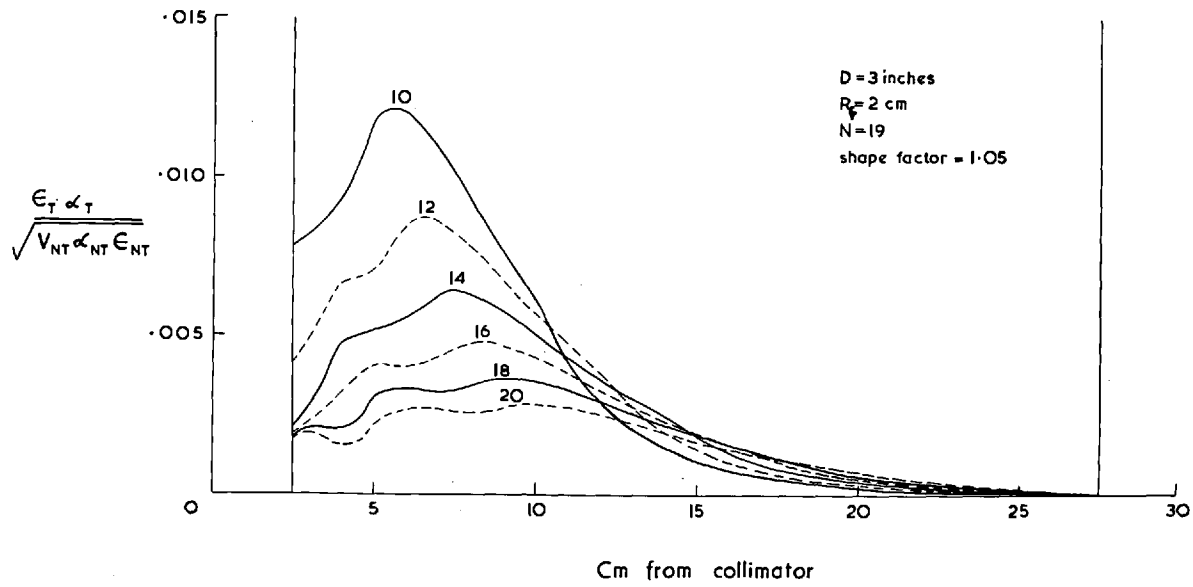

Fig. 4.6 The axial figures of merit for a point source of Tc-99m placed in a tank of water 25 cm wide at a distance 2.5 cm from the faces of the collimators of fig. 4.5.

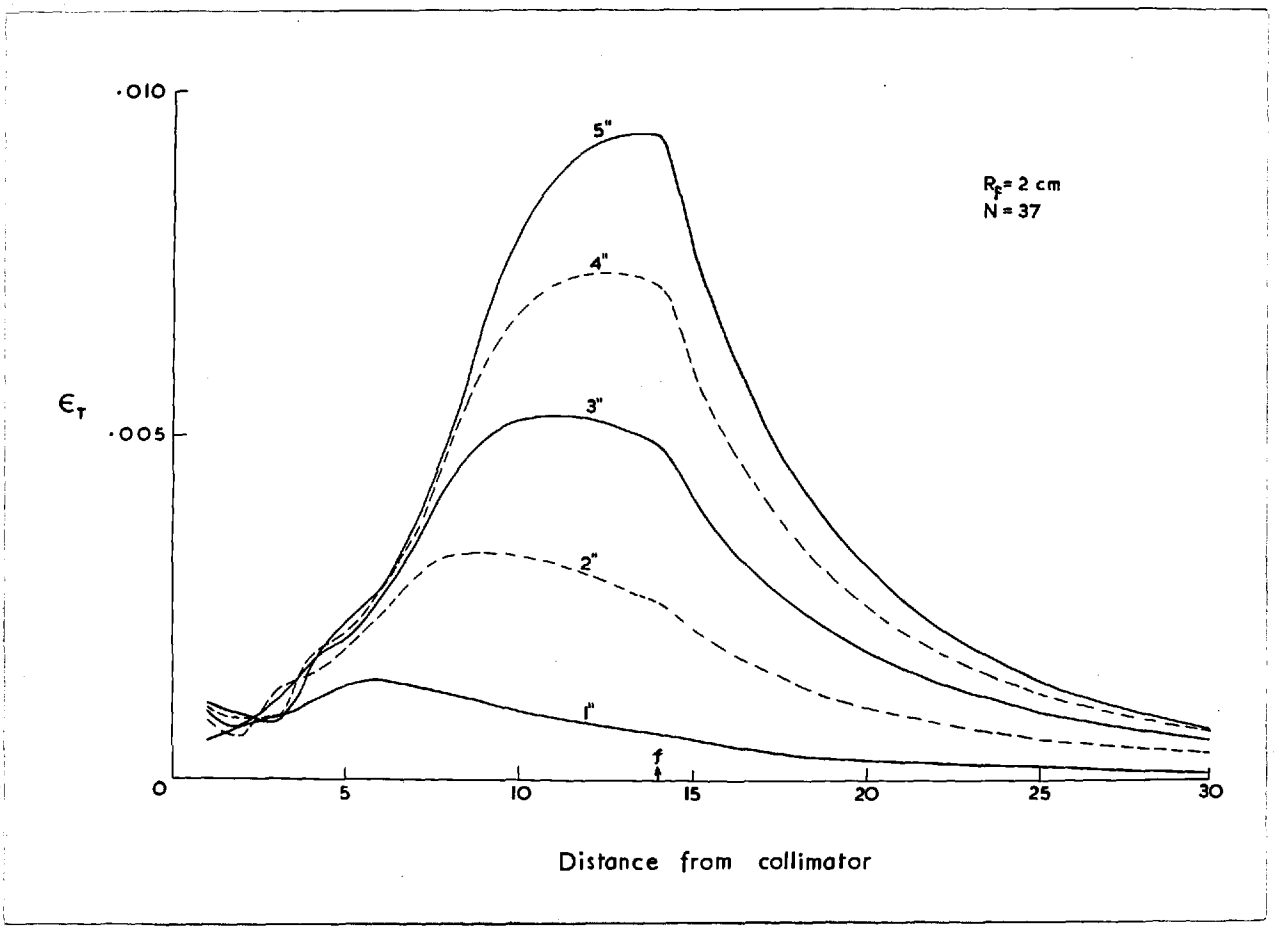

Fig. 4.7 The axial efficiencies in air of collimators designed for crystals of different diameters with the same focal lengths, radii of field of view in the focal plane, and numbers of holes.

increased from 0.26 for the 1" crystal to 2.51 for the 5" crystal. Figure 4.8 shows the axial figures of merit for the same collimators under the same conditions as before. At small depths, the figures of merit appear higher for the smaller than for the larger crystals. Some of the differences are however due to the different shape factors. The collimators for the smaller crystals have smaller shape factors and give the maximum point source efficiency closer to the collimator face. These maxima are less affected by attenuation and are therefore likely to be higher than those for larger crystals. A better comparison between collimators for different crystals is obtained from collimators with different numbers of holes, for which the shape factors are approximately the same. Figure 4.9 shows that a 7-hole collimator for a 3" crystal with a shape factor of 0.63 is slightly better than a 37-hole collimator for a 2" crystal with a shape factor of 0.79. Similarly, a 37-hole collimator for a 5" crystal with a shape factor of 2.51 is slightly better than a collimator for a 3" crystal with 91 holes and a shape factor of 1.82.

Influence of the radius of the field of view in the focal plane

Figure 4.10 shows point source efficiencies in air plotted against distance from the collimator for collimators

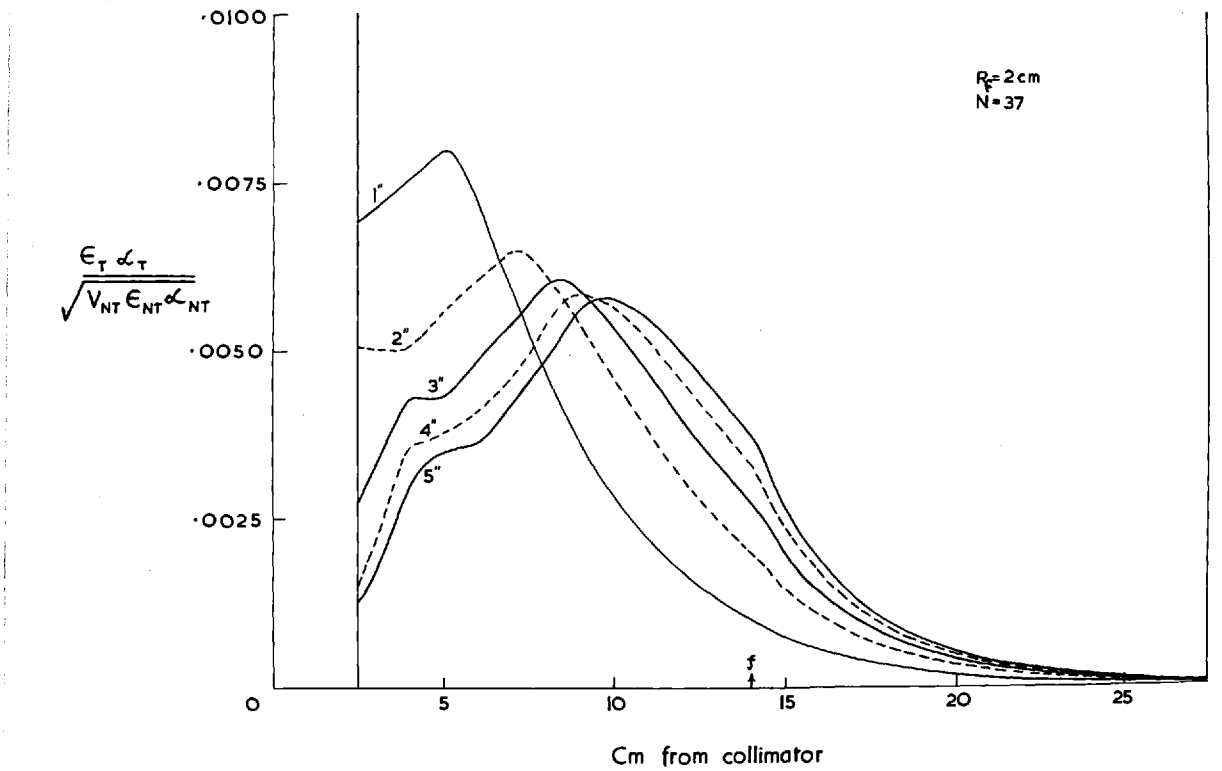

Fig. 4.8 The axial figures of merit for a point source of Tc-99m placed in a tank of water 25 cm wide at a distance 2.5 cm from the faces of the collimators of fig. 4.7.

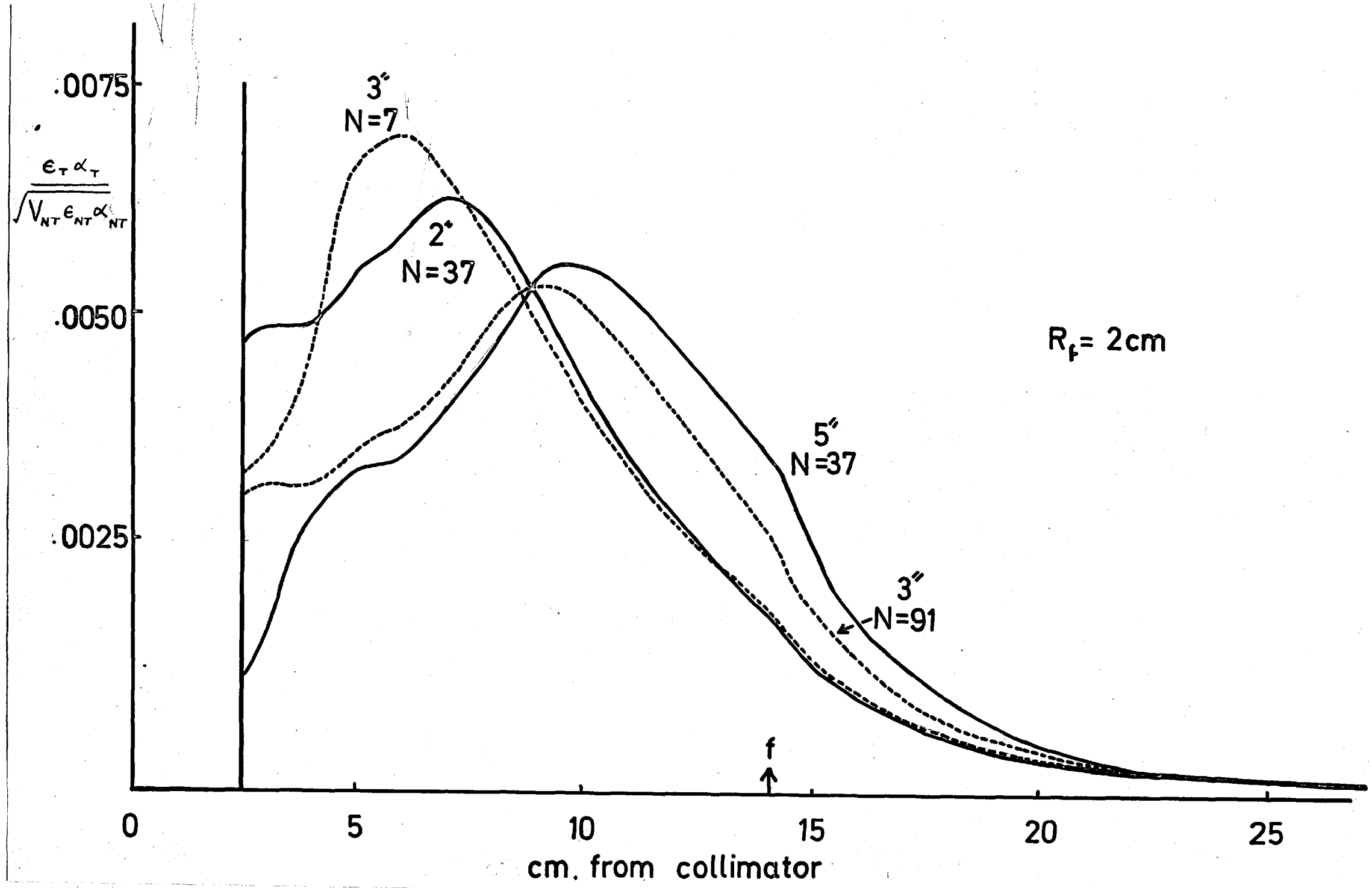

Fig. 4.9 The axial figures of merit of collimators for crystals of different diameters with the same focal lengths and radii of the field of view in the focal plane, but with different numbers of holes so that the shape factors are similar. The isotope, air gap and phantom size are as in fig. 4.8.

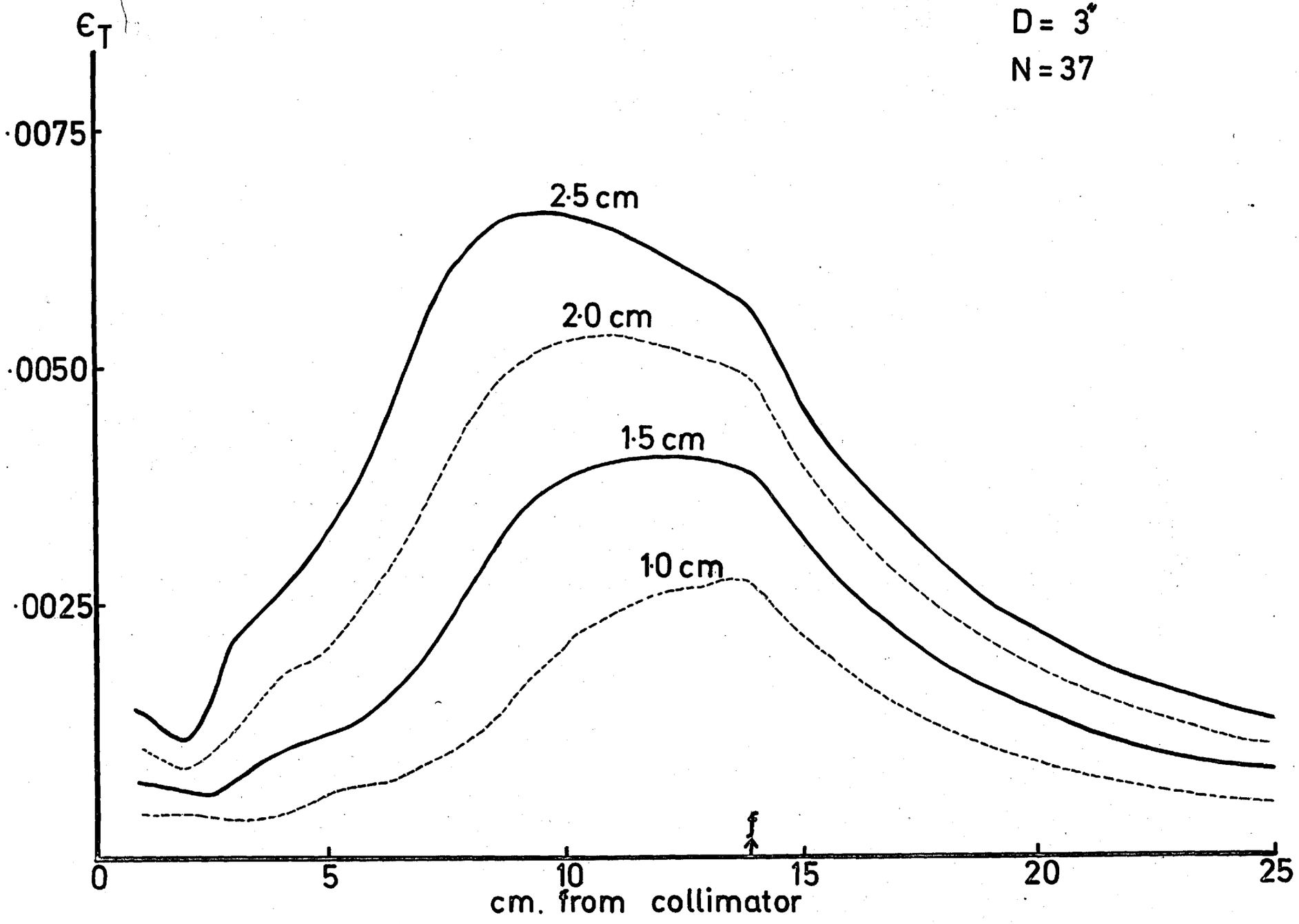

Fig. 4.10 The axial efficiencies in air of collimators with the same focal lengths and numbers of holes, but with different radii of the field of view in the focal plane.

with different values of the radius of the field of view in the focal plane. The collimator length varies between collimators but the other parameters are constant. As the radius of the field of view is increased, there is an increase in the collimator efficiency and a decrease in the shape factor from 3.2 when R_f = 1.0 cm to 0.8 when R_f = 2.5 cm in this example. Values of the collimator figures of merit cannot be used directly to compare collimators under these conditions. Equation (2.5) shows that the probability for detection of a lesion is proportional to the square root of the time in which counts accumulate. The time in which counts accumulate is determined by the time for which a point source lies within the field of view, and for the same scan speed and line spacing it is proportional to the area of the field of view. The probability for detection of a lesion is therefore proportional to the radius of the field of view. An estimate of the way in which collimators of different resolutions compare can thus be obtained by multiplying the collimator figures of merit by R_f. This method of comparison is only strictly correct in the focal plane; in other planes, the figures of merit should be multiplied by the radius of field of view in that plane rather than R_f.

In this example, the collimator figures of merit are similar and therefore the probabilities for detection of lesions are approximately proportional to the values of R_f.

4.3 Effects of alterations in practical conditions

Comparison of single and double-headed detector systems

Scanning systems which utilise detectors on each side of the body are now available commercially. Figure 4.11 shows the collimator figures of merit plotted against distance for a double-headed system equipped with two collimators of focal length 16 cm. The point source is assumed to be Tc-99m, situated in a tank of water 20 cm wide, placed at 2.5 cm from the faces of each collimator. The figures of merit for single headed systems with collimators of 16 and 20 cm focal length are also shown. Two detectors give the most uniform probability of detection throughout the body, but a single detector with the same collimator gives a higher probability for detection close to the body surface. Increasing the focal length of the collimator for the single detector decreases the probability of detection at most distances, although a small increase is obtained at

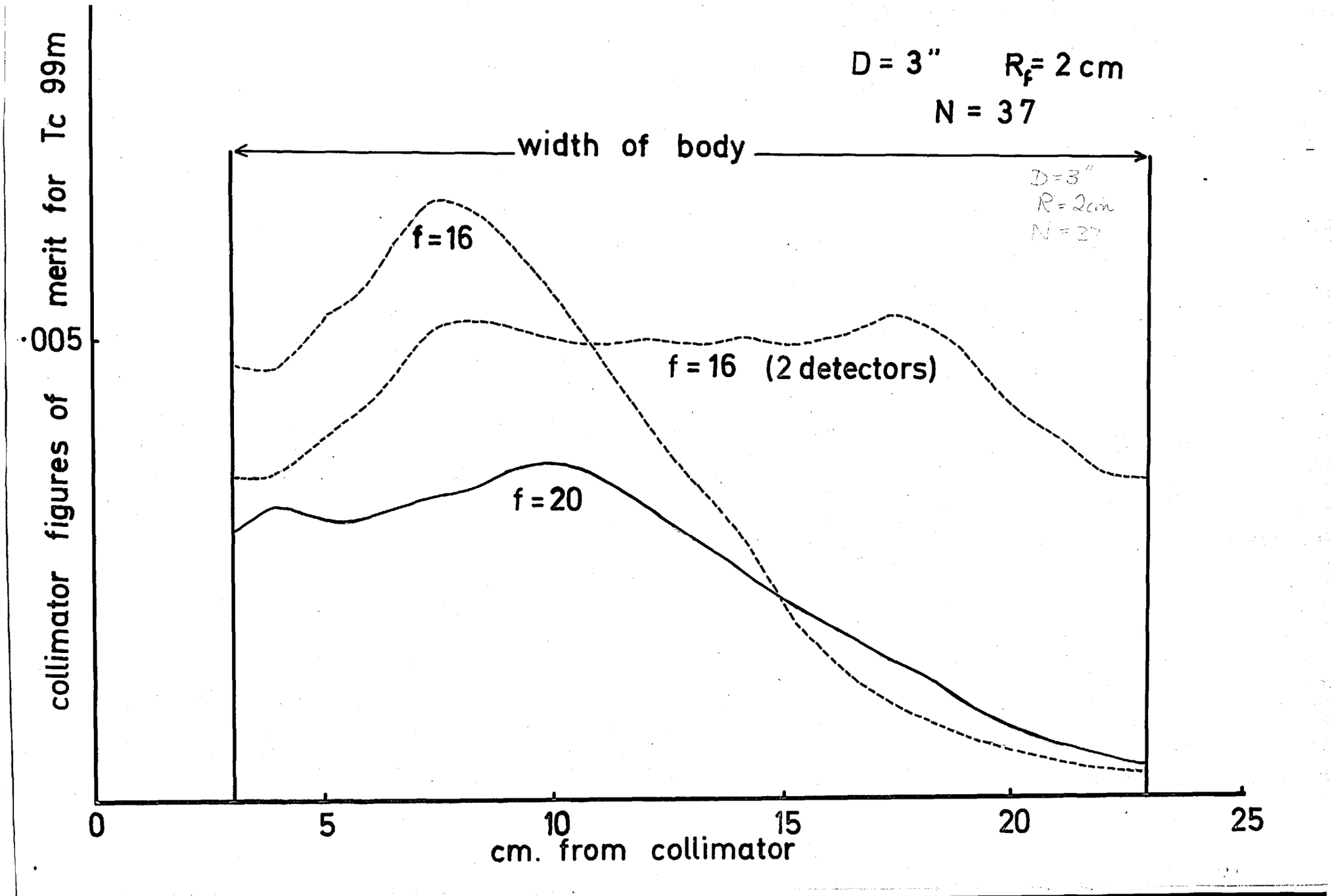

Fig. 4.11 The axial figures of merit for a point source of Tc-99m placed in a tank of water 20 cm wide with air gaps of 3 cm. Curves are shown for a double headed system with collimators with focal lengths 16 cm and for a single detector with collimators of focal lengths 16 and 20 cm.

large distances from the collimator.

Influence of air gap and phantom size

Figure 4.12 shows the influence of alterations in air gap size for a single detector. The axial efficiencies for a point source of Tc-99m in a 20 cm tank are plotted against distance from the edge of the phantom closest to the collimator. As the size of the air gap is increased, the efficiencies and probabilities for detection are increased for superficial lesions but decreased for deeply-lying lesions. There is also a greater variation in efficiency through the body. Figure 4.13 shows the influence of alterations in air gap size for a double-headed system. In this example, increasing the air gaps from 0 to 2 cm leads to a general increase in efficiency. Increasing the air gaps from 2 to 4 cm leads to a drop in efficiency at the centre of the plantom but an increase in efficiency at the edges. Further increases in air gap size lead to greater changes of this kind. For any two collimators, the shape of these curves depends on the size of the phantom as well as the sizes of the air gaps. The air gap for this 20 cm phantom which gives the highest efficiency is approximately 3 cm., giving a collimator separation of 26 cm. Similar sets of curves were drawn for

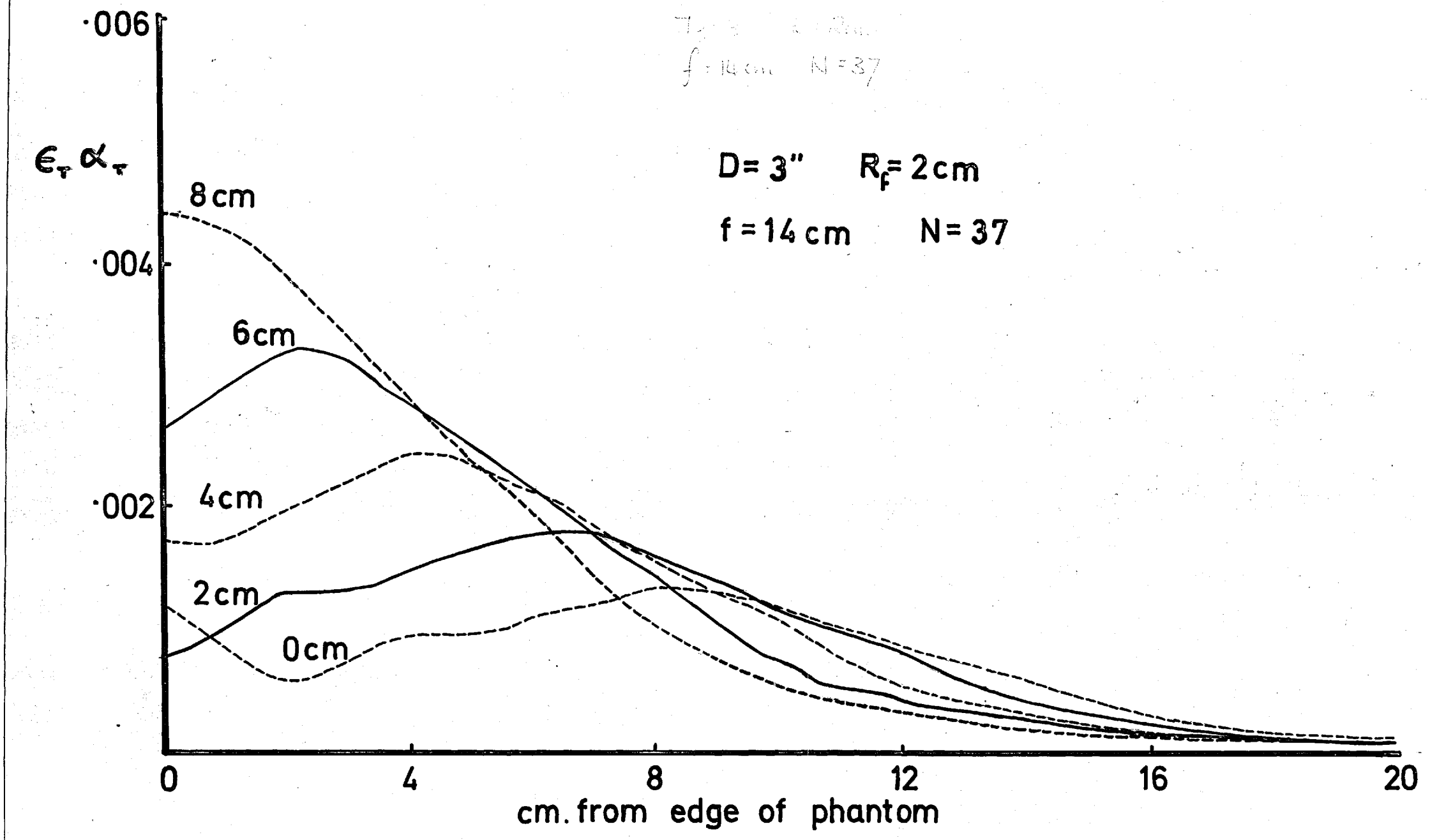

D= 3" R_f= 2cm

f = 14 cm N= 37

Fig. 4.12 The axial officiencies for a point source of Tc-99m in a water medium, 20 cm wide, for one collimator with different air gaps.

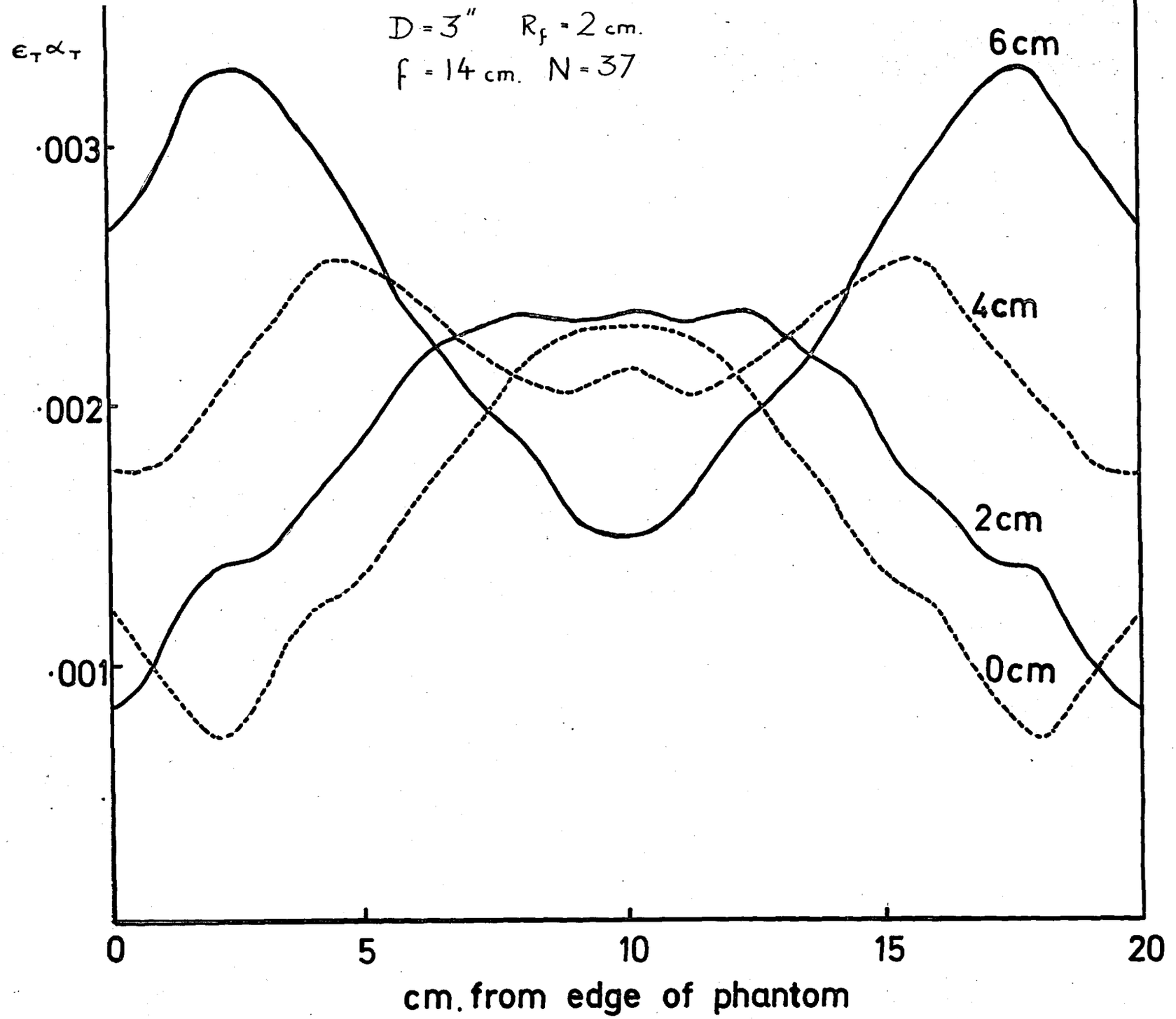

Fig. 4.13 The axial efficiencies for a point source of Tc-99m in a water medium, 20 cm wide, for a double headed system with the same collimators but with different air gaps.

phantoms of 10, 15 and 25 cm width and it was found that the highest values of efficiency were always obtained when the separation of the detectors was maintained at 26 cm.

4.4 Examples of collimator designs

The way in which a collimator is chosen from the many possible designs is illustrated in the following examples. For the design of a collimator for thyroid scanning using I-131 and a single detector, it was assumed that the neck thickness was 13 cm and that an air gap of 8 cm was required to allow for protrusion of the chin. The possible range of positions of the thyroid was assumed to be from 2 to 6 cm from the neck surface as denoted by the shaded region in fig. 4.14. The collimators with focal lengths of 11 cm lead to a wide variation of efficiency and probability for detection throughout the range of possible thyroid positions. The collimators of focal length 13 cm lead to a more uniform variation in efficiency, and of these the 37-hole collimator gives the highest probability of detection. Although this 37-hole collimator has a shape factor of 6.68, reference to fig. 3.3 shows that the resolution varies relatively little over the possible range of thyroid positions.

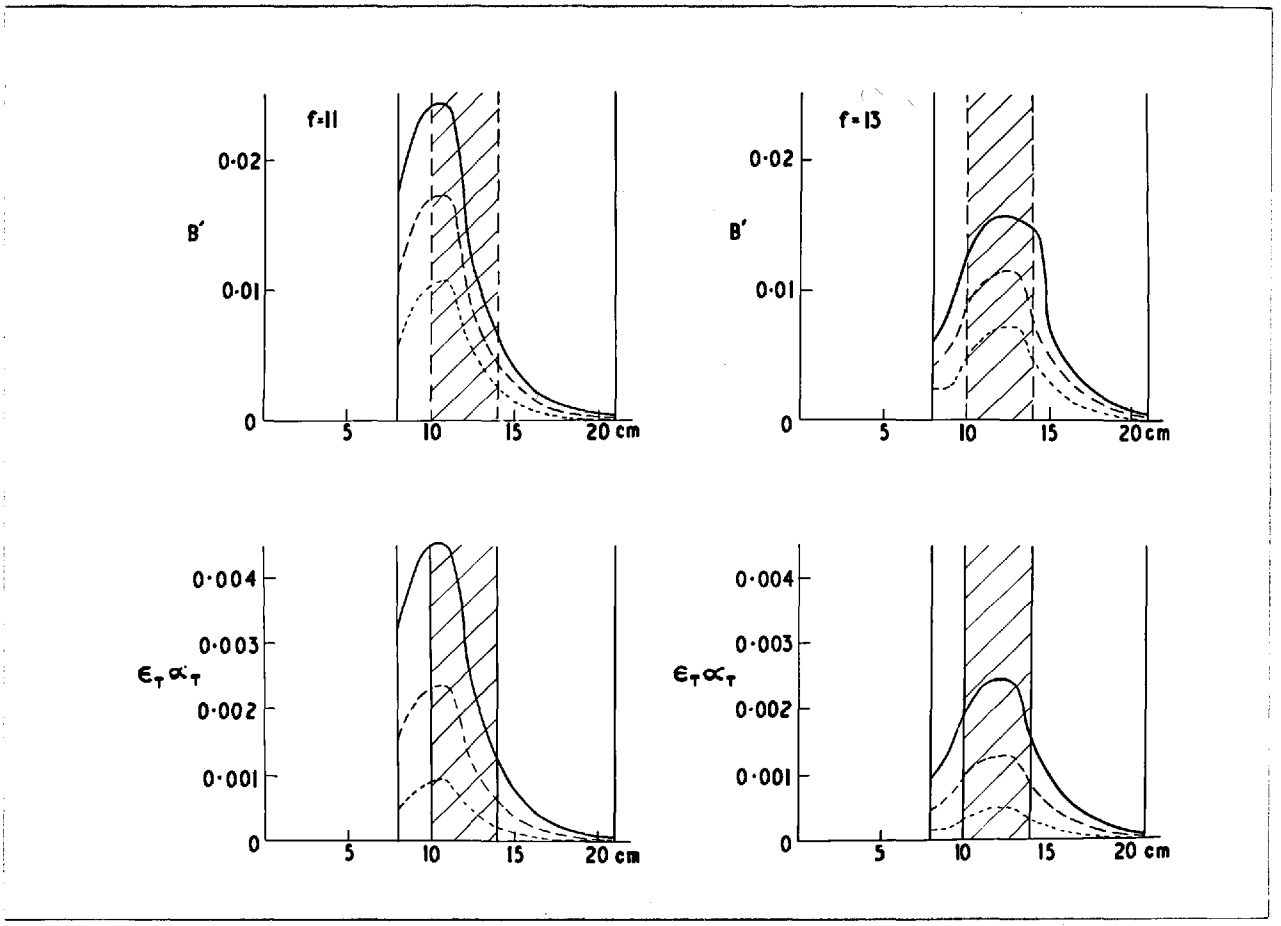

Fig. 4.14 Designs of possible collimators for thyroid scanning with I-131 using a single detector. Figures of merit and efficiencies are shown for 37, 19 and 7-hole collimators in order of decreasing height.

Collimators with greater numbers of holes had high penetration fractions and were therefore unsuitable.

Collimators for other applications of a single detector can be chosen in a similar manner. For scanning of large organs, such as the liver, the choice of collimator is usually difficult to make. A compromise between an order of magnitude drop in efficiency close to the surface and perhaps a 20 or 50 per cent increase in efficiency for deeply lying regions must often be made.

The choice of collimator for a double-headed system is illustrated in fig. 4.15 for Hg-197 for brain scanning. It has been assumed that the width of the head is 15 cm and that air gaps of 4 cm are required. Collimators with focal lengths of 9 cm are poor because the figure of merit falls to a low value at the centre of the phantom. Collimators with focal lengths of 13 cm give the most uniform variation of figure of merit but in general the values are about 20 per cent lower than those of focal lengths of 11 cm. Curves for collimators with focal lengths of 11 cm and different numbers of holes are all similar, and the collimator with the optimum shape factor can therefore be chosen.

Collimators designed for one scanning application are

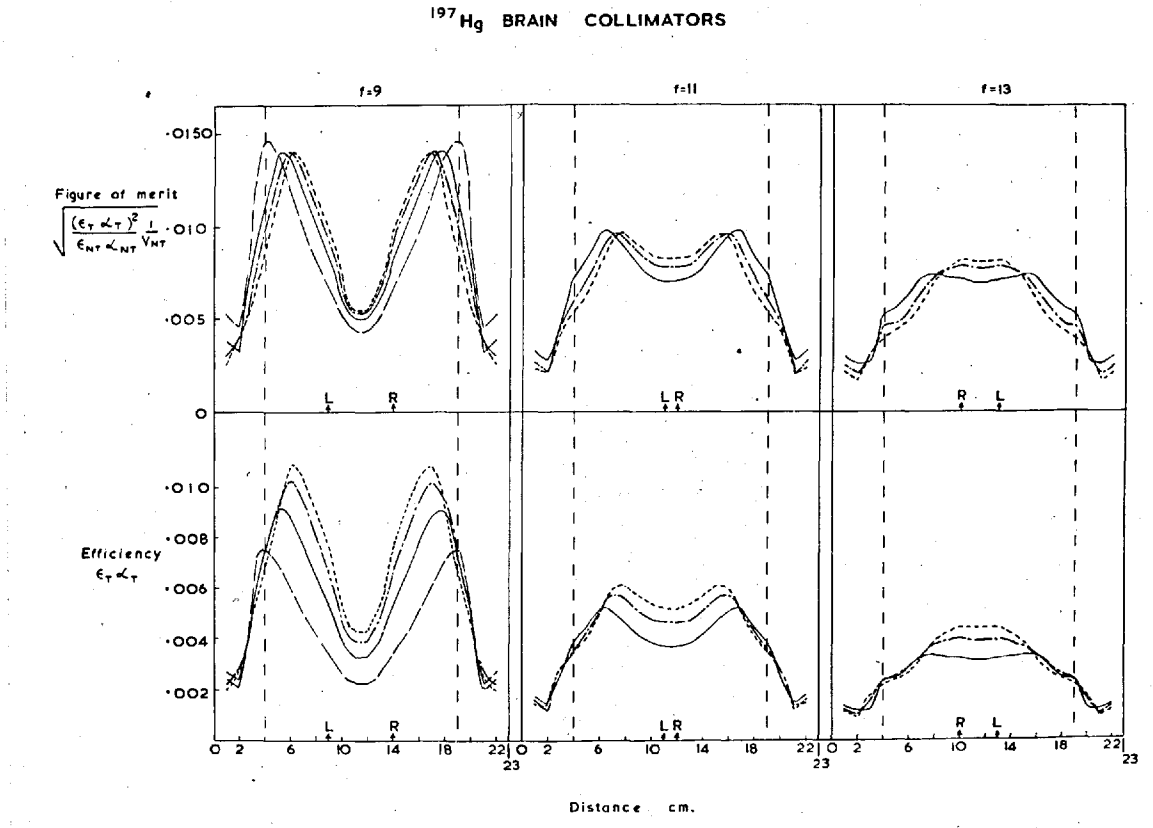

Fig. 4.15 Designs of possible collimators for brain scanning with Hg-197 using a double detector system. Figures of merit and efficiencies are shown for 61, 37, 19 and 7-hole collimators in order of decreasing efficiency when f = 9 cm.

in general not the most suitable for other applications, even using the same isotope, because of variations in body, organ and air gap size. Different collimators are also required for different gamma-ray energies. Some suggested collimators for a single 5" detector are given in Table 4.1. In order to obtain small shape factors for collimators for scanning of large organs, a small number of large holes is necessary. These collimators are long and limit septum penetration well. Therefore collimators designed for low energies may often be used for much higher energies as illustrated here. In some cases, collimators designed for low energies with small shape factors are so long that their weight makes them impracticable. Increasing the number of holes results in a shorter length and less weight, but may lead to an unacceptably high shape factor. Maintaining the same number of holes, but decreasing the collimator length, and increasing the septum thickness in order to maintain the same radius of field of view in the focal plane, may result in a smaller increase in shape factor. This is equivalent to designing the collimator for a higher energy.

Figure (4.16) shows figures of merit and attenuated efficiencies for collimators for single and double headed

Table 4.1

Suggested collimator designs for a 5" diameter crystal for round holes in a hexagonal array (dimensions in cm)

	Radius of field of view in focal plane	Focal length	No. of holes	Collimator length	Crystal face		Shape factor	Suggested γ-ray energies keV	Suggested Uses	Setting up conditions
					hole radius	septum thickness				
1	1	13	37	16.13	.620	.669	6.68	< 360	I-131 for thyroid	External collimator face 8 cm from body surface over thyroid
2	1	13	91	13.11	.504	.161	8.32	< 290	Tc-99m for thyroid	as above
3	2	9.5	19	11.4	1.20	.176	1.73	< 350	Hg-197, Tc-99m and Hg-203 for lateral brain	External collimator face 10.5 cm from mid-line of head
4	2	14	19	16.79	1.20	.176	1.73	< 420	Au-198, I-131, Cr-51, Hg-203, Tc-99m and Hg-197 for spleen, liver, kidneys and AP brain	External collimator face 15.5 cm from mid-line of body or head.

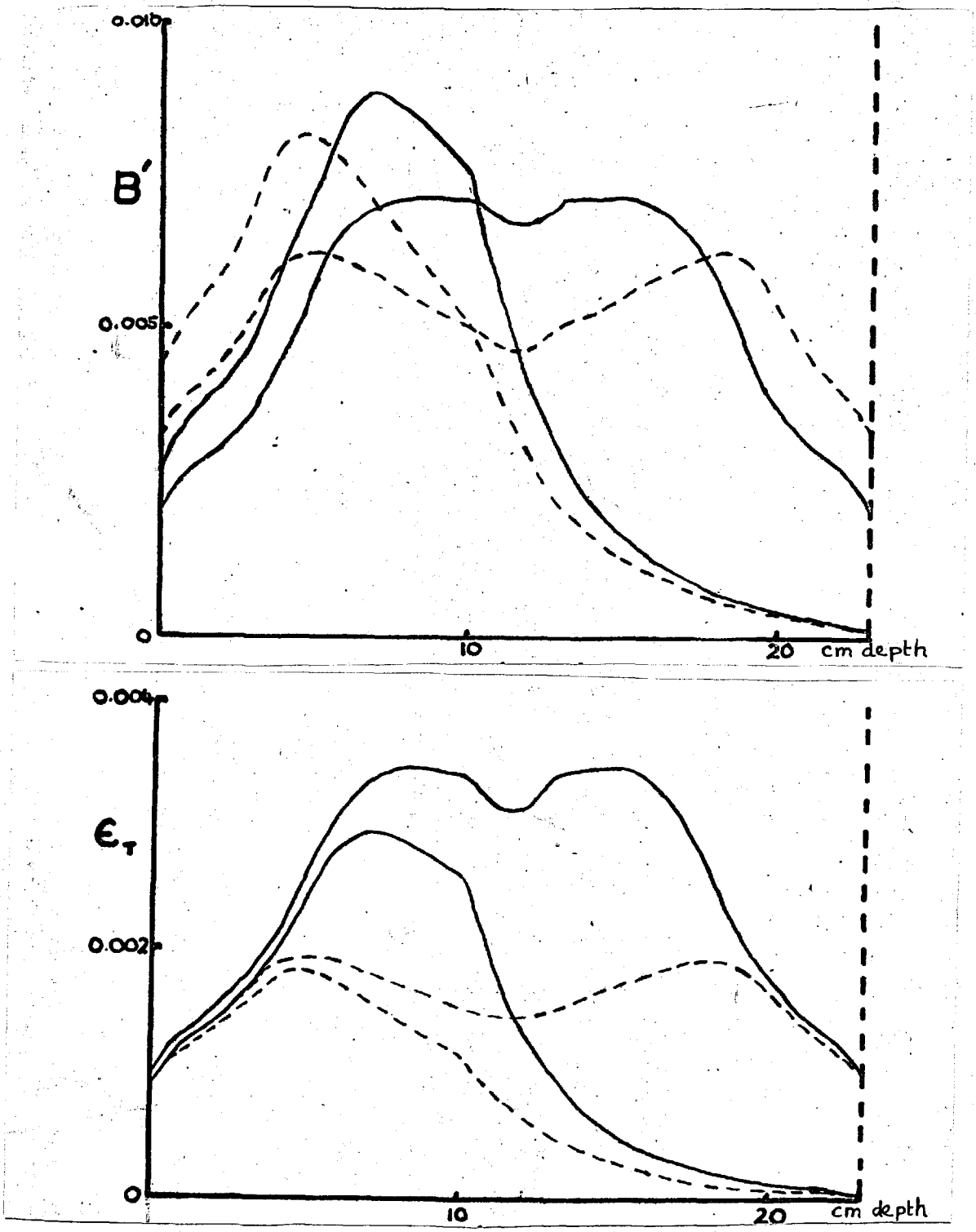

Fig. 4.16 Figures of merit and axial point source efficiencies for the most suitable collimators for detection of regions of increased or decreased concentration in a phantom 23 cm wide with air gaps of 4 cm. The solid curves are for single and double headed detector systems with 5" crystals and the dashed curves are for systems with 3" crystals. The dimensions of the collimators are given in Table 4.2.

detector system with 3" and 5" crystals. These collimators were selected as the optima from the ranges of possible designs for scanning a large organ such as the liver using In-113m. The same focal length was found most suitable for both single and double headed detector systems and for both 3" and 5" crystals. The dimensions of the collimators are given in Table 4.2. The shape factor of the collimators for the 5" crystals are rather large but it could not be reduced without a considerable reduction in efficiency and figure of merit. Although efficiencies for the 5" crystals are significantly higher than those for the 3" crystals, the differences between figures of merit are less pronounced. Up to the centre of the phantom, the single 5" detector gives a higher probability of detection than the double 3" crystal detector system although it has a wider variation in resolution. Single 5" crystal systems may on the whole be fractionally better for detection than single 3" systems and, similarly, double 5" systems may be better than double 3" systems. The 3" crystal systems are however superior for the detection of superficial lesions. Although 5" crystal systems have higher efficiencies they have the disadvantage of a wider variation in resolution. Similar results were obtained for collimators designed for scanning

Table 4.2

Dimensions of the most suitable collimators for detection of regions of increased or decreased concentration of In-113m in a 23 cm wide phantom (air gap 4 cm) using 3" and 5" diameter crystals and single or double headed detector systems

Dimensions are in cm. unless otherwise stated.

Crystal diameter inches	Radius of field of view in focal plane	Number of holes	Focal length	Collimator length	Crystal face		Shape factor	Penetration fraction
					Hole radius	Septum thickness		
3	1.5	19	14	13.1	0.704	0.139	1.42	0.019
5	1.5	37	14	15.7	0.844	0.148	3.30	0.022

the same phantom with Tc-99m.

4.5 Summary and discussion

The design procedure described here differs from the two methods suggested by Beck (1964b). In the first, s, f, R_f and D are specified and in the second, R_f, f, s and K are specified. The collimator with the highest plane source efficiency is then found. It also differs from that of Matthews (1967) in which the shape factor is specified and the collimator with the highest point source efficiency at the focus is found.

The results presented here show that the efficiency does not necessarily reflect the probability of detection which is proportional to the collimator figure of merit. Figures of merit have been calculated for point sources representing very small lesions, which are the most difficult to detect. When the diameter of the lesion is comparable to the diameter of the field of view of the collimator the point source figure of merit is probably still applicable. Assuming that the lesion is spherical and of uniform concentration, when seen from above through a layer of tissue the greatest increase or decrease in counts occurs opposite the centre of the lesion where it is of greatest thickness.

Therefore the highest probability of detection is obtained using a collimator with a high figure of merit for axial points. When the diameter of the lesion is much greater than the diameter of the field of view a plane source figure of merit may be more applicable. The plane source figure of merit is proportional to the plane source efficiency and therefore under these circumstances a high efficiency is required rather than a high point source figure of merit. The plane source efficiency depends on the axial point source efficiency and the shape of the resolution curve and therefore the plane source efficiencies of collimators with similar resolution can be compared using the point source efficiency. However, the variation of axial point source efficiency with distance does not reflect the probability of detection of large lesions because as the efficiency decreases the resolution tends to increase. Thus the plane source efficiency in air is approximately independent of depth. The probability of detection of large lesions therefore decreases with increase in depth owing to attenuation in tissue.

It has been assumed that the collimator with the highest point source efficiency for specified values of D, R_f, f and n is that with the smallest septum thickness.

This can be shown from the approximate expression for the efficiency of a point source at the focus :

$$\epsilon_T = \frac{N r^2}{4 (t+f)^2}$$

Substituting for r and t from equations (4.1), (4.3) and (4.4) :

$$\epsilon_T = \frac{NR^2}{4f^2} \quad \frac{[D-s'(n-1)]^2}{(nR_f + D)}$$

which is a maximum when s' is a minimum. The collimator figure of merit at the focus is proportional to the point source efficiency divided by the square root of the plane source efficiency (equation 3.10). Therefore,

$$B' \propto \frac{N}{2f\sqrt{\pi}} \quad \frac{[D-s'(n-1)]}{(nR_f + D)}$$

which is also a maximum when s' is a minimum. Thus the assumption is valid.

The importance of considering figures of merit as well as efficiencies has been emphasised in these results. In many cases an increase in point source efficiency is

accompanied by an increase in plane source efficiency and therefore the probability for detection is not necessarily increased. The effect on efficiency of increases in focal length has been discussed by Popovic and Fowler (1968). However, calculations of figures of merit show that there is a limiting focal length, beyond which further increases only result in a loss in detection probability.

Results on the effects of increase in crystal diameter confirm the theoretical calculations of Matthews (1967) that only a small improvement in detection is obtained by such an increase when the shape factor is kept small so that a reasonably uniform resolution is obtained. The efficiencies do however increase with increase in crystal diameter (Popovic and Fowler, 1968).

The relative merits of single and double headed detector systems have been discussed by Kibby (Appendix 3). Comparing the same detectors and collimators, a double-headed system gives a more uniform probability for detection throughout the body, although a single detector gives a higher probability for the detection of superficial lesions. This is because, for the double-headed system, the detector furthest from the source contributes only a little to the target counting rate, while doubling the non-target counting

rate. It is suggested that where a double-headed system is in use, the best results would be obtained by recording scans on paper or magnetic tape and playing back each response separately for the detection of superficial lesions. The combined response could then be played back for the detection of mid-line lesions. The results of subtracting the two responses could also be investigated.

Popovic and Fowler (1968) have discussed the effects of alterations in air gap size. These results have further shown that where a double-headed system is in use, the best results are obtained when the distance apart of the collimators is kept constant.

The results of alterations in the collimator parameters and practical conditions have been obtained with collimators designed for low energies, but it is reasonable to assume that they can be applied to collimators designed for higher energies provided the penetration is small. Calculations of figures of merit have been carried out for specified phantom sizes but alterations in phantom size are unlikely to affect these conclusions.

CHAPTER 5

A COMPARISON BETWEEN THEORETICAL AND EXPERIMENTAL VALUES OF POINT SOURCE EFFICIENCIES IN AIR

5.1 Introduction and experimental method

Experimental measurements were carried out in order to determine how accurately the theoretical calculations discussed above describe the response of a collimator to a point source in air. Preliminary measurements of the efficiencies of a 3" x 1" sodium iodide crystal were carried out as data were not available for this size of crystal.

Apparatus

The detecting system consisted of two 3" diameter by 1" thick sodium iodide crystals, each coupled to photomultiplier tubes, the outputs from which were fed to valve amplifiers. The amplifiers could be connected either to single channel amplifiers and thence to a scaling unit, or to a 512-channel analyser.

Four collimators suitable for low energy radiation were used with each crystal. They were designed to focus at 4" from the collimator face, with shape factors of

approximately one, and with different radii of the field of view in the focal plane. The collimators were cast in lead and their finished dimensions, which differed slightly from the design specifications, are given in Table 5.1.

The first value given for the focal length corresponds to that of the axial hole and was calculated from the equation:

$$f = \frac{t\,r'}{r - r'} \qquad (5.1)$$

The second value corresponds to that of the surrounding holes, calculated from the equation:

$$f = \frac{t\,(2r' + s')}{(2r+s) - (2r'+s')} \qquad (5.2)$$

The radii of the field of view in the focal plane were calculated from each focal length using the equation:

$$R_f = \frac{2rf}{t} \qquad (5.3)$$

The differences between the values of focal length and radius of field of view are small except for the 61-hole collimator which was particularly difficult to construct.

Each collimator incorporated a thickness of lead

Table 5.1

Collimator dimensions in cm., average values of measurements on both collimators

Number of holes	Collimator length	Crystal face		External face		Focal length	Radius of field of view in focal plane	Shape Factor
		Hole radius	Septum Thickness	Hole radius	Septum Thickness			
7	20.0	1.17	0.36	0.41	0.06	10.5 9.5	1.24 1.13	0.94
19	7.39	0.71	0.14	0.40	0.08	9.7 9.8	1.86 1.88	1.14
37	3.74	0.47	0.17	0.34	0.12	10.0 10.0	2.52 2.54	1.01
61	2.59	0.36	0.15	0.27	0.16	8.6 11.4	2.38 3.14	1.26

surrounding the holes, the minimum thickness being 3/4" at the crystal face. Each crystal was encased in 1/2" lead shielding in cylindrical form which also maintained the collimator in place. The length of the cylinder which protruded beyond the crystal could be adjusted to fit the collimator length. Extra lead was used to shield the crystal and could be slipped onto the outside of the cylinder. This external shielding was sufficient to reduce the effects of penetration to a negligible level at the energies used.

Sources

The point sources used for the measurements were made from perspex or glass and contained a cylindrical cavity which was filled with a radioactive solution. The cavity was approximately 0.4 cm in length and 0.4 cm in diameter.

The radioactive isotopes used were Hg-197, Tc-99m and Hg-203 (Table 5.2). The point sources were assayed for radioactivity by placing them in a ring of six Geiger tubes calibrated against an NPL ion chamber (Dale, Perry and Pulfer, 1961; Dale, 1961). The NPL ion chamber was calibrated for Tc-99m and Hg-203 using sources of known strength obtained from the NPL. The calibration factor for Hg-197 was obtained from measurements described in section 5.2. These factors (Table 5.2) agree with those of other workers

Table 5.2

Radioactive isotopes used for experimental measurements, with ion chamber calibration factors. The two photopeaks corresponding to the principle gamma-ray energies for Hg-197 could not be resolved with the detectors used. The maximum of the combined photopeak was therefore assumed to correspond to 71 keV.

Isotope	Decay Process	Principle gamma-ray energies keV	Fraction of disintegrations	Ion chamber calibration μμA/μCi (without brass filter)	
				Present work	Williams and Birdseye (1967)
Hg-197	Electron capture	77 69 (Au X-rays)	0.193 0.745	13.0	-
Tc-99m	Isomeric transition	140	0.901	9.7	9.6
Hg-203	β^- emission	279	0.815	10.8	10.8

within the limits of differences between chambers at these energies.

Measurements

Axial point source efficiencies were measured by determining the counting rate for a point source of known activity at different distances along the collimator axis. Measurements were also made with the source at different distances off the axis. For these readings, the amplifier was connected to a single channel analyser set to include the whole photopeak. The spectra of detectable radiation were measured for some source positions by connecting the amplifier to the 512-channel analyser. Approximately 100 channels of the analyser were used. Readings were taken with the 19, 37 and 61-hole collimators using all three isotopes. For the 7-hole collimator, measurements were only made with Tc-99m and Hg-203.

The dead-time of the detecting system was measured and found to be 3 μsec. The counting rates were corrected when necessary. Background counting rate corrections were also applied.

5.2 Crystal efficiencies

Measurements of the counting rate for a point source

of Hg-197 on the crystal axis were used to calibrate the NPL ion chamber for Hg-197. This calibration was based on the assumption that for large source to crystal distances at this energy the crystal efficiency was 100 per cent. The measured counting rate was connected for absorption of radiation in the 0.016" aluminium cap covering the crystal and the quantity of radioactivity (Q) in the source was then calculated from the equation:

$$Q = \frac{\text{cps}}{3.7 \times 10^4 \times \eta \times q \times \frac{\Omega}{4\pi}} \mu\text{Ci} \qquad (5.4)$$

where η is the crystal efficiency (1.0), q is the fraction of disintegrations resulting in detectable radiation and $\Omega/4\pi$ is the fraction of radiation emitted which is incident on the crystal surface, i.e.,

$$\frac{\Omega}{4\pi} = \frac{1}{2}\left[1 - \frac{d}{\sqrt{D^2/4 + d^2}}\right] \qquad (5.5)$$

where d is the distance of the source from the crystal and D is the crystal diameter. The distance d was corrected for a gap between the face of the crystal and the aluminium

protective cap. The size of the gap was found from radiographs of each crystal which showed that it varied from 0.35 cm at the centre to 0.7 cm at the edge.

Values of Q were calculated from equation (5.4) over a range of distances. The constant value at large distances was used to obtain a calibration factor for the NPL ion chamber (Table 5.2).

Measurements obtained with known amounts of Tc-99m and Hg-203 were used to calculate the crystal efficiencies from the expression:

$$\eta = \frac{\text{cps} / \mu\text{Ci}}{3.7 \times 10^4 \times q \times \frac{\Omega}{4\pi}} \qquad (5.6)$$

The results of these measurements are summarised in fig. 5.1 which shows the crystal efficiency plotted against energy for distances of 2, 5, 10 and 20 cm from the crystal housing. There is no available published data on efficiencies for a 3" x 1" crystal but the values obtained here lie between those for 3" x 3" and 2" x 1" crystals and therefore seem acceptable.

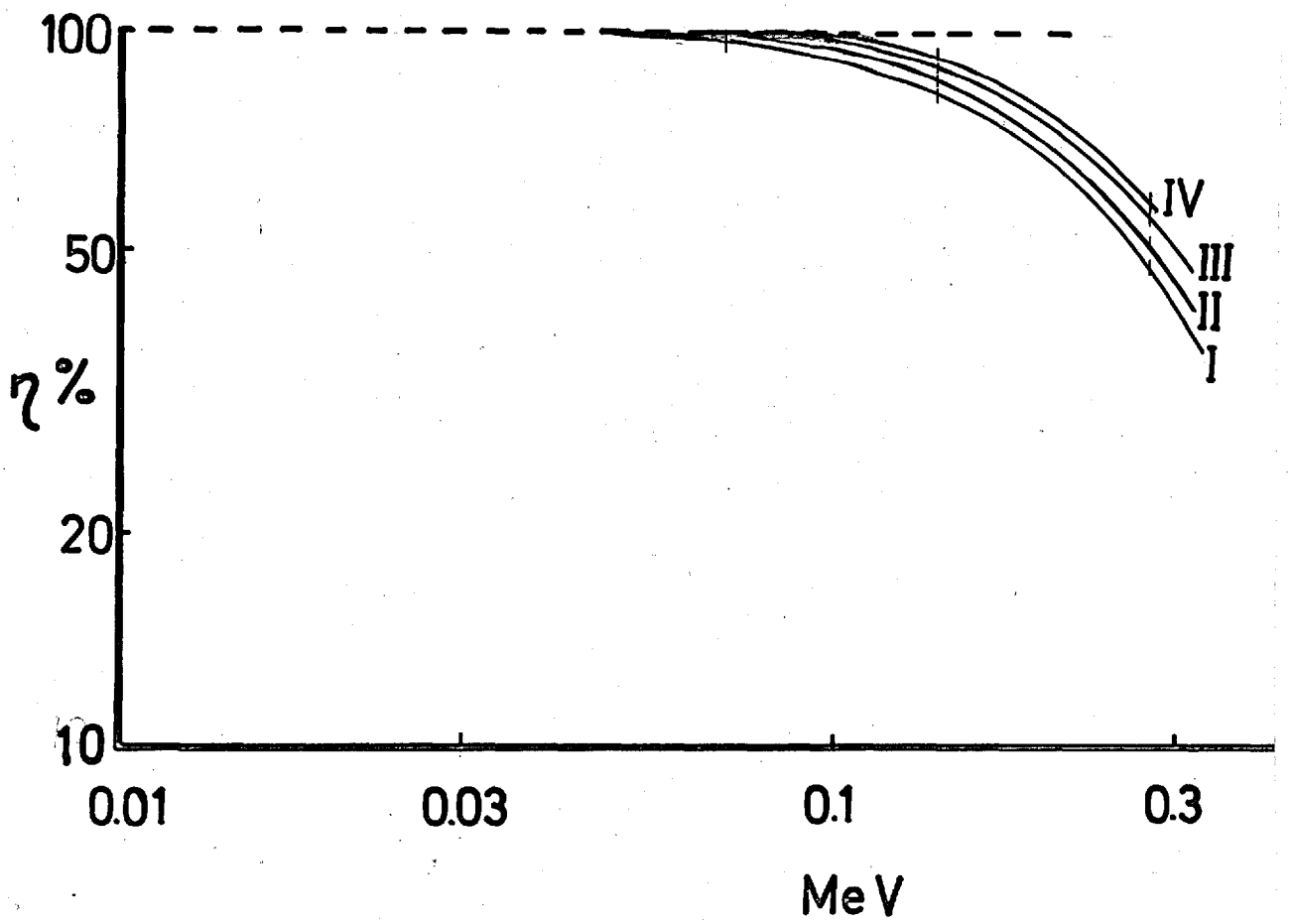

Fig. 5.1 Efficiencies for a 3" diameter x 1" sodium iodide crystal at distances of (i) 2 cm, (ii) 5 cm, (iii) 10 cm and (iv) 20 cm from the crystal.

5.3 Collimator efficiencies

Collimator efficiencies were calculated from experimental measurements using the equation:

$$\epsilon_T = \frac{\text{cps}/\mu\text{Ci}}{3.7 \times 10^4 \times \eta \times q} \qquad (5.7)$$

The results of axial measurements for the different collimators and isotopes are given in figs. 5.2, 5.3, 5.4 and 5.5. The theoretical curves based on the dimensions given in Table 5.1 are shown for comparison. In the calculation of the theoretical curves for the 7 and 61-hole collimators allowance has been made for the fact that the central hole focuses at a different distance from the other holes.

In general, the experimental points tend to be higher than the theoretical curve at small distances, but lower than the theoretical curve in the region of the focus. At large distances agreement between theory and experiment is better although experimental points are slightly higher than the theoretical curve for the 37 and 61 hole collimators. At small distances the experimental points for Hg-203 tend to be higher than those for Tc-99m and Hg-197. These differences are discussed in sections 5.4 and 5.5.

Some typical examples of off-axis measurements of

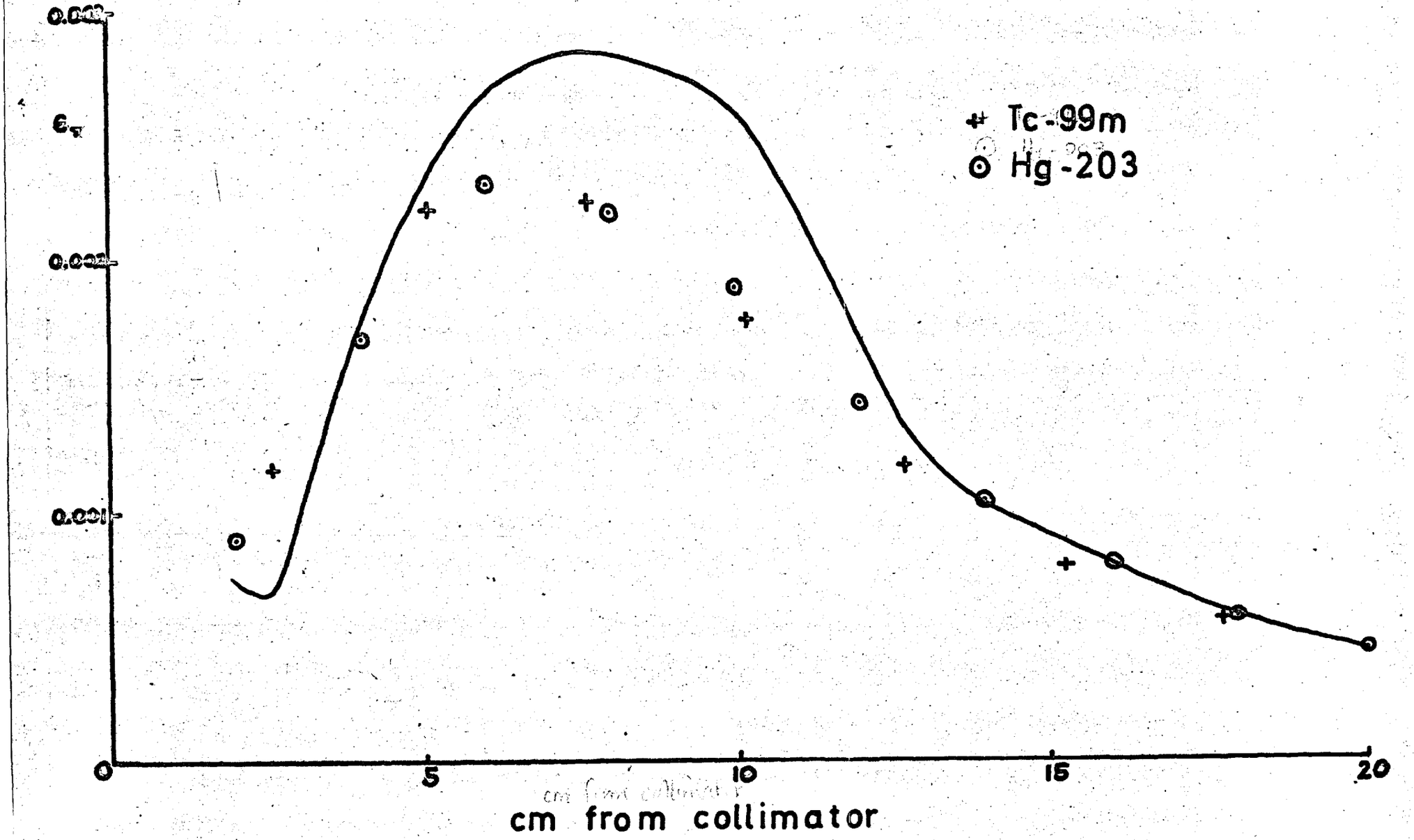

Fig. 5.2 Axial point source efficiencies in air for different distances from the face of the 7-hole collimator. The solid curve represents theoretical geometrical efficiencies.

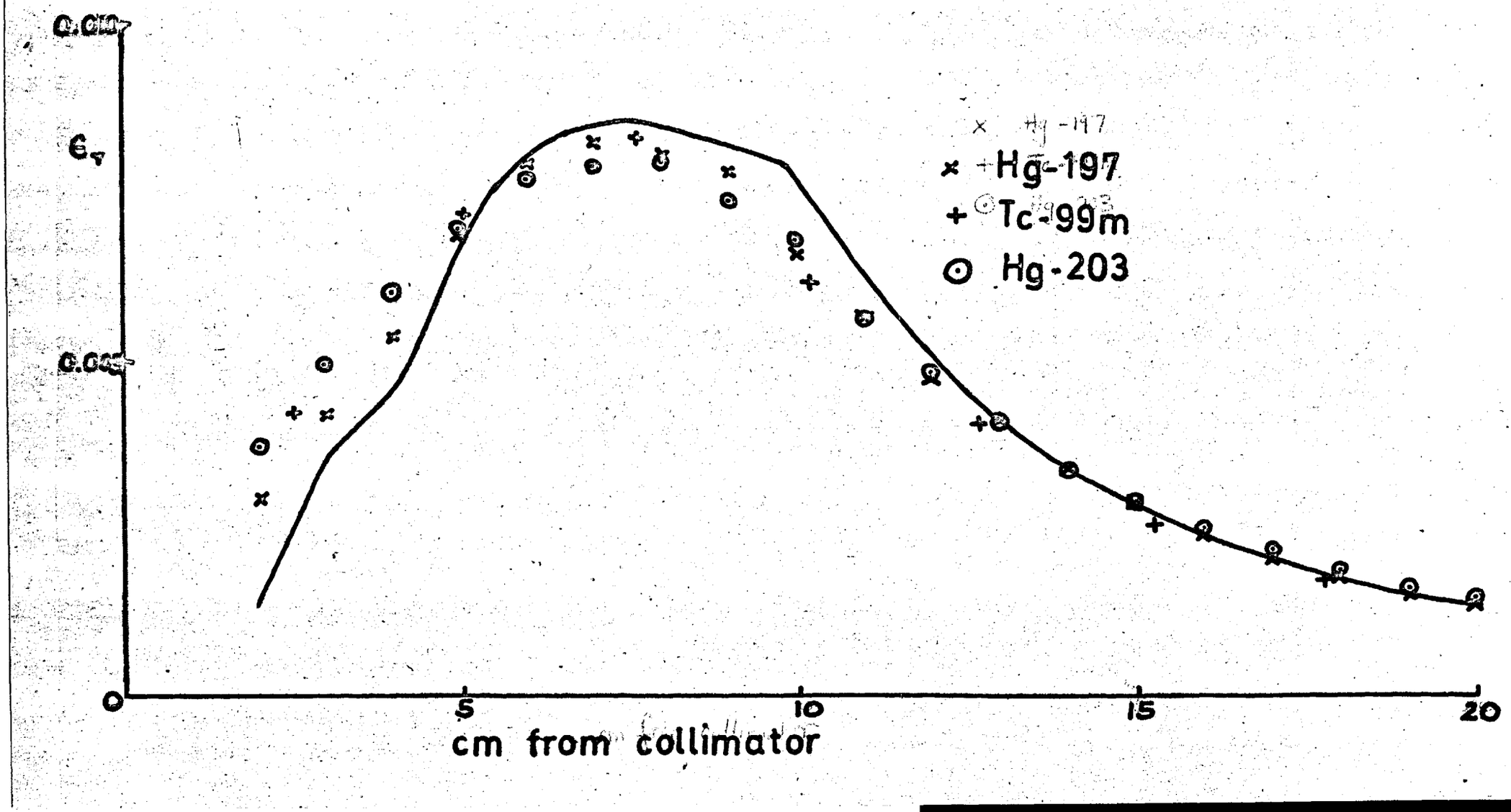

Fig. 5.3 Axial point source efficiencies in air for different distances from the face of the 19-hole collimator. The solid curve represents theoretical geometrical efficiencies.

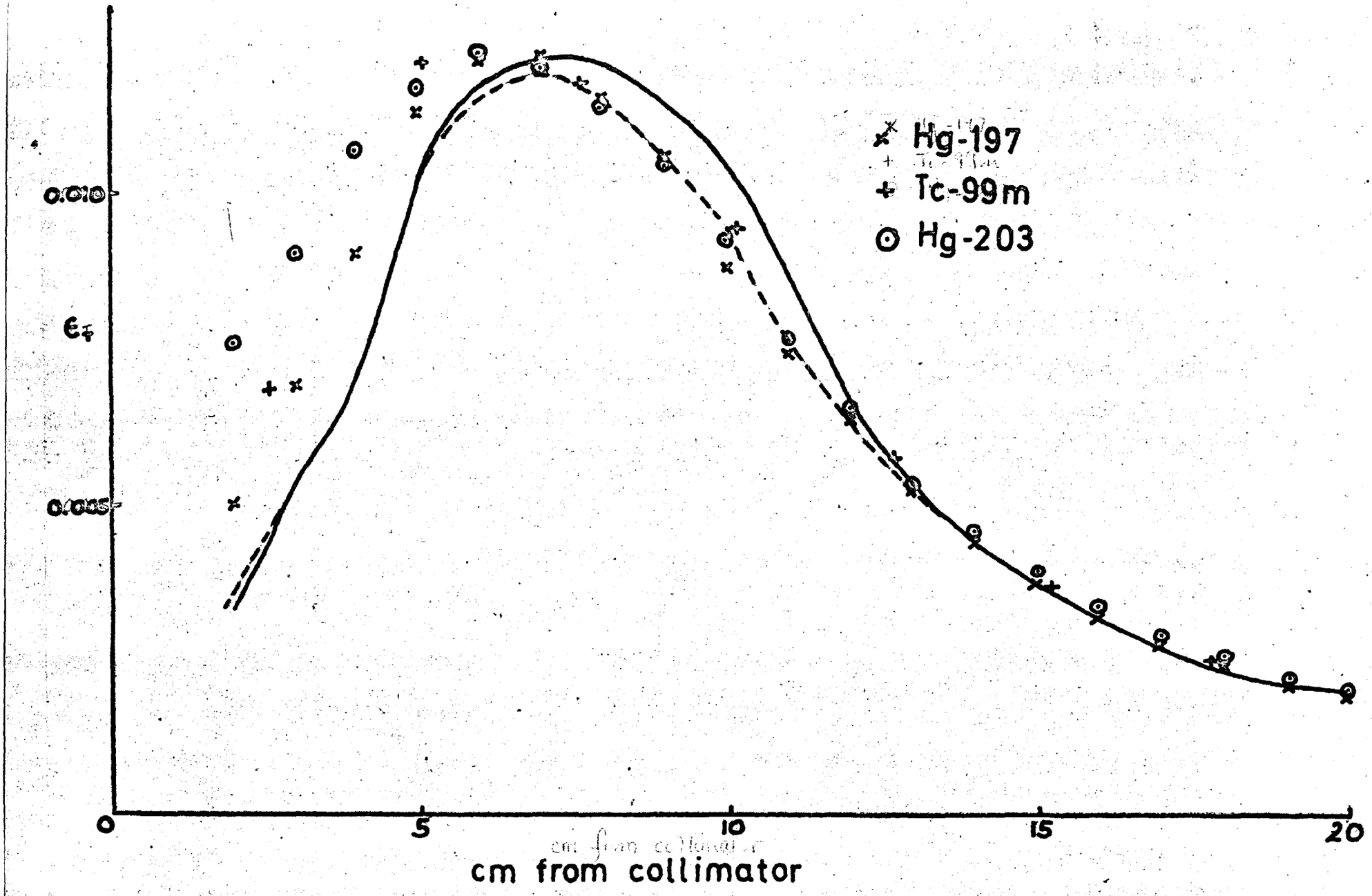

Fig. 5.4 Axial point source efficiencies in air for different distances from the face of the 37-hole collimator. The solid curve represents theoretical geometrical efficiencies. The dashed line represents theoretical values corrected for source size and error in positioning.

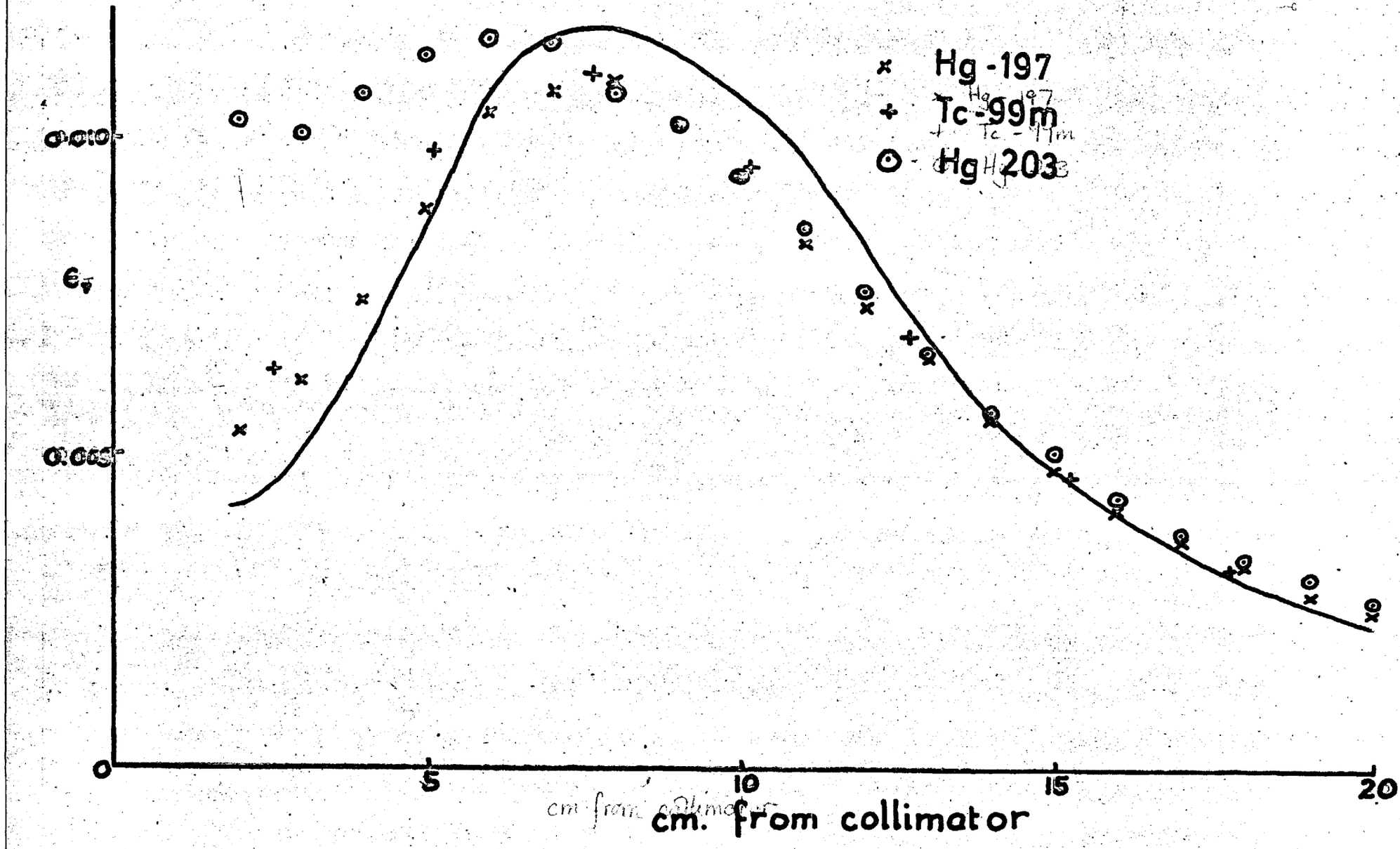

Fig. 5.5 Axial point source efficiencies in air for different distances from the face of the 61-hole collimator. The solid curve represents theoretical geometrical efficiencies.

collimator efficiency are given in fig. 5.6. The theoretical resolution curves for the 37-hole collimator at distances of 4, 10 and 16 cm from the collimator face were obtained by the method described in section 3.4 and are shown by the solid lines. Experimental points for Hg-197 and Hg-203 are given, one isotope on each side of the collimator axis. For Hg-197, agreement between experiment and theory is good except at very large distances from the axis. Agreement is less good for Hg-203 especially at large distances from the axis. These discrepancies between theory and experiment were less for the 19-hole collimator and greater for the 61-hole collimator.

Figure 5.7 shows spectra for Hg-203 obtained with the source in air at different distances along and perpendicular to the axis for the 37-hole collimator. There are no very distinctive differences between the spectra. No distinctive differences were observed for other collimators or for Hg-197.

5.4 Sources of error

Source size and positioning errors

The experimental points for axial efficiencies are in most cases the average of three readings; for the 7-hole

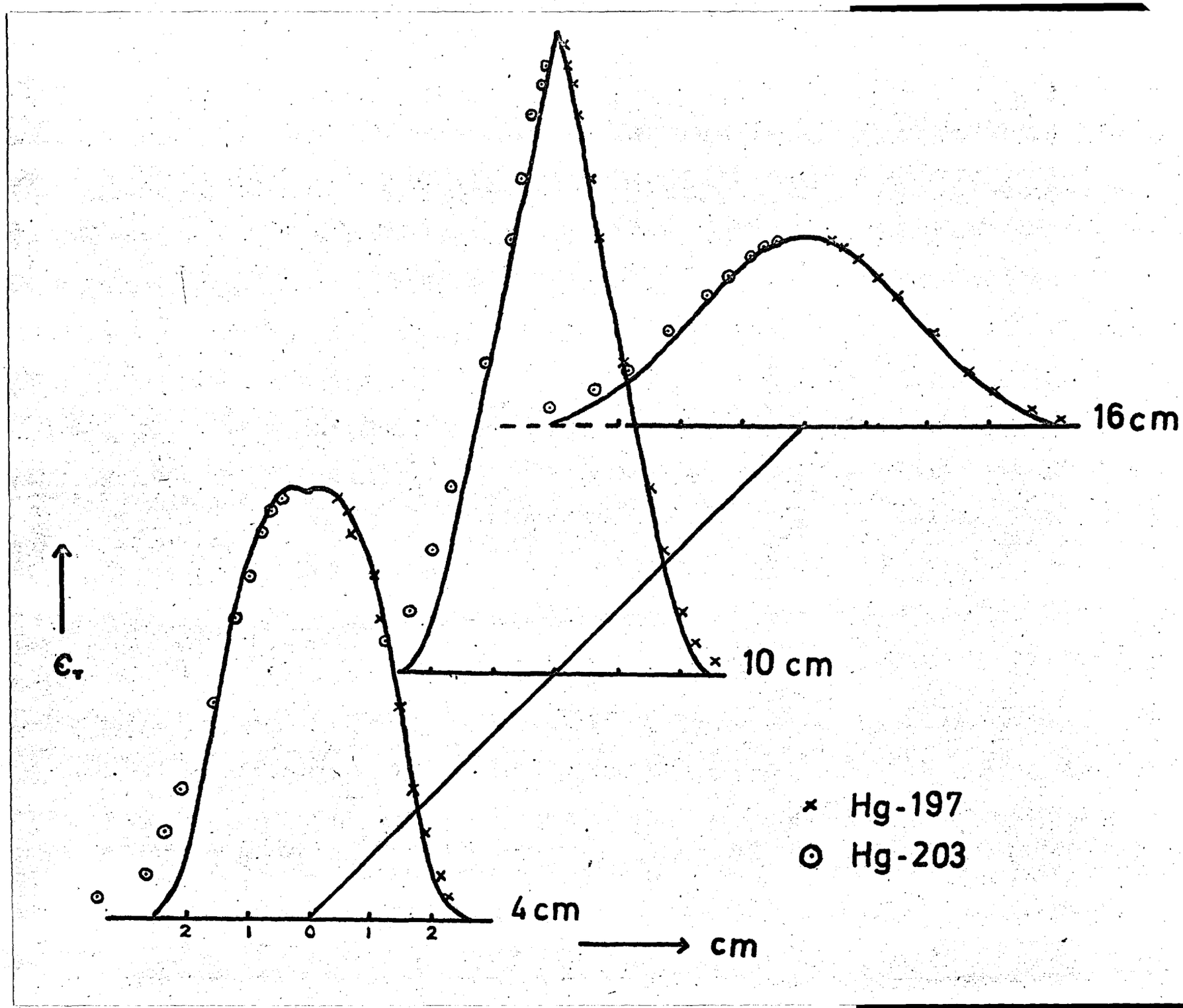

Fig. 5.6 Point source efficiencies at positions off the axis of the 37-hole collimator for distances of 4, 10 and 16 cm from the collimator face. The theoretical resolution curves are shown by the solid line. Experimental points have been normalised at the collimator axis.

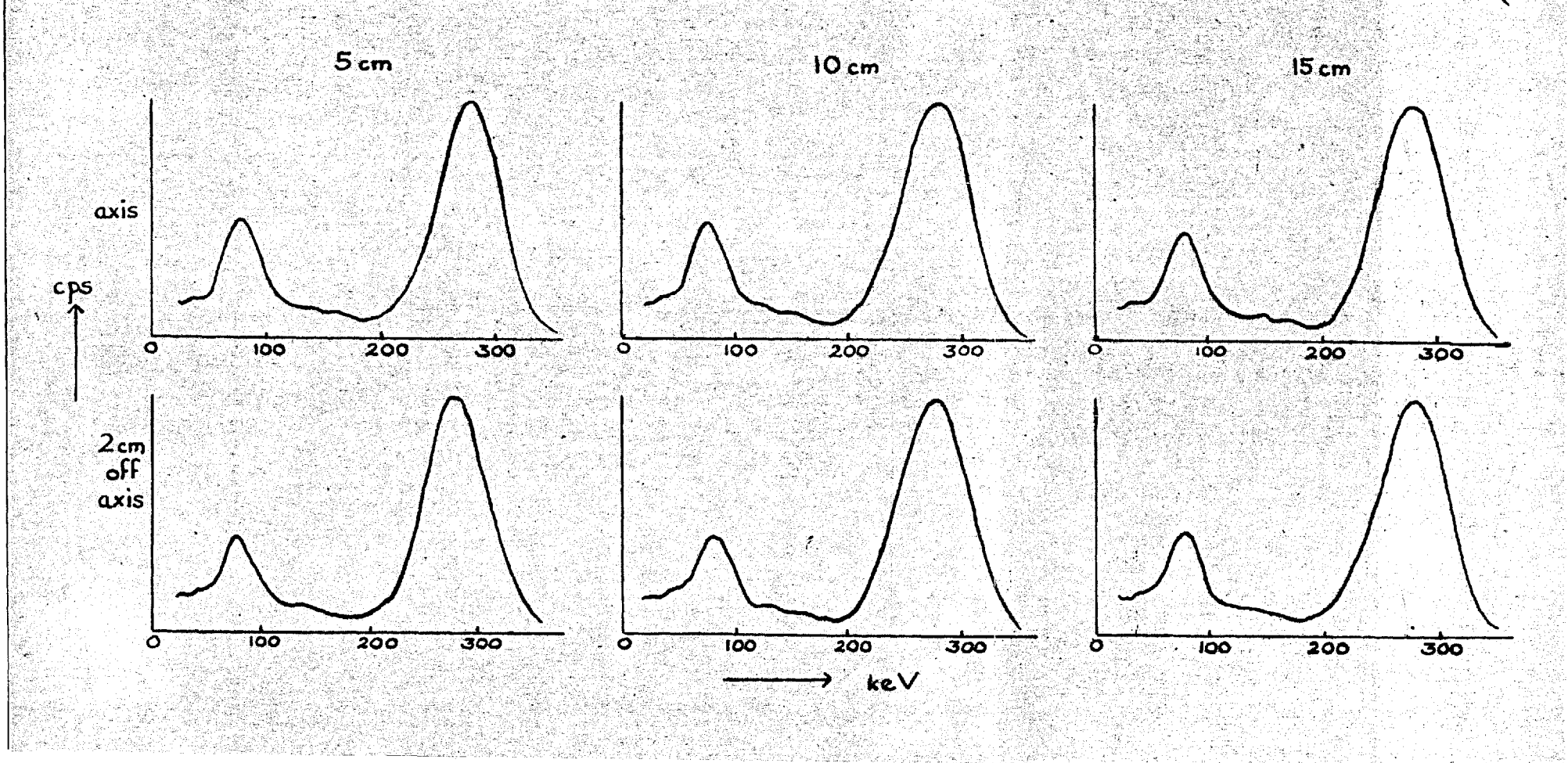

Fig. 5.7 Spectra obtained with point sources of Hg-203 in air at distances of 5, 10 and 15 cm from the 37-hole collimator, both on the axis and 2 cm off the axis. The peak at approximately 80 keV is due to incomplete absorption in the crystal.

collimator five readings were taken; in a few cases only two measurements were made. For Hg-197 and Hg-203, the error in the measurements was generally less than 5 per cent although it was as great as 10 per cent for some small source to collimator distances. For Tc-99m, using a less accurate positioning method, the error was generally less than 10 per cent increasing to 20 per cent for some small source-collimator distances. The errors tended to be greater for the 7 and 19-hole collimators, with smaller radii of field of view in the focal plane, for which positioning is more critical.

These experimental errors are however not a good indication of positioning errors in a plane perpendicular to the collimator axis, because, owing to the shape of the resolution curves, any error in positioning leads to a decrease in the experimental efficiency. The size of the source also leads to a decrease in the measured efficiency relative to the theoretical value. These errors increase as the resolution curves become more triangular in shape and hence are greatest in the region of the focus. Using theoretical resolution curves, the theoretical values of the axial efficiencies for the 37-hole collimator have been corrected for the size of the source and an assumed

positioning error of 0.1 cm and the corrected values are shown by the dashed line in fig. 5.4. The corrected curve lies below the original curve in the region of the focus. At small source-collimator distances, the corrected curve lies slightly above the original curve. This is due to undulations in the theoretical resolution curves which were described in section 3.4. Positioning errors and those due to the source size adequately explain the discrepancies between theory and experiment in the region of the focus for all collimators and isotopes for axial efficiency measurements.

Crystal efficiency

The values of crystal efficiency used in the calculation of collimator efficiencies from equation (5.7) were measured under conditions where the total area of the crystal was exposed. When the source is a small distance along the collimator axis, only the central portion of the crystal is exposed to direct radiation. The efficiency of this region of the crystal may be higher than the value for all the crystal because less radiation is likely to be lost from the edges. Therefore experimental values calculated from equation (5.7) using the efficiency for all the crystal area

may be higher than the true experimental values. The effect will be small for Hg-197 for which the crystal efficiency is high at all distances. For Hg-203, the true experimental values could be 15 per cent lower than those shown in fig. 5.5 for a source at 2 cm from the 61-hole collimator.

Scattering from the collimator walls

The possible magnitude of the contribution of radiation scattered from the collimator walls was estimated for a point source at 2 cm from the 19-hole collimator. At this distance, the majority of the efficiency is theoretically due only to radiation incident at the base of the axial hole, the contribution of surrounding holes being very small. The fraction of emitted radiation which is incident on the walls of the axial hole is given by : $\frac{\pi r^2(k^2-1)}{4\pi(t+d)^2}$.

At the gamma-ray energies used in the experiments, radiation incident on the collimator walls is either absorbed by the photoelectric effect or scattered by Compton or Rayleigh events. For Hg-203, the fraction of the incident radiation which undergoes coherent and incoherent scattering events is approximately 0.25. Neglecting the fact that some

scattered radiation may be further attenuated in the lead and assuming that the radiation is scattered isotropically, approximately a fraction $\frac{r^2}{t^2}$ of that scattered half-way down the collimator walls will be incident on the crystal. A larger fraction will be incident on the crystal for radiation scattered from the walls nearer the crystal, and a smaller fraction will be incident for radiation scattered near the collimator face. Radiation is not scattered isotropically, but Mather (1957) has suggested that the collimator walls are too rough for specular reflection and that this is therefore a good approximation. With the assumptions stated, the fraction of emitted radiation which is incident on the crystal after scattering events is given by the approximate expression:

$$\frac{r^2\,(k^2-1)}{4\,(t+d)^2} \times 0.25 \times \frac{r^2}{t^2}$$

Parts of the inside areas of the surrounding 18 holes may also contribute to the counting rate due to scattering, perhaps increasing the above expression by a factor of 6. Assuming that all scattered radiation incident on the crystal lies within the energies set by the analyser window, the percentage increase in efficiency due to scattering is

therefore:

$$\frac{6\,r^4\,(k^2-1)}{4\,t^2\,(t+d)^2} \times 0.25 \times \frac{4\pi\,(t+d)^2}{\pi\,r^2} \times 100$$

$$= 150\,\frac{r^2}{t^2}\,(k^2-1)$$

For a point source of Hg-203 at 2 cm on the axis of the 19-hole collimator the increase in efficiency due to scattering is therefore approximately 8 per cent. For Hg-197, the fraction of radiation incident on the walls which is attenuated by scattering events is slightly less (0.21) probably leading to a smaller increase in efficiency. The fraction of scattered radiation is likely to decrease in the region of the focus as the area of the collimator walls exposed to radiation decreases. For the 37 and 61-hole collimators, the areas of the walls of each hole over which scattering events may occur are smaller, leading to less scatter; this may be compensated however by the greater numbers of holes. At 2 cm from these collimators, the theoretical efficiencies are much higher than that for the 19-hole collimator and therefore the percentage increase in efficiency is likely to be less.

Multiple scattering in the lead may also add to the

scatter contribution. Of those photons which have undergone one scattering event, 25 per cent (for Hg-203) may be further scattered and this would increase the scatter contribution to 12 per cent in the above example. The probability of being detected within the analyser window setting is however less for multiply scattered photons.

The maximum angle through which radiation can be scattered from a point half way down the 19-hole collimator and be subsequently incident on the crystal is approximately 22^{o}.

The energy of a scattered photon ($h\nu'$) is related to the energy of the initial photon ($h\nu$) by the expression:

$$\frac{h\nu}{h\nu'} = 1 + \alpha(1-\cos\phi)$$

where $\alpha = h\nu/m_{o}c^{2}$ and ϕ is the angle of photon scattering. For Hg-197, the energy of the scattered photons is therefore greater than 99 per cent of the initial photon energy and for Hg-203, it is greater than 96 per cent of the initial energy. Some radiation may be scattered through greater angles and multiple scattering may also occur, both effects resulting in lower photon energies, but it appears that scattered radiation is unlikely to be observed on energy spectra obtained with the crystals used in these measurements.

Radiation which is absorbed in the collimator walls by the photoelectric effect gives rise to X-rays characteristic of the collimator material. The K X-ray peak for lead is at 75 keV and lies well below the photopeaks of Tc-99m and Hg-203. The L X-ray peak is at 10.5 keV well below the photopeak of Hg-197. X-rays emitted from the collimator material do not therefore contribute to the photopeak counts.

Since the magnitude of scattering from the collimator walls and of the X-ray peak is relatively small for the collimators used in these experiments, some separate measurements were carried out to demonstrate these effects. Spectra were obtained for a point source of Tc-99m at 8" from one of the crystals, firstly with no collimator, then with a cylindrical collimator 4" in length, and then with a cylindrical collimator 8" in length. These spectra are shown in fig. 5.8. The presence of the 75 keV X-ray peak and of scattering is evident.

Penetration of collimator septa

The probable magnitude of the effects of penetration through complete septa and through the edges of septa were estimated in one particular case. For a point source of 2 cm from the 19-hole collimator, the minimum path through one

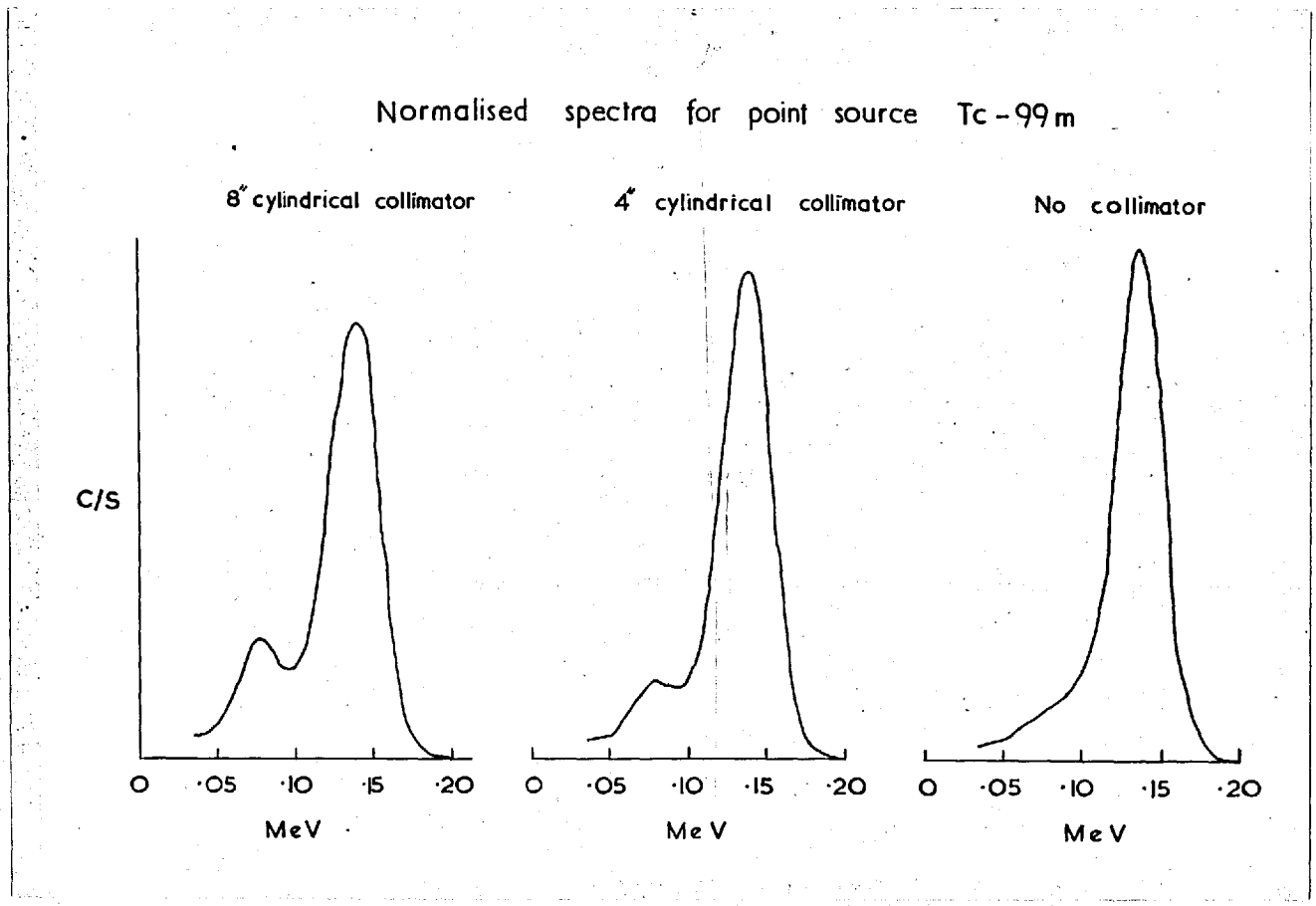

Fig. 5.8 Spectra obtained with a point source of Tc-99m at 8" from a 3" x 1" crystal with cylindrical lead collimators of 8" and 4" in length and with no collimator.

complete septum was calculated as 0.38 cm. The linear absorption coefficients for Hg-197 and Hg-203 in lead are 38/cm and 5.1/cm respectively giving percentages < .01% and 14% for penetration of radiation incident in this direction. The majority of radiation will pass through greater thicknesses of septa, but because there is a relatively large amount incident on the septa compared with that reaching the crystal by geometrical paths, it is probable that penetration is significant for Hg-203. Penetration of complete septa is likely to decrease in the region of the focus for which radiation must pass through much greater lengths of septa. The 37 and 61-hole collimators are shorter in length than the 19-hole collimator and therefore radiation may pass more acutely through the septa. There is therefore likely to be greater penetration for these collimators.

In order to estimate the magnitude of the effect of penetration through the edges of septa, it was assumed that radiation travelling through more than one half-value layer was totally attenuated and that travelling through less than one half-value layer was unattenuated. On this basis, the apparent increases in hole radii were calculated. For a point source of Hg-203 at 2 cm along the axis of the 19-hole

collimator this led to a 12 per cent increase in efficiency; the increase being less than 1 per cent for Hg-197. This effect is likely to decrease in the region of the focus and to be greater for the 37 and 61-hole collimators.

5.5 Discussion and conclusions

The source size and errors in positioning are sufficient to explain the discrepancy between experiment and theory in the region of the foci of the four collimators. The theoretical curves have been corrected for these errors and the resulting difference between theory and experiment at small source-collimator distances have been expressed as a fraction of the theoretical efficiency. These values are given in Table 5.3 for the 19, 37 and 61-hole collimators for Hg-197 and Hg-203 for which the most reliable results were obtained. For Hg-197, errors due to penetration and crystal efficiency are probably small and the discrepancies at small distances from the collimator are probably primarily due to scattering from the collimator walls. For Hg-203, the discrepancies are probably mainly due to penetration, with a further contribution from scattering. At distances beyond the focus, the higher experimental efficiencies for Hg-203 for the 37

Table 5.3

Experimental values of the combined scatter and penetration fractions for point sources of Hg-197 and Hg-203 at different distances from the collimators.

Theoretical penetration fractions for an extended source are also shown.

Distance cm.	Hg-197			Hg-203		
	19-hole	37-hole	61-hole	19-hole	37-hole	61-hole
2	0.45	0.39	0.26	0.85	1.11	1.45
3	0.20	0.28	0.21	0.40	0.67	0.98
4	0.10	0.16	0.12	0.25	0.55	0.62
5	0.05	0.11	0.04	0.08	0.15	0.33
6	0.04	0.05		0.01	0.06	0.10
P	.01	.01	.02	.12	.76	2.6

and 61-hole collimators are probably attributable to penetration. The same effects are most likely to account for differences between experiment and theory in the resolution curves. It is difficult to confirm the presence of scattered radiation from spectra obtained with these collimators because the majority of the scattered radiation lies close to the photopeak. Evidence that scattering from the collimator walls can occur has however been shown in a separate experiment.

Table 5.3 also shows the penetration fractions (P) calculated from equation (4.6) for these collimators and isotopes. This equation is based on penetration from an extended source and hence does not directly correspond with these point source measurements. However, on the basis of the calculated penetration fractions, all of these collimators would have been considered suitable for use with Hg-197 ($P < 0.2$) but none of them would have been considered suitable for use with Hg-203. These conclusions have been confirmed by the experimental results presented here and support the validity of the use of equation (4.6) in the collimator design procedure used in Chapter 4.

CHAPTER 6

THE INFLUENCE OF RADIATION SCATTERED FROM TISSUE

Experimental measurements were carried out in order to assess the magnitude of the contribution of scattered radiation from a point source situated in water, representing a tissue medium. The effects of scattered radiation from an extended radioactive source were also investigated.

Apparatus and sources

The apparatus and point sources were the same as those described in section 5.1. The volume source consisted of a perspex tank 15 x 20 x 20 cm high filled with 5 litres of radioactive solution. The concentration of activity in the source was determined by counting 50 ml. samples on the ring of six Geiger tubes calibrated against the NPL chamber for this volume (section 5.1).

Measurements

Point source measurements were carried out with the source placed in the tank containing 5 litres of water. The tank was placed at 2.5 cm from the collimator surface

with its shortest length along the direction of the collimator axis. The source counting rate was measured at different distances along and perpendicular to the collimator axes, with the single channel analyser set to include the whole photopeak. Measurements of spectra were made for some source positions using approximately 100 channels of the 512 channel analyser. Counting rate and spectra measurements were also made with the tank filled with radioactive solution placed in the position described above.

6.2 Optimisation of the setting of the lower level of the analyser window

Preliminary calculations were carried out in order to determine the setting of the lower level of the analyser window which gave the maximum figure of merit for each isotope. The spectra obtained with the 19-hole collimator for a point source at a depth in water of 7.5 cm and for the tank of radioactivity are shown in fig. 6.1. A large amount of scattered radiation is apparent in the spectra for the volume source and the aim in optimising the analyser setting is to reduce the counting rate due to scattered

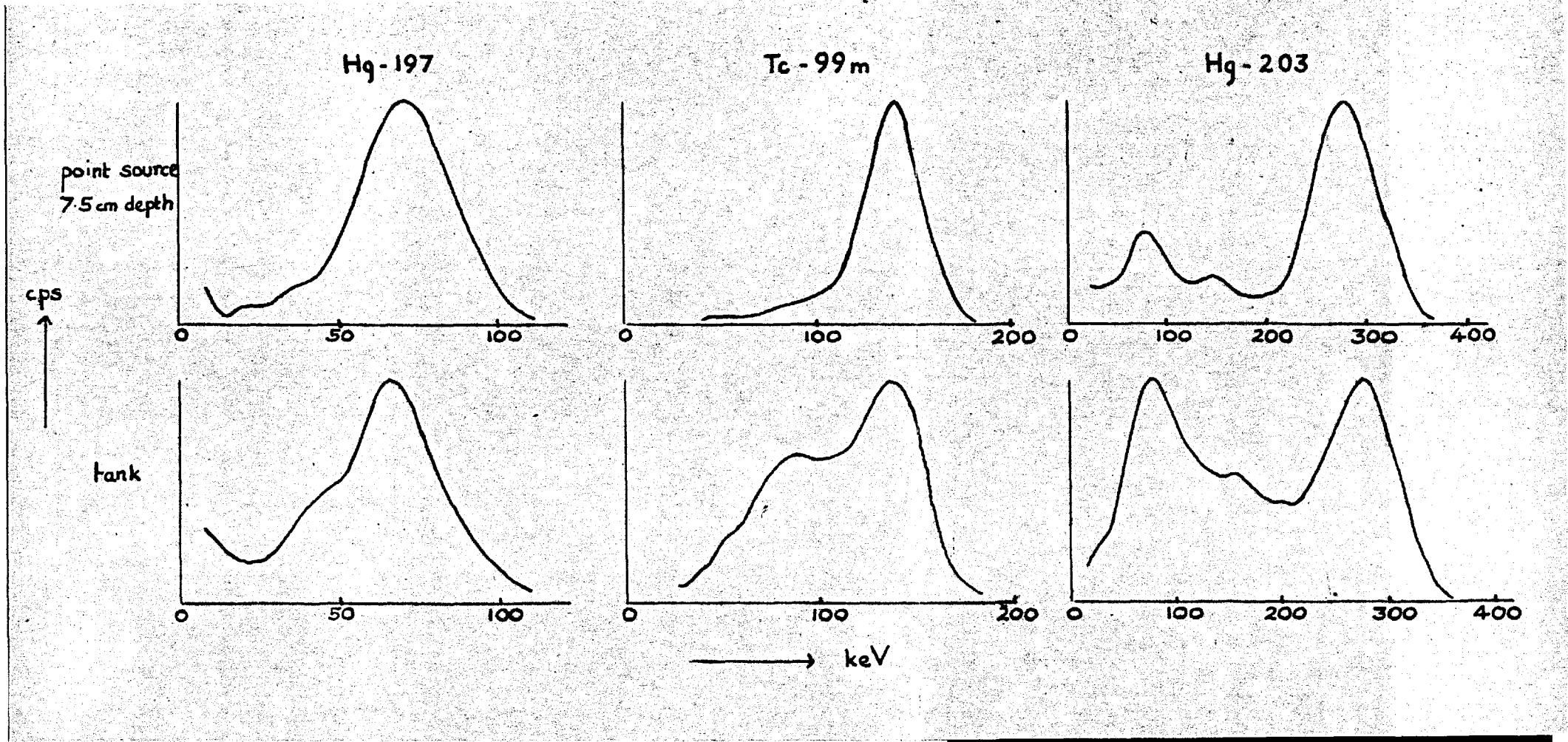

Fig. 6.1 Spectra obtained with the 19-hole collimator using Hg-197, Tc-99m and Hg-203 for a point source at 10 cm from the collimator in a tank of water and for a tank filled with 5 litres of radioactive solution. The air gap between the collimator face and the tank was 2.5 cm.

radiation without too much reduction in the photopeak counts.

The collimator figure of merit is proportional to the counting rate for a point source divided by the square root of the counting rate for a volume source. For each isotope, the areas under the point source and volume source spectra were found for a range of settings of the lower level of the analyser window. The upper level of the analyser window was set to include all the high energy side of the photopeak. Factors proportional to the figure of merit were then plotted against lower level analyser setting as illustrated in fig. 6.2 for Hg-203. The lower level analyser setting corresponding to the maximum of the curve was considered the optimum for that isotope. The spectra for point and volume sources showed only small variations between collimators and therefore it was assumed that the optimum setting was independent of the collimator dimensions.

6.3 Point and volume source scattering

Point sources

Scatter fractions for point sources (equation (2.4)) were calculated in the first instance from measurements taken with the analyser set to include the whole photopeak of each

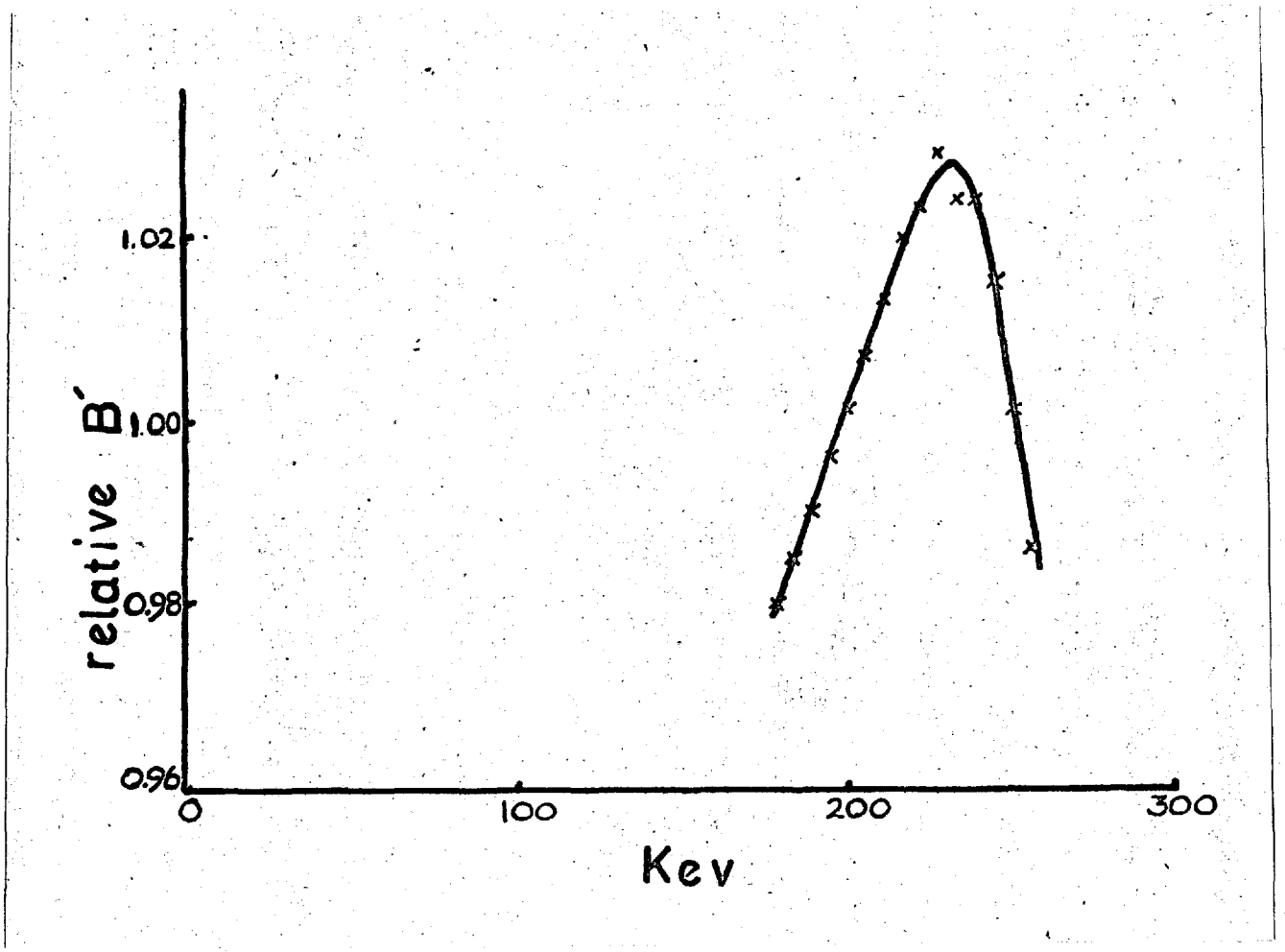

Fig. 6.2 The relative collimator figure of merit plotted against the lower setting of the analyser window for Hg-203 and the 19-hole collimator.

isotope. The axial counting rates in air, obtained as described in the previous chapter, were corrected for attenuation in water using the total linear absorption coefficients (Siegbahn, 1965). The difference between the measurement with the source in the tank and the measurement with the source in air, corrected for attenuation, was expressed as a fraction of the latter. These scatter fractions are given in Table 6.1 for a point source at 10 cm from the collimator face, that is, at a depth in water of 7.5 cm.

Scatter fractions were then calculated for the optimum settings of the lower level of the analyser window. The experimental measurements for point sources in air and in water were corrected to the values which would have been obtained at the optimum analyser settings, by multiplying them by the ratios of the areas under the spectra for the optimum and whole photopeak analyser settings. The scatter fractions were obtained as described above and are shown in fig. 6.3 as a function of distance from the collimator face (air gap 2.5 cm). The scatter among the points is due to the fact that these values are dependent on the difference between two relatively similar readings, both of which may incur an error of 5 - 10 per cent. There is

Table 6.1

Point source axial water scatter fractions at 10 cm from the collimators, and volume source penetration plus scatter fractions for whole photopeak analyser settings.

Isotope	Lower level analyser window setting keV	Point source No. of holes in collimator				Volume source No. of holes in collimator			
		7	19	37	61	7	19	37	61
Hg-197	36		0.12	0.22	0.22				
Tc-99m	90	0.12	0.09	0.17	0.20	1.02	1.07	1.44	1.25
Hg-203	190	0.06	0.11	0.10	0.10	0.67	0.99	1.49	1.87

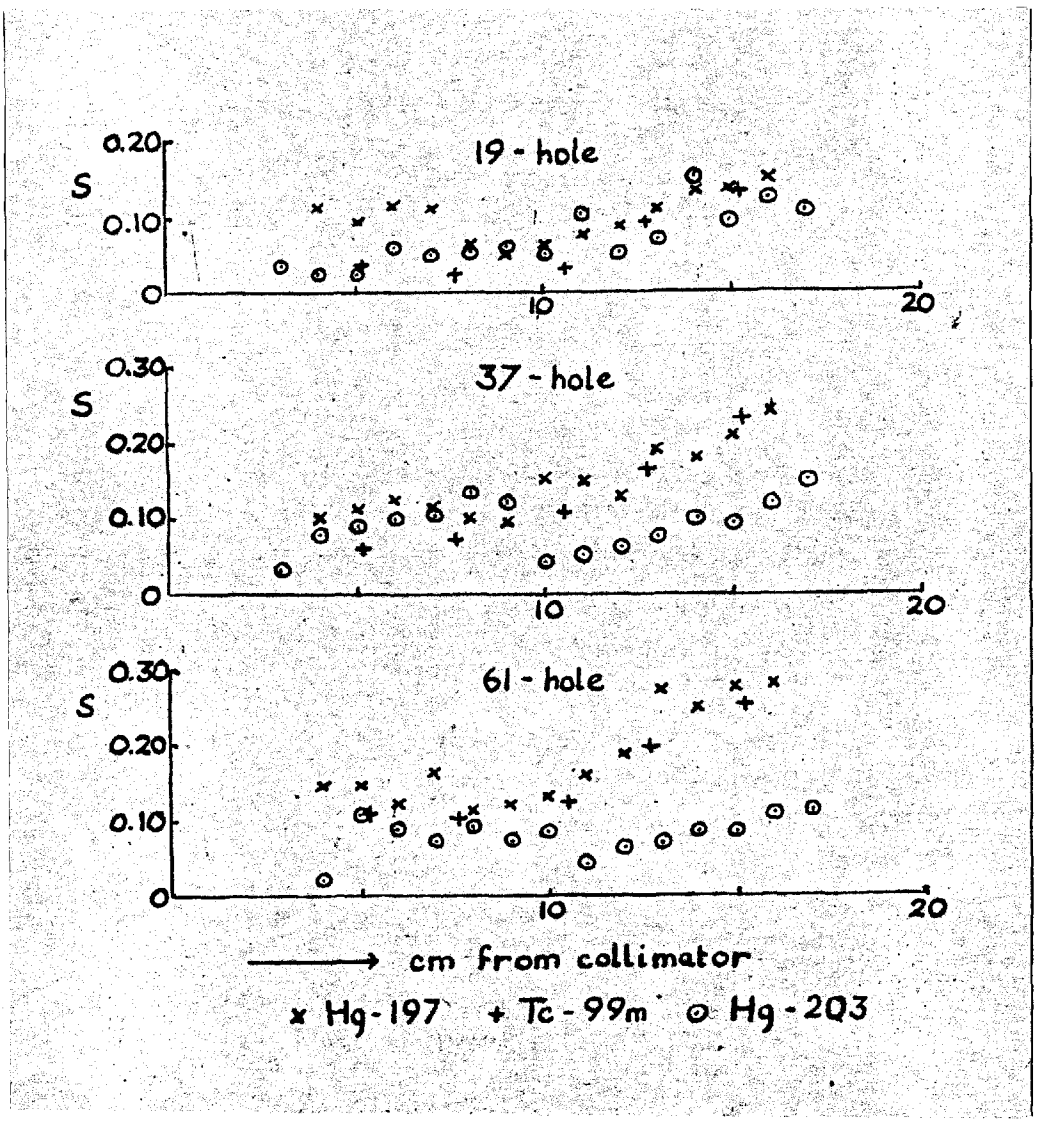

Fig. 6.3 Experimental values of the axial point source scatter fraction plotted against distance from the faces of the 19, 37 and 61-hole collimators. The analyser settings were the optimum for each isotope.

no consistent correlation with distance in the region up to 10 cm from the collimator but, beyond this region, the scatter fractions increase with distance. The amount of scattering is slightly greater for Hg-197 than for Tc-99m. The scattering for Hg-203 is considerably lower than that for other isotopes at large distances from the collimator. The average values of the scatter fractions at 10 cm from the collimator with the optimum analyser settings are shown in Table 6.2. In general there is increased point source scattering for collimators with greater numbers of holes.

Volume sources

Theoretical values of volume source efficiency were calculated for each collimator and isotope from equation (4.8). The volume source scatter fractions were then calculated as the difference between experimental and theoretical efficiencies divided by the theoretical efficiency. They therefore include the effects of penetration of septa and scattering from the collimator walls as well as those of scattering from water. The effects of septum penetration are most likely to affect the volume source measurements with Hg-203 for the 37 and 61-hole collimators. The volume

Table 6.2

Point source axial water scatter fractions at 10 cm from the collimators, and volume source penetration plus scatter fractions for the optimum analyser settings

Isotope	Lower level analyser window setting keV	Point source No. of holes in collimator				Volume source No. of holes in collimator			
		7	19	37	61	7	19	37	61
Hg-197	51		0.06	0.13	0.14				
Tc-99m	120	0.06	0.05	0.10	0.12	0.54	0.52	0.69	0.63
Hg-203	228	0.04	0.07	0.07	0.07	0.40	0.74	1.29	1.46

source scatter fractions are shown in Tables 6.1 and 6.2 for the whole photopeak and optimum analyser settings. The results obtained with Hg-197 were unfortunately not consistent and have therefore not been included. Scatter fractions with the volume source of Tc-99m are similar for all the collimators. Scatter fractions with the volume source of Hg-203 show an increase for collimators with greater numbers of holes although part of the increase may be due to septum penetration as explained above. Septum penetration of Hg-203 is likely to be small for the 7-hole collimator because it is relatively long and in this case the scatter fraction is lower than the values for Tc-99m.

Resolution curves

Some examples of resolution curves obtained with the source in water are given in fig. 6.4 for the 37-hole collimator, at distances 4, 10 and 16 cm from the collimator face (air gap 2.5 cm). The solid curves represent the results of theoretical calculations for point sources in air, obtained as described in section 3.4. The effects of attenuation on the shape of these curves is probably very small and therefore discrepancies with experimental measurements are largely due to septum penetration, collimator

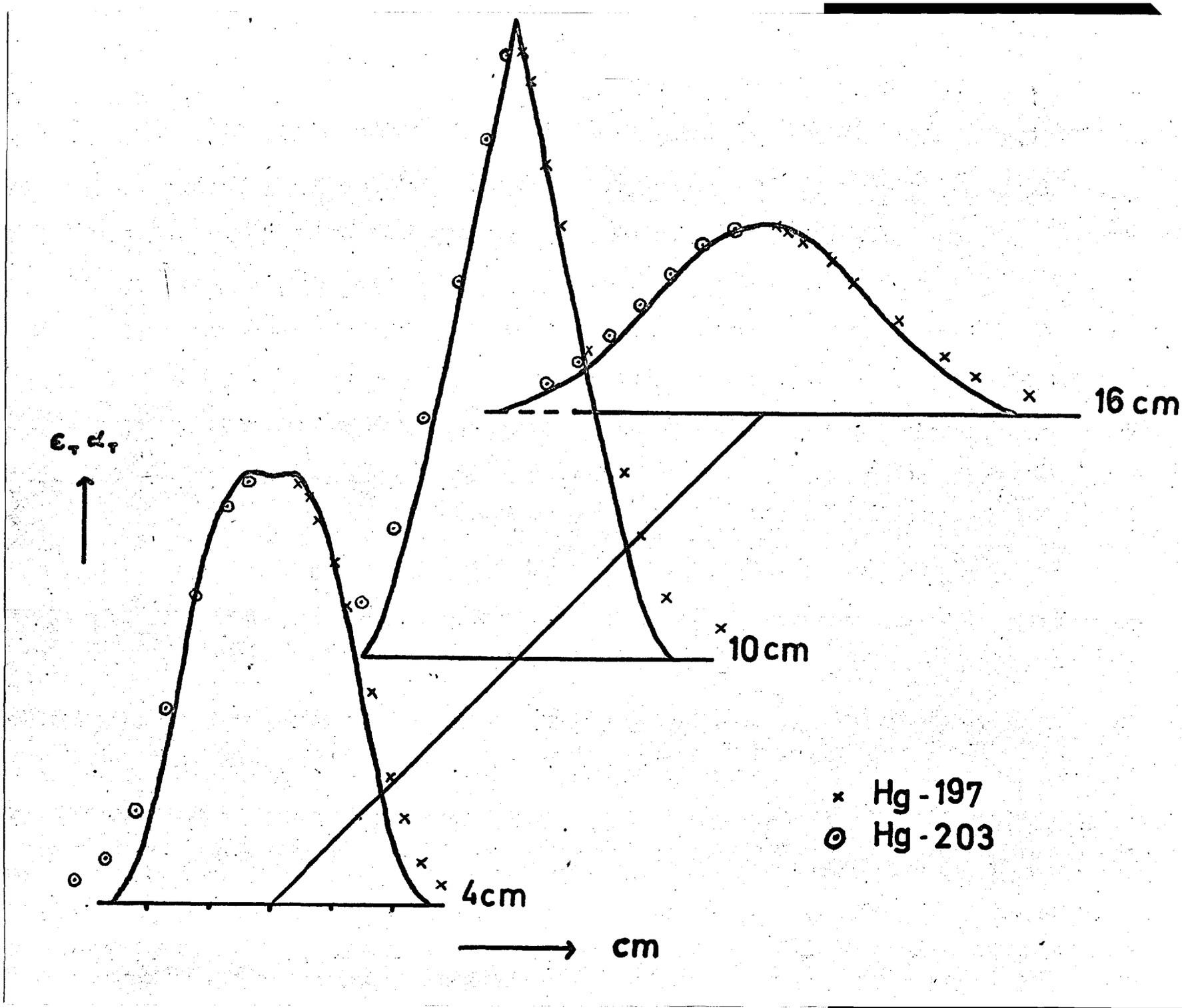

Fig. 6.4 Experimental and theoretical resolution curves obtained with point sources of Hg-197 and Hg-203 in a water medium at distances 4, 10 and 16 cm from the face of the 37-hole collimator. The theoretical results are shown by the solid lines. Experimental points have been normalised at the collimator axis.

scattering and scattering from water. The effects of septum penetration and collimator scattering were shown in fig. 5.6. Comparing fig. 6.4 with fig. 5.6 one can see that scattering from water has only a small effect on the resolution curves for Hg-203. Scattering has a larger effect for Hg-197 and leads to a broadening of the resolution curves, particularly at large distances from the collimator axis.

Figure 6.5 shows the spectra obtained from a point source of Hg-203 placed in water at distances 5, 10 and 15 cm from the collimator face (air gap 2.5 cm). Spectra are shown with the source on the axis and 2 cm off the axis. The spectra in air were shown in fig. 5.7. The presence of scattered radiation is evident in all the spectra shown in fig. 6.5, but particularly when the source is displaced from the axis.

6.4 Theoretical method

Magnetic tapes loaned by Dr. W.H. Ellett enabled theoretical calculations of spectra to be made. These tapes contained details of the interactions of gamma-rays of a given initial energy emitted from a point in an infinite

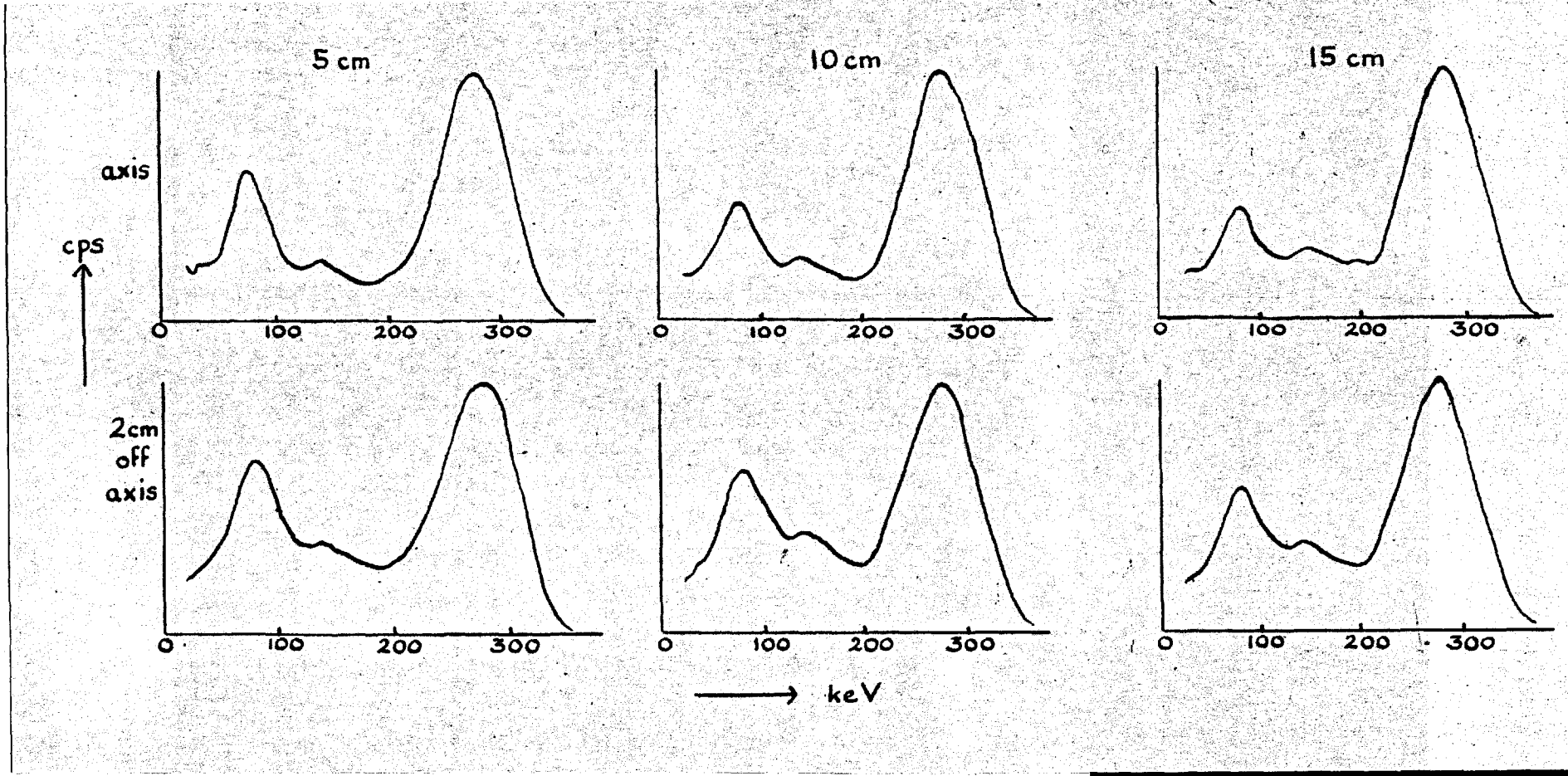

Fig. 6.5 Spectra obtained with a point source of Hg-203 placed in water at distances 5, 10 and 15 cm from the face of the 37-hole collimator at positions on the axis and 2 cm off the axis.

tissue medium ($C_5H_{40}O_{18}N$) (Ellett, Brownell and Reddy, 1968). Each interaction was characterised by three positions and one energy co-ordinate. Only photoelectric and Compton events were considered as higher energy effects do not contribute to attenuation at the energies considered. Coherent scattering was also neglected. Details of the first interaction of a photon of the specific initial energy were stored; if this was a Compton event, details of the next interaction of the scattered photon were then stored. The gamma-ray 'history' was continued in this way until the scattered photon was completely absorbed by a photoelectric event. The next history was then started. The assumptions used in producing these magnetic tapes have been discussed by Ellett, Brownell and Reddy (1968).

A computer program was written (by P.M. Kibby) in Fortran and FAP (Fortran II Assembly Programming Language) for an IBM 7090 which enabled the interaction co-ordinates to be read from the magnetic tapes and then sorted. The program has been summarised in the flow-chart in fig. 6.6. It was assumed that all photons originate from the centre of a sphere whose radius is set by the input data. The path of each initial photon was traced until either it was completely absorbed within the sphere or it emerged from

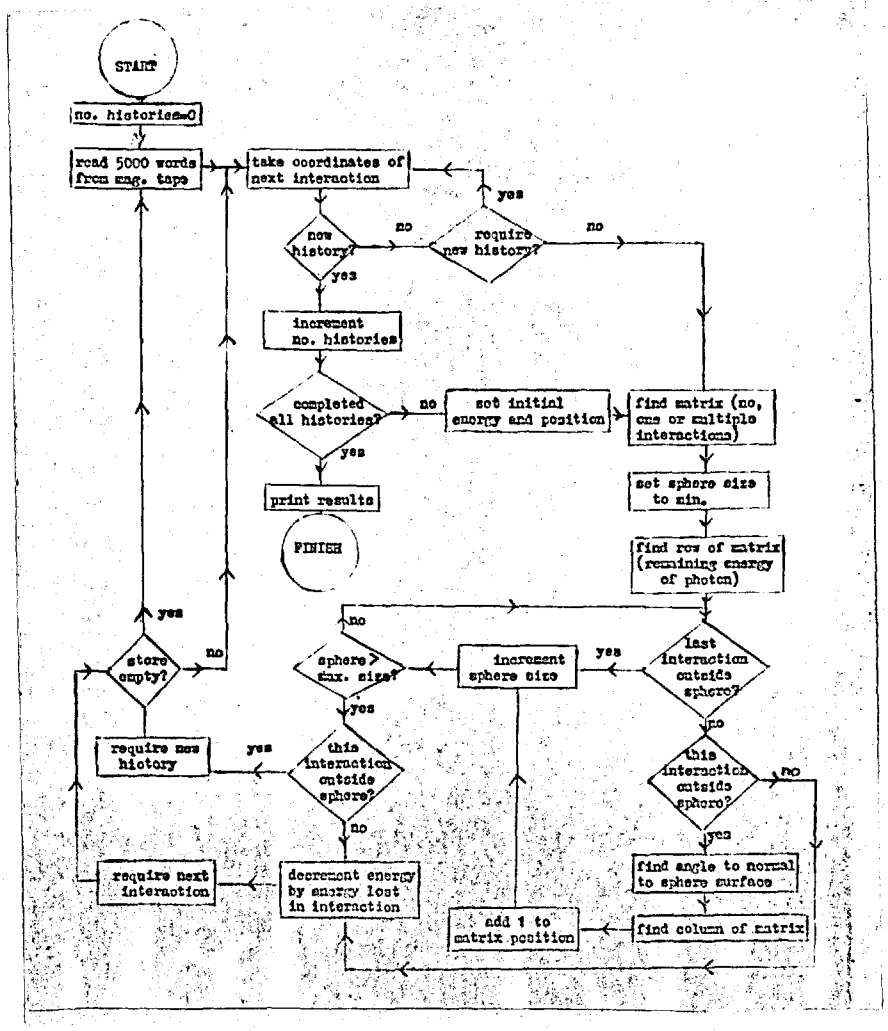

Fig. 6.6 Flow diagram for the computer program for calculating spectra at the surface of a spherical medium.

the surface. The energy and direction of the emergent photons were recorded in a matrix of angular and energy intervals. Photons which had undergone only one interaction were entered in a different matrix from those which had undergone more than one interaction. Photons which were directly emitted from the sphere were recorded separately. The position on the surface of the sphere at which each photon emerged was ignored as the spectra were the same for all points on the surface. Thus, the spherical symmetry enabled statistically significant results to be obtained with the 60,000 gamma-ray histories available on each tape. A much larger number of histories would be required for a cubic medium, resulting in considerable computer running time and cost. The limitation of a spherical medium is that the results can only be related to experimental measurements for large source to collimator distances for which the effects of the difference between the curved and a plane surface are small.

The angular intervals of the matrices corresponded to units of 0.1 in $\sin\theta$ where θ is the angle to the normal to the surface. The energy intervals were set by decrements of one twentieth of the initial photon energy.

In order to relate the spectra of photons emergent from

a sphere to the spectra of photons incident on a detector after passage through a collimator, further calculations were required and these are described in section 6.6.

6.5 Theoretical scattering from a point source

Scattered radiation was investigated from sources at the centre of spheres of 10, 15 and 20 cm radius, using magnetic tapes containing data on the interactions of photons of initial energies 80 and 140 keV.

The Klein-Nishina cross-section for the number of photons scattered with energies between $h\nu'$ and $(h\nu' + d(h\nu'))$ (Davisson and Evans, 1952) is proportional to the expression:

$$\left[\frac{h\nu}{h\nu'} + \frac{h\nu'}{h\nu} - \frac{2h\nu}{a} \left(\frac{1}{h\nu'} - \frac{1}{h\nu} \right) + \left(\frac{h\nu}{a} \right)^2 \left(\frac{1}{h\nu'} - \frac{1}{h\nu} \right)^2 \right]$$

This function has been plotted in fig. 6.7 for initial photon energies of 80 and 140 keV. The spectra of photons emitted from the surfaces of spheres containing a point source at the centre differ from the Klein-Nishina distribution partly because of the inclusion of photons which have undergone more than one interaction, that is, multiply scattered photons. In addition, photons which have been scattered through large angles have a higher probability of

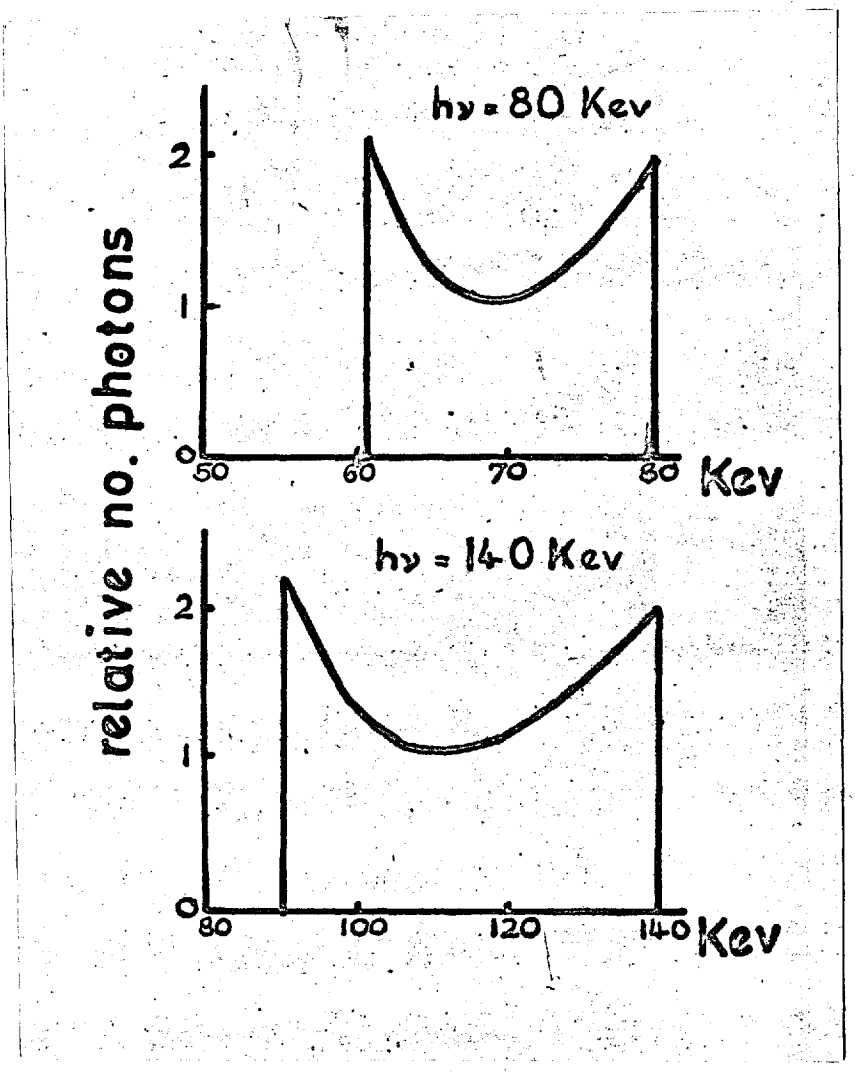

Fig. 6.7 The Klein-Nishina distribution of scattered photons for initial energies of 80 and 140 keV.

total absorption because of their lower energies and because their path lengths in the sphere have been increased. This latter effect tends to bias the distribution towards high energies.

Figure 6.8 shows the results of calculations of theoretical spectra for a point source of 80 keV radiation at the centre of a 10 cm tissue sphere. The histograms are for scattered photons within four ranges of angles to the normal to the surface. The solid lines show the total numbers of scattered photons and the shaded regions show the contribution of photons which have undergone only one interaction. Fewer scattered photons emerge at large angles to the normal and the proportion of singly scattered radiation decreases.

In order to apply the theoretical results to collimator theory, one should consider the number of photons emitted within a specified angle to the normal rather than the number emitted within specified angular intervals. Figures 6.9 and 6.10 show the spectra of scattered radiation emitted within the stated angles to the normal, for point sources of 80 keV and 140 keV radiation at the centre of a 10 cm radius sphere. The majority of radiation scattered within small angles to the normal has undergone only one interaction,

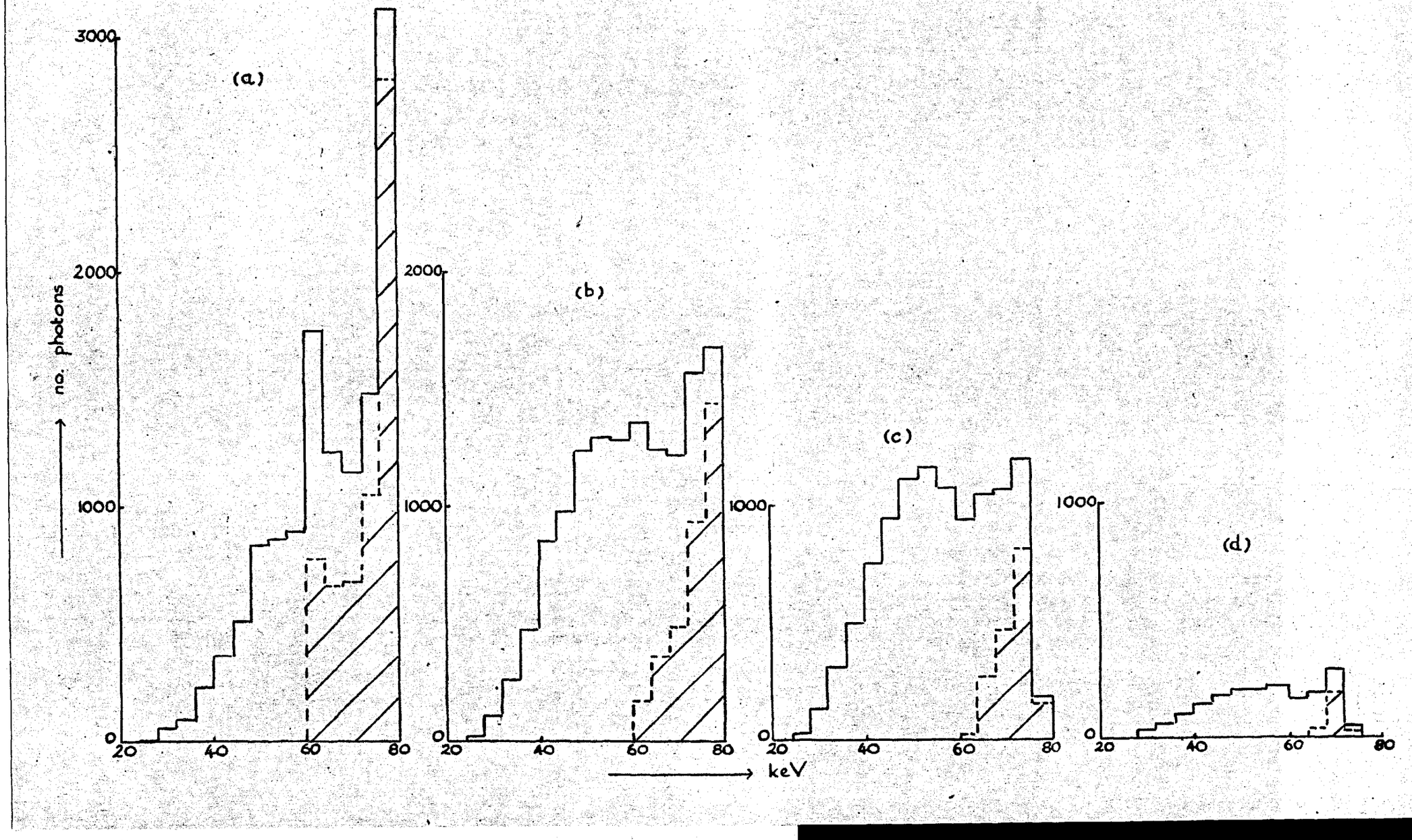

Fig. 6.8 Theoretical spectra of scattered radiation at the surface of a 10 cm sphere of tissue containing a point source of 80 keV radiation at the centre. Spectra are shown for radiation emitted within the following angles to the normal to the surface (a) 0 - 17.5°, (b) 17.5° - 36.9°, (c) 36.9° - 64.1° and (d) 64.1° - 90°.

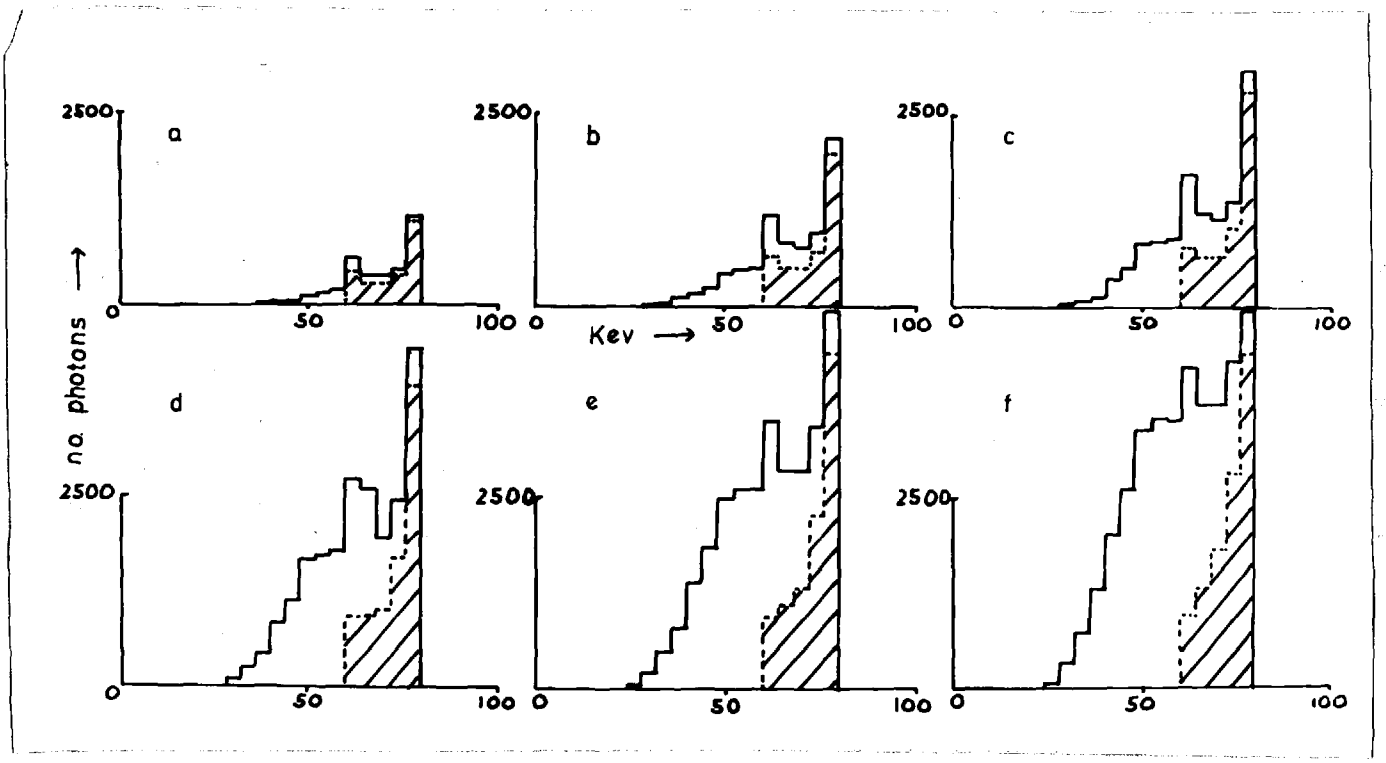

Fig. 6.9 Theoretical spectra of scattered photons emitted from a 10 cm radius sphere when a point source of 80 keV radiation is situated at the centre. The spectra are for all photons emitted within the following angles to the normal (a) 5.7°, (b) 11.5°, (c) 17.5°, (d) 30°, (e) 44.4° and (f) 90°.

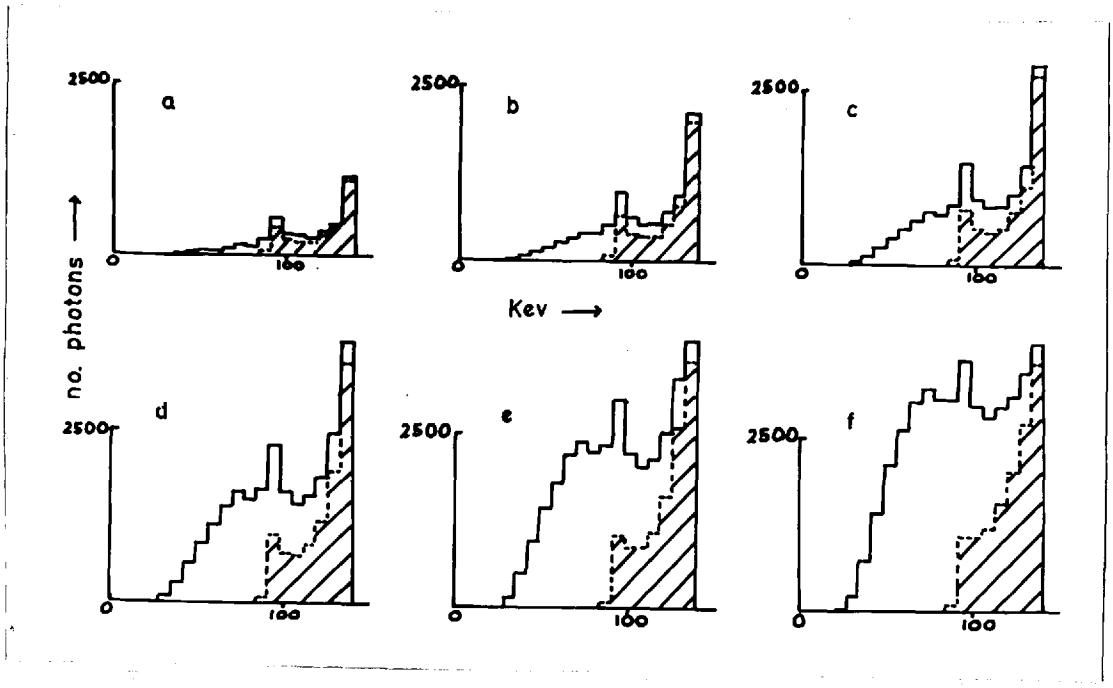

Fig. 6.10 Theoretical spectra of scattered photons emitted from a 10 cm radius sphere of tissue when a point source of 140 keV radiation is situated at the centre. Angles as for fig. 6.9.

probably because it is unlikely for a photon to undergo two or more interactions with only a small change in direction. Within greater angles to the normal, the spectra include a large proportion of lower energy photons which have been multiply scattered.

Figure 6.11 shows spectra of scattered radiation from a point source of 140 keV radiation at the centre of a 20 cm sphere. There is significantly more multiply scattered radiation than from a source in a 10 cm sphere (fig. 6.10) especially when radiation at large angles to the normal is included. This multiple scattering gives rise to a scatter peak at approximately 60 keV.

Figure 6.12 shows spectra from point sources of 80 keV radiation at the centre of 10, 15 and 20 cm spheres. The angular intervals 0° - 11.5° and 0° - 90° are shown. As demonstrated for 140 keV radiation, an increase in the sphere size leads to a marked increase in the amount of multiply scattered radiation. In this case, a multiple scatter peak occurs at about 50 keV. As these histograms were obtained using the same initial number of photons, they show that the total amount of scattered radiation decreases as the sphere size is increased owing to the greater probability of absorption. The number of photons which

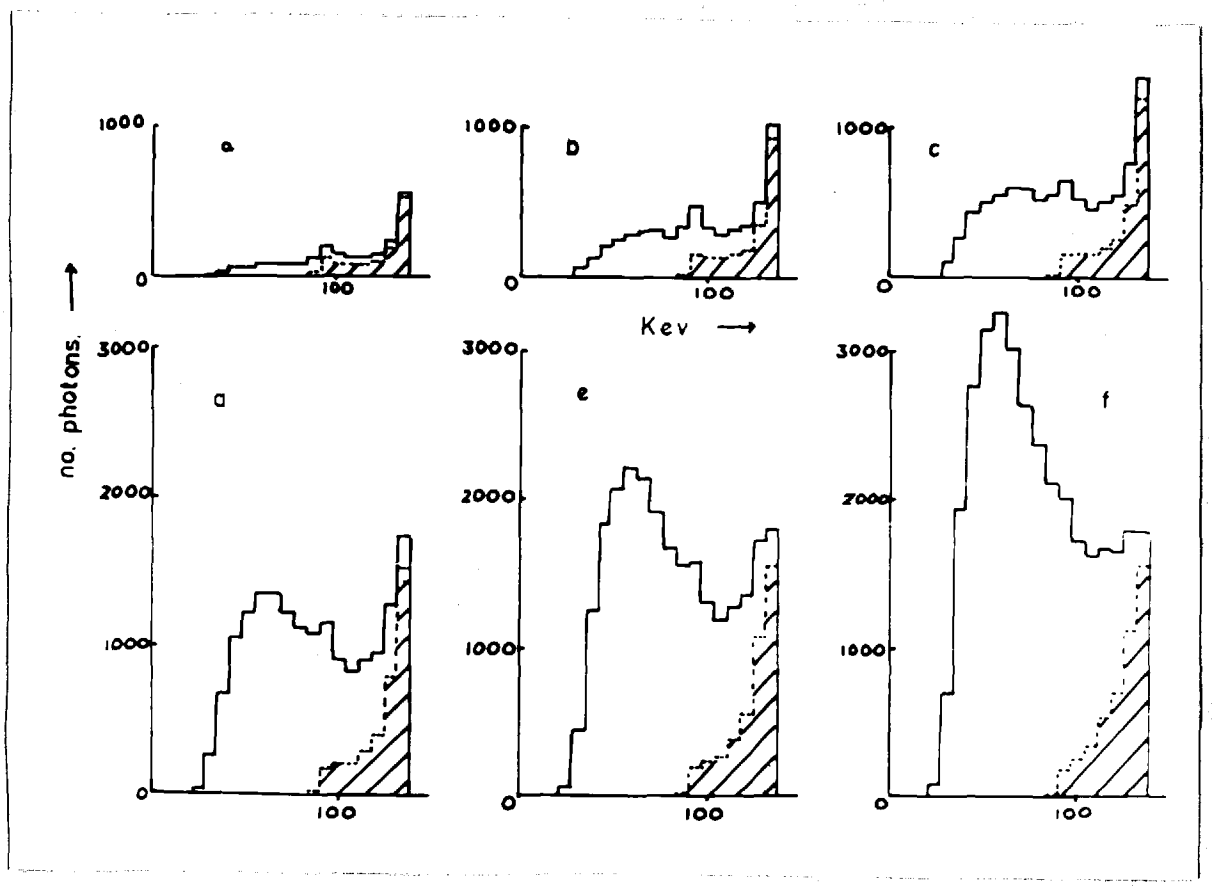

Fig. 6.11 Theoretical spectra of scattered photons emitted from a 20 cm radius sphere of tissue when a point source of 140 keV radiation is situated at the centre. Angles as for fig. 6.9.

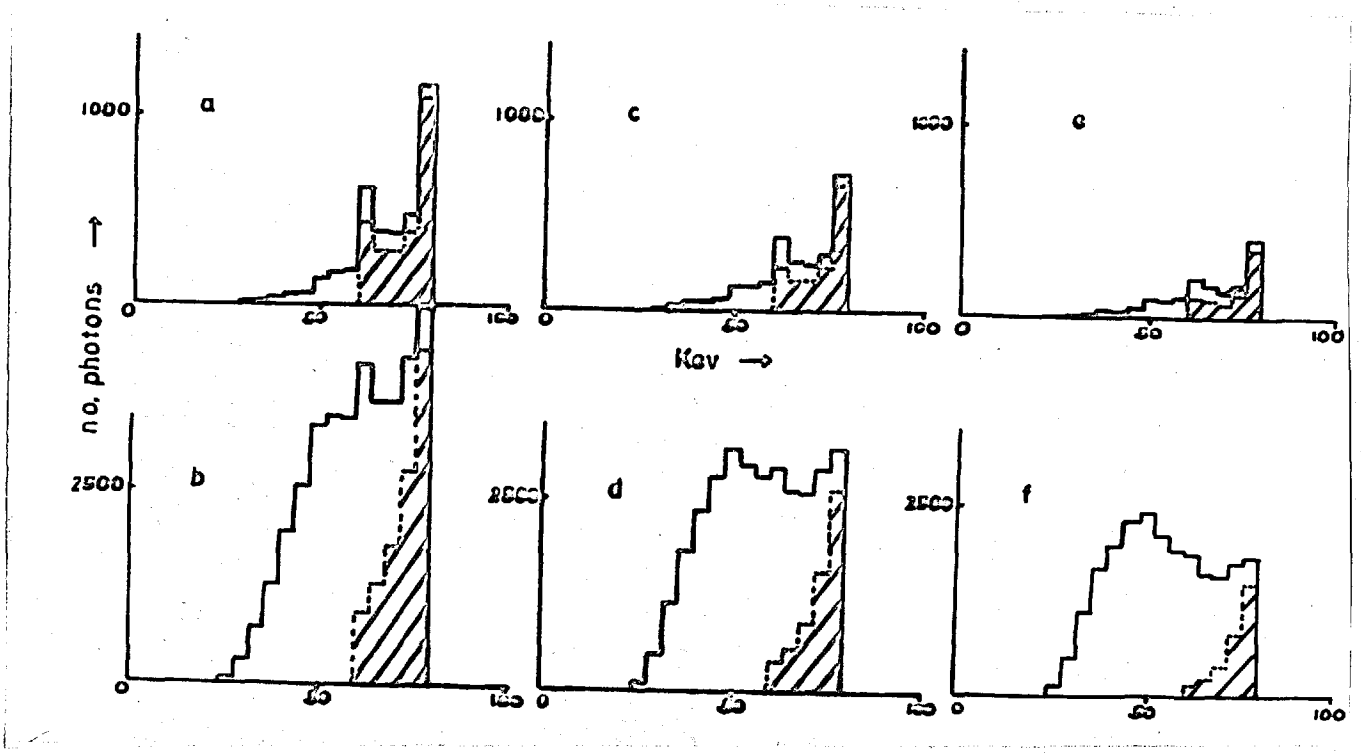

Fig. 6.12 Theoretical spectra of scattered photons emitted from 10 cm (a and b), 15 cm (c and d) and 20 cm (e and f) radius spheres of tissue when a point source of 80 keV radiation is situated at the centre. All photons emitted within the following angles to the normal are included (a, c and e) 11.5°, (b,d and f) 90°.

emerge from the sphere without undergoing an interaction also decreases and the scatter fractions (number of scattered photons divided by the number which undergo no interaction) show an increase with depth.

6.6 Interpretation of theoretical results

The spectrum of output pulses from a collimated scintillation detector differs from the spectrum of radiation emitted at all angles from the surface of the subject in two main ways; firstly, the collimator allows radiation emitted within only small angles to the normal to the surface to be incident on the detector; and secondly, the 'collimated' spectrum is smoothed by the finite energy resolution of the detector. Beck (1968) has suggested a method for allowing for the latter effect. A correction was not however attempted since the error introduced by neglecting it was likely to be small compared with the error introduced by allowing for the effect of the collimator.

Point source scatter fractions

The spectrum and amount of scattered radiation incident on a collimated detector is the sum of contributions from all parts of the surface of the subject within the field

of view of the collimator. These contributions are different from each point on the surface and hence the accurate calculation of spectra and scatter fractions is extremely complex.

In this work, scatter fractions have been calculated using a simplified technique in which it has been assumed that there is some limiting angle to the normal to the surface inside which all scattered radiation has equal probability of detection and outside which no radiation is detectable. This limiting angle has been found by considering the resolution curve at the distance of the surface from the collimator. The height of the curve at any point represents the probability of detection and therefore the mean height of the curve in revolution gives the mean probability. Assuming that the resolution curve approximates to a Gaussian distribution, the mean probability equals half the axial probability, i.e., $\epsilon_T/2$ where ϵ_T is the axial efficiency. The mean probability of detection can also be expressed as the fraction of the solid angle subtended by the mean detector area exposed at a point on the surface, i.e.,

$$\frac{\epsilon_T}{2} = \frac{\pi x^2}{(a + t)^2} \times \frac{1}{4\pi} \qquad (6.1)$$

where x is the radius of the area and a is the distance from the collimator to the surface of the subject. The limiting angle to the normal at which radiation is incident is given by:

$$\tan \theta = \frac{x}{(a + t)}$$

Therefore, from equation (6.1), $\tan\theta = \sqrt{2 \epsilon_T}$. Using theoretical values for ϵ_T (equations 3.6 and 3.7) one obtains for the collimators used in the experimental work:

7-hole	:	$\theta = 2.1^\circ$
19-hole	:	$\theta = 4.1^\circ$
37-hole	:	$\theta = 5.3^\circ$
61-hole	:	$\theta = 5.4^\circ$

The scatter fractions for radiation emitted from a point on the surface within these angles to the normal represent the mean scatter fractions for radiation emitted from the whole surface.

The smallest angle to the normal for which theoretical results were obtained was 5.7°. The scatter fractions for radiation within this angle are given in fig. 6.13 as a function of the lower analyser setting, for point sources

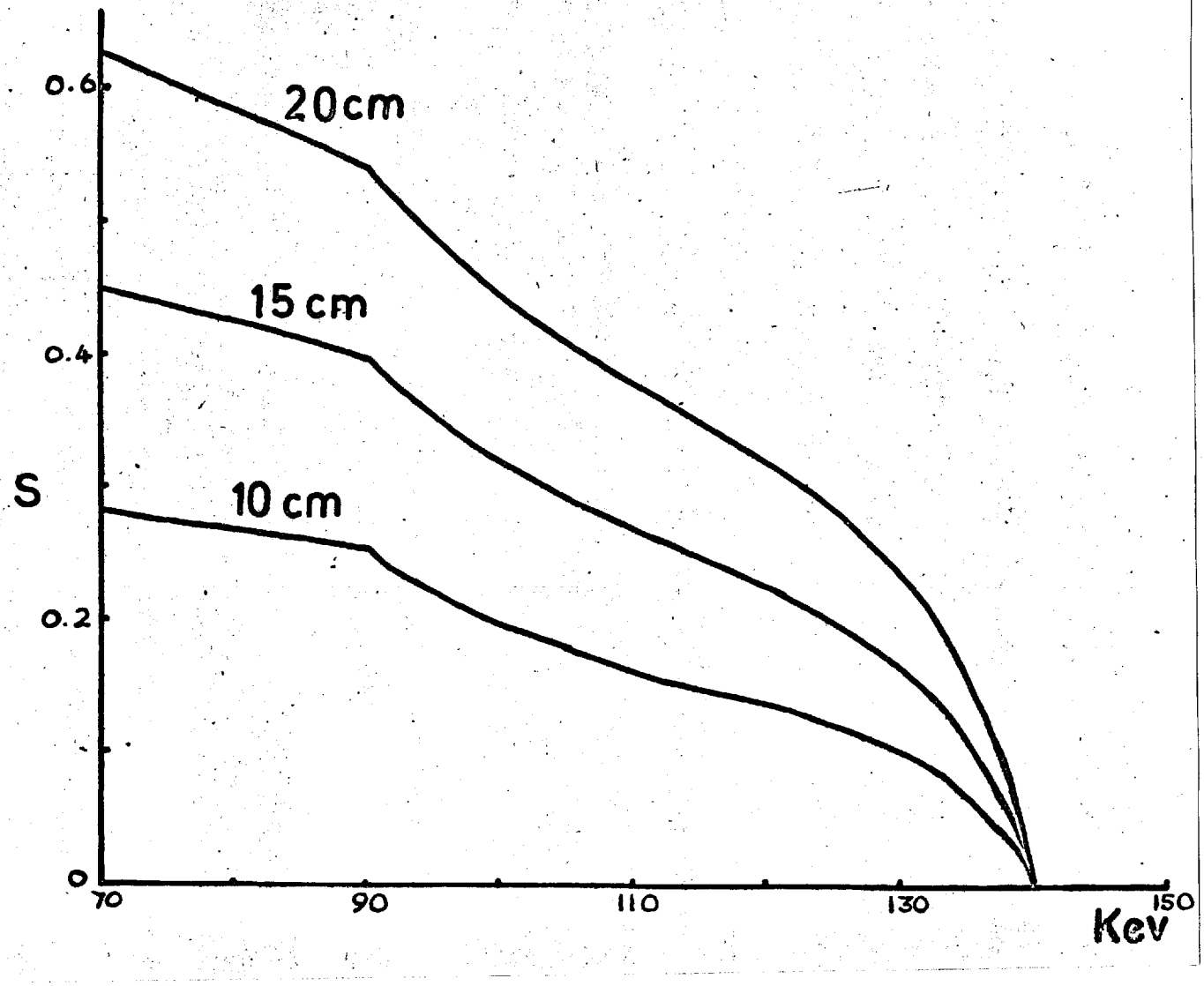

Fig. 6.13 Theoretical scatter fractions as a function of lower level analyser setting for point sources of 140 keV at the centre of 10, 15 and 20 cm radius spheres of tissue. Radiation scattered within 5.7° of the normal is included.

of 140 keV radiation at the centre of spheres of 10, 15 and 20 cm radius. The change in slope at 90.6 keV corresponds to the minimum energy of a scattered photon after one interaction (fig. 6.7). Since the dependence of the scatter fraction on the angle to the normal was not investigated for $\theta < 5.7^{\circ}$, theoretical point source scatter fractions for the collimators used in the experiments were obtained by multiplying the scatter fractions at 5.7° by the ratio $\theta/5.7$. The results of these calculations for 140 keV radiation are given in Table 6.3 with a comparison with experimental figures for Tc-99m at 12.5 cm from the collimator face, that is, at 10 cm depth corresponding to the results for the 10 cm sphere. Values are given for the whole photopeak and optimum analyser settings. The agreement between theoretical and experimental results is good considering the errors, approximations and assumptions involved. The theoretical figures confirm the experimental observation that the scatter fraction for a point source increases beyond 10 cm in depth. They also substantiate the experimental evidence that point source scatter fractions are smallest for the 7-hole collimator and increase in magnitude for the collimators with larger numbers of holes. In order to compare experimental results for Hg-197 (71 keV)

Table 6.3

Theoretical and experimental point source scatter fractions for 140 keV radiation

Lower level analyser window setting	90 keV				120 keV			
Distance from (air gap collimator 2.5 cm) face	12.5 cm		17.5 cm	22.5 cm	12.5 cm		17.5 cm	22.5 cm
No. of holes in collimator	Exp.	Theory			Exp.	Theory		
7	0.13	0.09	0.14	0.20	0.06	0.05	0.08	0.12
19	0.16	0.18	0.28	0.38	0.09	0.10	0.16	0.23
37	0.27	0.24	0.37	0.50	0.16	0.13	0.21	0.30
61	0.32	0.24	0.38	0.52	0.19	0.13	0.22	0.30

with the theoretical results for 80 keV radiation, it has been assumed that there is no difference in scattering at these two energies, and that the whole photopeak and optimum analyser settings for 80 keV radiation correspond to the same fraction of the photopeak energy as those for Hg-197, i.e., 40 and 57 keV. These results are given in Table 6.4 and show similar agreement to those for 140 keV radiation.

Plane and volume source scatter fractions

Lack of symmetry makes it difficult to obtain theoretical results on scattering from a volume source distribution within the limits of computer cost and running time. An attempt was therefore made to calculate approximate volume scatter fractions from the results on point sources which have already been described. This was done by first considering plane source scatter fractions.

Consider a plane source of radioactivity at a depth d in a tissue medium and let σ photons be emitted per cm^2 per minute from the plane (fig. 6.14). In order to calculate the number of unscattered photons passing through an element of area δA at the surface, consider the radiation emitted from the ring of width dx at a perpendicular distance x from the normal to the surface through δA. The number of

Table 6.4

Theoretical point source scatter fractions for 80 keV radiation and experimental values for Hg-197

Lower level analyser window setting	40 keV				57 keV			
Distance from (air gap collimator 2.5 cm)	12.5 cm		17.5 cm	22.5 cm	12.5 cm		17.5 cm	22.5 cm
Number of holes in collimator	Exp.(lower analyser setting 36 keV)	Theory			Exp.(lower analyser setting 51 keV)	Theory		
7		0.13	0.21	0.30		0.11	0.17	0.24
19	0.20	0.25	0.41	0.60	0.10	0.22	0.34	0.48
37	0.29	0.33	0.53	0.78	0.17	0.29	0.44	0.62
61	0.33	0.34	0.54	0.80	0.21	0.30	0.45	0.64

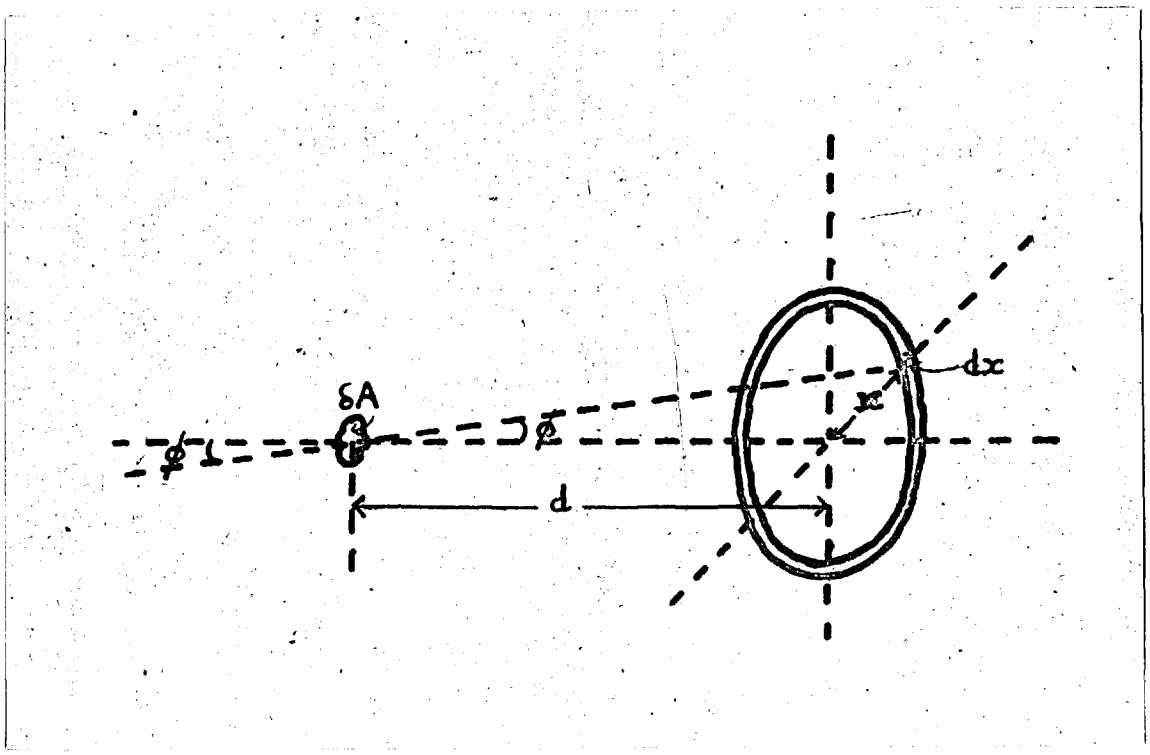

Fig. 6.14 To illustrate the calculation of plane source scatter fractions.

photons emitted from the ring = $2\pi x dx \times \sigma$. Therefore the number of unscattered photons passing through δA

$$= \frac{\delta A \cos \phi}{4\pi(d^2+x^2)} \times 2\pi x dx \times \sigma \times e^{-\mu \sqrt{d^2+x^2}}$$

where $\tan \phi = \frac{x}{d}$ and μ is the linear absorption coefficient of the medium. These photons will pass through the area at the angle ϕ to the normal to the surface. Using the concept of the limiting angle θ, developed in the earlier part of the section, the total number of unscattered photons passing through δA within the limiting angle

$$= \int_0^{d\tan\theta} \frac{\delta A \cos\phi}{4\pi(d^2+x^2)} \times 2\pi x dx \times \sigma \times e^{-\mu \sqrt{d^2+x^2}}$$

$$= \frac{\delta A \, \sigma \, d}{2} \int_0^{d\tan\theta} e^{-\mu \sqrt{d^2+x^2}} \frac{x}{(d^2+x^2)^{3/2}} dx \qquad (6.2)$$

When $x > d\tan\theta$, although no unscattered photons can pass through δA within the limiting angle, scattered photons may still enter the collimator. Let $S(\phi)$ be the scatter fraction per unit solid angle for radiation emitted normal to the surface, that is, at an angle ϕ to the direction of

unscattered radiation (fig. 6.14). Then, when the angle θ is small, the number of photons emitted from the elemental ring, which pass through δA within the limiting angle after being scattered

$$= S(\phi) \times \frac{\delta A \cos\phi}{4\pi(d^2+x^2)} \times 2\pi x dx \times \sigma \times e^{-\mu\sqrt{d^2+x^2}} \times \pi \tan^2\theta$$

The total number of scattered photons emitted from the plane which pass within the angle θ to the normal is therefore:

$$\frac{\delta A \sigma \, d\pi \tan^2\theta}{2} \int_0^\infty S(\phi) \, e^{-\mu\sqrt{d^2+x^2}} \frac{x}{(d^2+x^2)^{3/2}} \, dx \qquad (6.3)$$

Using expressions (6.2) and (6.3), one obtains for the scatter fraction S for a plane source at depth d:

$$S = \frac{\pi \tan^2\theta \int_0^\infty S(\phi) e^{-\mu\sqrt{d^2+x^2}} \frac{x}{(d^2+x^2)^{3/2}} \, dx}{\int_0^{d\tan\theta} e^{-\mu\sqrt{d^2+x^2}} \frac{x}{(d^2+x^2)} \, dx} \qquad (6.4)$$

In order to simplify this expression for integration, several assumptions and approximations must be made. Since θ is small for the collimators used, the denominator may be

simplified giving for $x \ll d$,

$$\int_0^{d\tan\theta} e^{-\mu\sqrt{d^2+x^2}} \frac{x}{(d^2+x^2)}\,dx = \int_0^{d\tan\theta} e^{-\mu d} \frac{x}{d^3}\,dx$$

$$= e^{-\mu d} \frac{\tan^2\theta}{2d}$$

The function $S(\phi)$ can be approximately evaluated from the previous results if it is assumed that the scatter fractions for a source at depth $\sqrt{d^2+x^2}$ are the same as those for a source at depth d. The results of integration by hand using incremental steps showed that the majority of the scattered radiation arose from regions of the plane for which $x \ll d$ and for which the above assumption was valid. The contribution to scattered radiation decreased to 1 per cent at approximately x = 0.8d. It was found that the function $S(\phi)$ could be represented by two straight lines over the region x = 0 to x = d on a plot of log $[S(\phi)]$ against $\tan\phi$, i.e.,

$$S(\phi)_1 = S_{o_1} e^{-k_1 \tan\phi}$$

$$\text{and } S(\phi)_2 = S_{o_2} e^{-k_2 \tan\phi}$$

where S_o and k are constants. The integration of the numerator of equation (6.4) was therefore carried out in two parts using mean values of $x(\overline{x_1}$ and $\overline{x_2})$ over the two ranges of integration. These mean values were used in the expressions $e^{-\mu\sqrt{d^2+x^2}}$ and $(d^2+x^2)^{3/2}$ which were found to vary less rapidly with x than $S(\phi)$. Therefore,

$$S = \frac{2\pi d}{e^{-\mu d}}\left[\frac{e^{-\mu\sqrt{d^2+\bar{x}_1^2}}}{(d^2+\bar{x}_1^2)^{3/2}} S_{o_1}\int_0^{x_1} e^{-k_1\frac{x}{d}}\, x\, dx\right.$$

$$\left. + \frac{e^{-\mu\sqrt{d^2+\bar{x}_2^2}}}{(d^2+\bar{x}_2^2)^{3/2}} S_{o_2}\int_{x_1}^{x_2} e^{-k_2\frac{x}{d}}\, x\, dx\right]$$

$$= \frac{2\pi d}{e^{-\mu d}}\left[\frac{e^{-\mu\sqrt{d^2+\bar{x}_1^2}}}{(d^2+\bar{x}_1^2)^{3/2}} S_{o_1}\frac{d}{k_1}\left[e^{-k_1\frac{x}{d}}\left(x+\frac{d}{k_1}\right)\right]_{x_1}^{0}\right.$$

$$\left. + \frac{e^{-\mu\sqrt{d^2+\bar{x}_2^2}}}{(d^2+\bar{x}_2^2)^{3/2}} S_{o_2}\frac{d}{k_2}\left[e^{-k_2\frac{x}{d}}\left(x+\frac{d}{k_2}\right)\right]_{x_2}^{x_1}\right] \qquad (6.5)$$

This expression was evaluated for plane sources of 80 keV and 140 keV radiation at depths of 10, 15 and 20 cm. The results are shown for 80 keV radiation in fig. 6.15

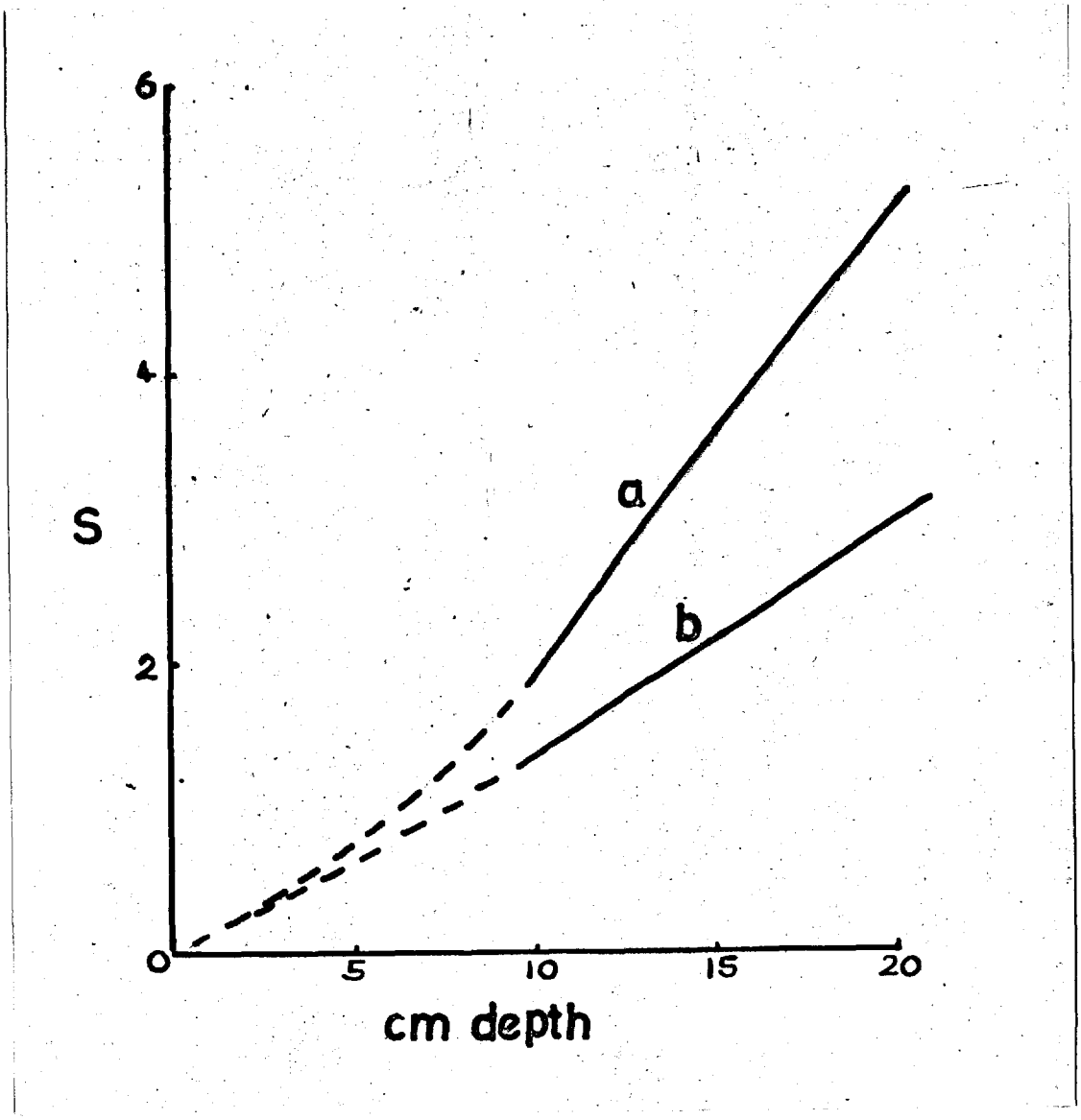

Fig. 6.15 Plane source scatter fractions for 80 keV radiation plotted against distance from the collimator face assuming an air gap of 2.5 cm. Curves are shown for lower level settings of the analyser of (a) 40 keV and (b) 57 keV.

where the scatter fraction is plotted against distance of the plane from the collimator face, for base line settings of 40 and 57 keV. The scatter fractions show a rapid increase with depth. Since equation (6.5) is independent of θ when θ is small, the same scatter fractions apply to all collimators used in the experiments.

In order to obtain volume source scatter fractions it is necessary to assume some relationship between the scatter fraction and depth of the plane. The simplest solution is to assume that the scatter fraction is linearly related to the depth of the source. Then $S = md$ where m is a constant. Since the counting rate from a plane at depth d is proportional to $\epsilon_{pl} e^{-\mu d}$ where ϵ_{pl} is the plane source efficiency, the volume scatter fraction is given by the expression:

$$S = \frac{\int_0^H \epsilon_{pl} \, e^{-\mu d} \, S \, d(d)}{\int_0^H \epsilon_{pl} \, e^{-\mu d} \, d(d)}$$

$$= m \left[\frac{1}{\mu} - \frac{H e^{-\mu H}}{(1-e^{-\mu H})} \right] \qquad (6.6)$$

where H is the volume thickness.

This expression was used to obtain the volume scatter fractions shown in Tables 6.5 and 6.6. The experimental values for Tc-99m (Tables 6.1 and 6.2) are higher than the theoretical values but this difference could be accounted for in several ways. The theoretical values were obtained using several assumptions and approximations which could incur considerable error. In particular, the assumption that the scatter fraction for a plane source is linearly dependent on depth is in doubt. No theoretical values were obtained for sources closer than 10 cm to the collimator and it is this region which probably contributes the majority of the volume source counting rate at these energies for which absorption is considerable. In addition, the theoretical results were obtained by assuming an infinite source whereas the experimental source was bounded laterally. This probably has a relatively small effect however as the majority of the scattered radiation is contributed from points near the axis of the collimator. The higher experimental values include the contribution of penetration and scattering from the collimator walls.

6.7 Summary

Point sources

Experimental and theoretical results show that the

Table 6.5

Theoretical plane and volume source scatter fractions for 80 keV radiation

Lower level analyser window setting	Plane source scatter fractions at given depths			Volume source scatter fraction for 15 cm wide source
	10 cm	15 cm	20 cm	
40 keV	1.92	3.62	5.20	1.00
57 keV	1.37	2.15	2.99	0.64

Table 6.6

Theoretical plane and volume source scatter fractions for 140 keV radiation

Lower level analyser window setting	Plane source scatter fractions at given depths			Volume source scatter fractions for 15 cm wide source
	10 cm	15 cm	20 cm	
91 keV	0.97	1.67	2.26	0.54
119 keV	0.50	0.75	1.12	0.26

amount of scattered radiation detected from a point source of radiation in a tissue medium tends to be greater for collimators with coarser resolution and shorter length. Experimental results indicate no definite trend in the variation of scatter fractions with sources up to 10 cm depth. At greater depths, both theoretical and experimental results indicate an increase in point source scatter fractions. The scattered radiation from a point source is probably primarily from photons which have undergone only one interaction with only a small change in direction and loss of energy. Point source scatter fractions show a decrease with increase in gamma-ray energy.

Volume sources

Experimental volume source scatter and penetration fractions are similar for all the collimators using Tc-99m and increase for collimators with larger numbers of holes using Hg-203. The theoretical work indicates that the volume scatter fractions should be independent of the collimator, provided its field of view is not too great. The experimentally observed variation for Hg-203 is probably due to the larger penetration and contributions for the collimators with more holes. Theoretical volume source scatter fractions

are lower than experimental values but the discrepancy is probably due to the approximations involved in the former calculations. Theoretically, volume source scatter fractions for 80 keV are significantly greater than those for 140 keV radiation which experimentally are slightly higher than those for 279 keV radiation. From the theoretical results, it is difficult to determine the probable spectrum from a volume source of radiation. However, since the plane source scatter fractions include a significant contribution from radiation scattered at $\tan\theta = 0.5$, it is reasonable to assume that volume source scatter fractions include a similar contribution. This would indicate (figs. 6.9 and 6.10) that multiply scattered radiation contributes significantly to the response.

6.8 Discussion

Beck (1968) has calculated optimum base line settings and volume source scatter fractions using a half-theoretical and half-experimental approach. He has estimated the contributions of scattered radiation by subtracting a smoothed Klein-Nishina distribution from an experimental volume source spectrum. The curves are matched at the base

of the photopeak, where it is assumed that the contribution of multiply scattered radiation, which has not been included, is negligible. The results obtained here suggest that even in this region, multiply scattered radiation has some effect and will introduce some error into his method. Based on the analysis described, Beck obtains optimum base-line settings of 126 keV and 254 keV for Tc-99m and Hg-203, using a 5" x 5" crystal. These values are higher than those obtained for the 3" x 1" crystals used in the present experiments (Table 6.2). Recently, experimental measurements on a 5" x 3" crystal at the Churchill Hospital, Oxford, gave a value of 115 keV for the optimum base-line setting for Tc-99m, again lower than Beck's figure. These differences are probably due to the different energy resolutions of the detectors. Since the experimental determination of optimum analyser settings can be carried out in a relatively short time, it is suggested that this simple method should be employed for all crystals and isotopes in use in a department.

In the same paper, Beck gives scatter fractions for a 16 cm volume source for different lower settings of the analyser (AS) as follows :

Tc-99m : AS = 106 keV, S = 0.68; AS = 126 keV, S = 0.38

Hg-203 : AS = 225 keV, S = 0.45; AS = 254 keV, S = 0.24

It is difficult to compare values for the optimum analyser settings (second results) because of the different energy resolution of the detector used by Beck. For the whole photopeak settings, the value for Tc-99m is similar to the value obtained theoretically in this work (0.54). The experimental values (Table 6.1) are however higher. The value for Hg-203 quoted by Beck is similar to the experimental value obtained here for the 7-hole collimator (Table 6.1). The larger experimental values for the other collimators are probably due to penetration. The values obtained in this work are therefore in reasonable agreement with those of Beck. The theoretical result derived here, that collimators of different designs have similar volume source scatter fractions, has been observed experimentally by Beck (1968).

CHAPTER 7

FINAL SUMMARY AND CONCLUSIONS

7.1 The theoretical evaluation of focusing collimators for scanning

Several important results have been obtained from the theoretical calculations on the effects of altering the parameters of focusing collimators. Firstly, although the collimator efficiency is higher for a larger crystal, the collimator figure of merit may be only slightly higher if the same variation in resolution is maintained. Secondly, there is a limit to the increase in efficiency which can be gained by increasing the number of holes of a collimator while decreasing the collimator length to maintain the same radius of the field of view and resolution in the focal plane. Increasing the number of holes has no significant effect on the figure of merit and leads to a wider variation in resolution. Thirdly, although increasing the focal length results in a small increase in point source efficiency at greater depths, the figure of merit for deeply-lying regions is not significantly increased when the focal length is increased beyond some limit.

The theoretical calculations have also shown that several aspects of collimator performance can be evaluated from the shape factor. Collimators with high shape factors have a wide variation in resolution with distance and are therefore only suitable for thin organs such as the thyroid. Collimators with smaller shape factors have more uniform resolution and are suitable for both thick and thin organs. Collimators with small shape factors also have a more uniform variation in axial efficiency with distance and therefore approach the ideal of uniform resolution and response over a large region more closely than collimators with high shape factors. The shape factor is large for collimators with a radius of field of view in the focal plane which is small relative to the crystal diameter. Shape factors are also large for short collimators with a large number of holes.

It has been shown that the probability of detection of regions of increased or decreased concentration, which are comparable or smaller in diameter than the field of view of the collimator, is proportional to the collimator figure of merit for a specified dose and scan time. Therefore these results suggest that, for the detection of small regions, there may be no advantage in using very large

crystals and large numbers of holes and that there may be some disadvantage owing to the wider variation in resolution. The higher efficiencies gained by using a large crystal or a collimator with more holes may in fact be misleading. The higher counting rates may seem to justify a reduction in dose or scan time and this may reduce the probability of detection below that for a smaller crystal, or for a collimator with fewer holes using a higher dose but obtaining the same counting rate.

For regions of increased or decreased concentration which are larger than the collimator field of view, it has been shown that the probability of detection is proportional to the plane source efficiency multiplied by a factor which allows for attenuation in tissue. Therefore, in these cases, larger crystals and collimators with greater numbers of holes may give improved detection.

These considerations are important when determining the relative merits of single and double headed detector systems with 3" and 5" crystals. The figures of merit for a single detector are higher than those of a double detector system, using the same size crystals, up to almost the centre of the body and then they are considerably lower. Therefore, for the detection of small regions, as already suggested,

the best procedure is undoubtedly to record the individual responses of the detectors of a double headed system and to play back the detector responses both individually and summed. A double detector system with 5" crystals may be slightly superior to one with 3" crystals as the figures of merit are higher near the centre of the body; they are however lower towards the front and back surfaces of the body. If recording is not possible, a double headed system with 5" crystals is probably the system of choice provided the low detection probabilities for superficial lesions can be tolerated. For the same total scan time, two views with a single 5" detector result in similar detection probabilities to one view with a double 3" detector system. A single 3" detector system gives a high probability for the detection of superficial regions but a low probability for central regions.

For large regions of increased or decreased concentration, double headed systems always have higher efficiencies and therefore give higher probabilities of detection than single detector systems using the same size crystal. Larger crystals give higher probabilities of detection than smaller crystals and therefore a double 5" crystal detector system is the most suitable under these conditions. Similar detection

probabilities can be obtained in the same total scan time from either two views with a single 5" detector or from one view with a double headed 3" detector system. A single 3" detector system gives relatively poor probabilities for the detection of large regions.

Therefore, when the detection of regions of increased or decreased concentration is the primary object of scanning, a double 5" detector system is probably the most suitable for all sizes of lesion. Single 5" detectors and double 3" detector systems are comparable in performance but give lower detection probabilities in the same total scan time. Although variation in resolution is of secondary importance to detection under these circumstances, the wider variation obtained with collimators for crystals greater than 5" in diameter is probably undesirable. When the concentrations in the subject being scanned are such that the probability of detection is very high, it may be important to have a uniform variation in efficiency and resolution with depth. Under these circumstances a 3" double detector system may be preferable to a 5" double detector system because of the smaller variation in resolution which can be obtained with suitable collimators.

7.2 The design of focusing collimators for scanning

Previous methods of focusing collimator design have been based on finding a collimator with a suitable shape factor which gives the highest plane source efficiency or point source efficiency in air at the focus, assuming that the optimum focal length is known. It has been shown here that it is important to consider both collimator figures of merit and efficiencies when determining the collimator which gives the highest probabilities of detection. The method of design presented is an improvement over previous methods of design because the most suitable collimator from the possible range is chosen by considering the variation in figure of merit and efficiency with depth under practical conditions. The thickness of septa required to limit penetration has been obtained using an equation derived by Beck (1964a), the validity of which has been established in the experimental work.

Results obtained with this design procedure show that long collimators are often required even at very low energies in order to limit the variation in resolution. These collimators limit septum penetration well and may often be the most suitable designs for much higher energies.

7.3 The effects of scattered radiation on focusing collimator performance

The experimental results for the efficiencies of point sources in air have shown that scattered radiation from the collimator walls may significantly increase the counting rate at small source to collimator distances. Differences between experiment and theory at small source to collimator distances have also been observed by Myhill (1961) and by Popovic and Mallard (1968) at 0.32 MeV and 0.36 MeV. These differences were attributed to penetration of the corners of septa, but the approximate calculations presented here suggest that they are more likely to be due to scattering from the collimator walls. Although the way in which the amount of scattered radiation depends on the collimator parameters and gamma-ray energy is complex, scattered radiation in general coarsens the resolution.

Scattered radiation from tissue has a two-fold effect on collimator performance; firstly, coarsening the resolution and secondly, decreasing the probability of detection. The way in which scattered radiation affects the probability of detection can be analysed with reference to equation (2.5). For a region of increased concentration, the target and non-

target counting rates are given by the expressions :

$$C_T = \rho_T E_T(1+S_T) + \rho_{NT}(E_{NT}-E_T) + \rho_{NT}E_{NT}S_{NT}$$

$$C_{NT} = \rho_{NT}E_{NT}(1+S_{NT})$$

The target counting rate includes the direct and scatter contributions from the target, the direct non-target contribution from all regions within the geometrical field of view except that occupied by the target, and the non-target scatter contribution from all regions assuming that it is not affected by the presence of the target. Equation (2.5) then gives :

$$\ell = \frac{\sqrt{T\rho_{NT}}E_T \left[\frac{\rho_T}{\rho_{NT}} (1+S_T) - 1 \right]}{\sqrt{2E_{NT}(1+S_{NT}) + E_T \left[\frac{\rho_T}{\rho_{NT}} (1+S_T) - 1 \right]}}$$

Since $E_T \left[\frac{\rho_T}{\rho_{NT}} (1+S_T)-1 \right] \ll 2E_{NT}(1+S_{NT})$ under conditions when the figure of merit is applied, the denominator may be simplified to give $\sqrt{2E_{NT}(1+S_{NT})}$. Therefore,

$$\ell = \frac{\sqrt{T\rho_{NT}}\left(\frac{\rho_T}{\rho_{NT}} - 1\right)E_T}{\sqrt{2E_{NT}}} \times \frac{\left[1 + \frac{\frac{\rho_T}{\rho_{NT}}}{\left(\frac{\rho_T}{\rho_{NT}} - 1\right)} S_T\right]}{\sqrt{1 + S_{NT}}} \qquad (7.1)$$

For a cold lesion, the target and non-target counting rates are given by the expressions :

$$C_T = \rho_{NT}(E_{NT} - E_T) + \rho_{NT}E_{NT}S_{NT}$$

$$C_{NT} = \rho_{NT}E_{NT}(1 + S_{NT})$$

Equation (2.5) then gives :

$$\ell = \sqrt{T} \times \sqrt{\rho_{NT}} \times \frac{E_T}{\sqrt{2E_{NT}(1+S_{NT}) - E_T}}$$

Assuming $E_T \ll 2E_{NT}(1+S_{NT})$

$$\ell = \sqrt{T}\sqrt{\rho_{NT}} \frac{E_T}{\sqrt{2E_{NT}}} \times \frac{1}{\sqrt{1 + S_{NT}}} \qquad (7.2)$$

Equations (7.1) and (7.2) show that for regions of both increased and decreased concentration, scattered radiation from the non-target region decreases the probability of detection. The factors by which theoretical figures of merit should be multiplied to allow for non-target scattering can be obtained from the experimental and theoretical results obtained in this work. For Hg-203, the non-target scatter fractions for the whole photopeak and optimum analyser settings are approximately 0.67 and 0.40, taking the experimental values for the 7-hole collimator which are less likely to include a contribution from penetration. For Tc-99m, the non-target scatter fractions are 1.20 and 0.60 taking the average experimental values. For Hg-197, since no reliable experimental values were obtained, one can assume values of 2.20 and 1.40, obtained by multiplying the theoretical values for 80 keV radiation by the ratio of the experimental and theoretical values for Tc-99m, thus allowing for the lower theoretical results. These figures result in the following multiplication factors for the theoretical figures of merit:

	Hg-203	Tc-99m	Hg-197
Whole photopeak	0.77	0.68	0.56
Optimum setting	0.84	0.79	0.65

The corrected figures of merit are directly applicable to the detection of regions of decreased concentration. For regions of increased concentration, they must be multiplied by a further factor to allow for scattered radiation from the region itself. When the target to non-target concentration ratio is 2 the corrected figures of merit are increased by a factor $(1 + 2S_T)$. Using the experimental results obtained here for point sources (Tables 6.1 and 6.2) at a depth of 7.5 cm, one obtains the following multiplication factors for the theoretical figures of merit.

	Hg-203	Tc-99m	Hg-197
Whole photopeak	0.84	0.78	0.67
Optimum setting	0.89	0.85	0.72

These are average values for the collimators used. The factors are greater for shorter collimators with coarser resolution and for greater depths of the source. They are also greater for smaller concentration ratios, but under these circumstances the probability of detection is very low since $\ell \ll 3$ (equation (7.1)). For larger concentration ratios the multiplication factors are smaller, reaching a limit between the two sets of correction factors.

Scatter fractions increase with increase in source size, and therefore the correction factors are larger for larger sources. The same values are probably approximately correct for double headed detector systems.

The increased scattering for large depths of the source is particularly advantageous for detection of regions of increased concentration using a single detector system, for which it is difficult to design a collimator with a high probability for the detection of deeply-lying lesions. Since however greater scattering from the target also leads to a greater loss in resolution it is doubtful whether high target scattering is a favourable property of a collimator. Since the scattering from the non-target volume is independent of the collimator and since the target scattering is probably similar for collimators of the same resolution, scattering does not invalidate the comparisons between collimators involved in the suggested design procedure.

These conclusions demonstrate that scattered radiation from the non-target region leads to a decreasing probability of detection as the gamma-ray energy is decreased. A relative improvement is gained however by using the optimum rather than the whole photopeak analyser settings. The

optimum settings are theoretically dependent on the amount of scattered radiation detected from the target but, since most of this scattered radiation lies within the photopeak, the effect is likely to be small.

7.4 The design of multichannel collimators for cameras

The designs of multichannel collimators giving the highest point source efficiency under specified conditions, and the methods by which they were obtained, have been published in detail in the paper 'The design of multichannel collimators for radioisotope cameras' (Kibby, 1969). Although the work described in this paper forms a significant part of the thesis, duplication was thought unnecessary and the reader is referred to the reprint bound at the end of the thesis. The work is summarised below.

It was necessary to develop two methods of collimator design based on slightly different definitions of resolution. For a collimator with a very large number of small cylindrical channels, even when a point source is a relatively small distance from the collimator, it is directly imaged in several channels. Therefore the resolution can be defined as the full width at half maximum of the curve obtained when

the point source efficiencies of consecutive channels are plotted against distance across the crystal. This definition of resolution was employed in the first method of design of lead collimators for energies below 0.3 MeV. At higher gamma-ray energies, it is necessary to increase the septum thickness and the collimator length in order to limit penetration of septa. This means that, even for quite large distances from the collimator, the source is mainly imaged in just one channel and hence the FWHM is difficult to interpret. Under these conditions it was assumed that two point sources are resolved if the total efficiencies of consecutive channels show a minimum when plotted against distance across the crystal. This definition of resolution was employed in the second method of collimator design for energies between 0.3 and 0.5 MeV.

The resolution and the minimum path length through one complete septum, which determines the amount of penetration, depend on the collimator length, the septum thickness and the channel radius. Therefore, if the collimator length is specified, the septum thickness and channel radius which give the required resolution and minimum path length can be calculated. In both methods of collimator design, total point source efficiencies were calculated for a range of

collimators of different lengths. The design giving the highest point source efficiency was thus found.

Since the point source efficiency is approximately independent of position in any plane parallel to the crystal face, and of distance from the collimator, the counting rate from a volume source is directly related to the counting rate from a point source. The probability of detection of a region of increased or decreased concentration, which is proportional to the target counting rate divided by the square root of the non-target counting rate, is therefore related to the point source efficiency. The collimator with the highest point source efficiency can therefore be assumed to give the highest probabilities of detection under the specified conditions.

The optimum collimator designs obtained using the first and second methods of design are reproduced in fig. 7.1 and fig. 7.2. The optimum collimator length was found to be independent of the required resolution. The channel radii (r) and septum thicknesses (s) are given for a resolution of 1 cm at 10 cm from the collimator, but, since they are directly proportional to resolution, they can be calculated for other resolutions. The total point source efficiency (ϵ_T) is also given for a resolution of 1 cm at 10 cm from

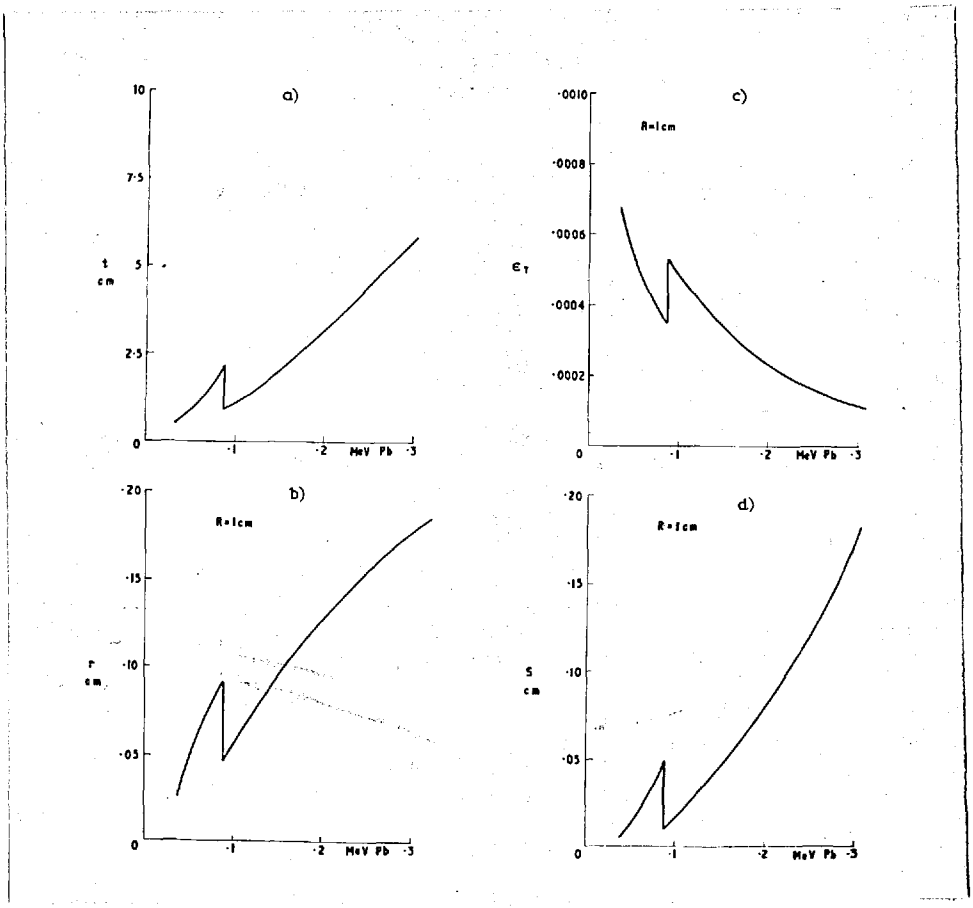

Fig. 7.1 Maximum efficiency lead collimator designs for photon energies below 0.3 MeV. The hole radii (r), septum thickness (s) and point source efficiencies (ϵ_T) are given for a resolution of 1 cm at 10 cm from the collimator face. The discontinuity at 0.088 MeV is due to the K-absorption edge for lead. t represents the collimator length.

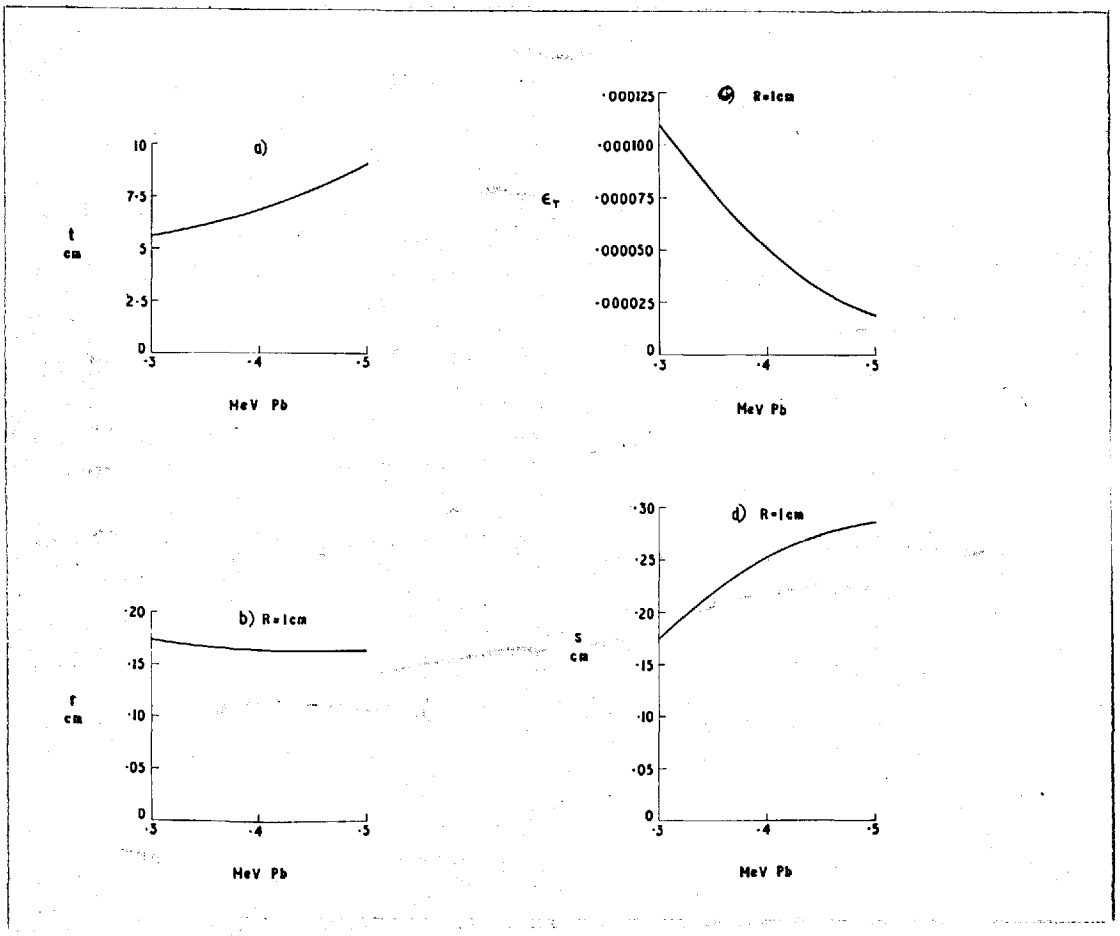

Fig. 7.2 Maximum efficiency lead collimator designs for photon energies between 0.3 and 0.5 MeV. The hole radii (r), septum thickness (s) and point source efficiencies (ϵ_T) are given for a resolution of 1 cm at 10 cm from the collimator face. t represents the collimator length.

the collimator face, but, since it is proportional to the square of the resolution, it can also be calculated for other resolutions. Although these results are based on a minimum path length through one complete septum of five mean free paths at the specified gamma-ray energy, they can be used to obtain the optimum collimator designs for different values of the minimum path length, and also for collimator materials other than lead. The optimum collimators all show a large increase in resolution with increase in distance from the collimator and in this type of design the resolution can only be made more uniform by using a collimator with a substantially lower efficiency.

Calculations of point source efficiency have shown that the approximate expression of Anger (1964) has an accuracy of ± 5% provided that the source is imaged in more than one channel. They have also shown that the formula for resolution derived by Anger can overestimate the FWHM by up to 15% under the same conditions. Keller (1968) has derived a method of multichannel collimator design based on Anger's equations and below 0.3 MeV his method gives similar collimators to those described here within the limits of accuracy described above. When the minimum path length through one complete septum is set to five mean free paths, more detailed

considerations of resolution are required above 0.3 MeV as explained above. The method of Keller is therefore no longer applicable.

The effect of the air gap between the crystal and the collimator has been ignored in this work. The air gap has a significant effect only for very short collimators for very low energies and leads to a slight broadening of the resolution and a slight decrease in efficiency.

7.5 Suggestions for further work

In this thesis, it has been assumed that the point source figure of merit is proportional to the probability of detection of regions of increased or decreased uptake which are comparable or smaller in diameter than the diameter of the field of view of the collimator (section 4.5). This was based on the fact that, when a spherical region of uniform concentration is viewed through a layer of tissue, the greatest increase or decrease in counting rate occurs opposite the centre of the region where it is of greatest thickness. It has also been assumed that the plane source efficiency is proportional to the probability of detection of regions which are much larger than the field of view of the collimator.

It would be interesting to confirm these assumptions by scanning a phantom containing different size lesions using two collimators, both having similar resolution and point source figures of merit, but one having a considerably higher plane source efficiency.

It would also be interesting to examine how the resolution of a double headed detector system is related to the resolution of the individual collimators and to determine the dependence of the resolution of a double headed system on attenuation in tissue.

A more complete analysis of tissue scattering for focusing collimators is required over a wider range of energies, and further investigation of the optimum analyser settings and their dependence on the energy resolution of the detector would be of value. It would also be interesting to examine the effects of scattered radiation on the response of camera systems.

ACKNOWLEDGEMENTS

I am indebted to Dr. Christine M.E. Matthews for her initial suggestion of this work, for her continued enthusiasm and encouragement, and for many valuable discussions. I am also indebted to my supervisor Dr. D.K. Bewley for many helpful discussions and for his advice and constructive criticism during the preparation of the manuscript. I should also like to thank Mr. D.D. Vonberg, the director of the MRC Cyclotron Unit, for his interest and for allowing the work to be done while employed by the Medical Research Council.

I am grateful to Mr. W. Verney and the members of the MRC Cyclotron Unit workshop staff for making the lead collimators and other parts of the experimental apparatus. I am also grateful to all the other members of the MRC Cyclotron Unit who have helped in numerous ways. I should like to thank Professor J.F. Fowler and the members of the Medical Physics Department at the Royal Postgraduate Medical School at Hammersmith Hospital who have helped through discussion, and in particular Dr. W.H. Ellett who initiated the theoretical work on scattering from tissue.

Finally, I should like to thank all those who encouraged

me to complete this work, particularly my parents, Mr. and Mrs. L.J. Kibby and my husband Dr. J.J. Davies.

REFERENCES

Anger, H.O. 1958 Rev. Sci. Instr. 29 (1), 27 Scintillation camera

Anger, H.O. 1964 J. Nucl. Med. 5, 515. Scintillation camera with multichannel collimators

Anger, H.O. 1966a J. Nucl. Med. 7, 331. Whole-body scanner Mark II (abstract)

Anger, H.O. 1966b ISA Trans. 5, 311. Survey of radioisotope cameras

Beck, R.N. 1961 J. Nucl. Med. 2, 314. A theoretical evaluation of brain scanning systems

Beck, R.N. 1964a Med. Radioisotope Scanning, Athens, I, 35. A theory of radioisotope scanning systems

Beck, R.N. 1964b Med. Radioisotope Scanning, Athens, I, 211. Collimators for radioisotope scanning systems.

Beck, R.N. 1966 ISA Trans. 5, 335. Radioisotope scanning systems

Beck, R.N. 1968 To be published. Effects of scattered radiation on scintillation detector response

Beck, R.N., Charleston, D.B., Eidelberg, P. and Harper, P.V 1967 J. Nucl. Med. 8, 1. The ACRH brain scanning system

Bell, T.K. and Johnston, A.R. 1968 Phys. Med. Biol. 13, 401. Penetration effects in wide aperture collimators

Bender, M.A. and Blau, M. 1962 Progress in Med. Radioisotope Scanning, Oak Ridge, 151. The autofluoroscope

Brownell, G.L. 1958 Int. J. appl. Radiat. Isotopes 3, 181. Theory of radioisotope scanning

Brownell, G.L. 1959 Med. Radioisotope Scanning, Vienna, 1. Theory of isotope scanning

Brownell, G.L. and Sweet, W.H. 1953 Nucleonics 11 (11), 40. Localization of brain tumours with positron emitters

Cassen, B. 1964 J. Nucl. Med. 5, 95. Theory of the performance characteristics of radioisotope distribution imaging systems

Concannon, J.P. and Bolhuis, F. 1957 Amer. J. Roent. 78 (5), 855. Studies with a modified collimator for use with a scintillation counter for total body scanning

Cradduck, T.D., Fedoruk, S.D. and Reid, W.B. 1966 Phys. Med. Biol. 11, 423. A new method of assessing the performance of scintillation cameras and scanners

Cradduck, T.D. 1968 J. Nucl. Med. 9, 210. Assessing the performance of radioisotope scanners; data acquisition

Dale, J.W.G. 1961 Int. J. appl. Radiat. Isotopes 10, 72 A beta-gamma ionisation chamber for substandards of radioactivity II Instrument response to gamma radiation

Dale, J.W.G., Perry, W.E. and Pulfer, R.F. 1961 Int. J. appl. Radiat. Isotopes 10, 65. A beta-gamma ionisation chamber for substandards of radioactivity I. Uses and calibration.

Davis, T.P. and Martone, R.J. 1966 J. Nucl. Med. 7, 114 The hybrid radioisotope scanner

Davisson, C.M. and Evans, R.D. 1952 Rev. mod. Phys. 24 (2), 79 Gamma-ray absorption coefficients

Dewey, W.C. and Sinclair, W.K. 1961 Int. J. appl. Radiat. Isotopes 10, 1. Criteria for evaluating collimators used in 'in vivo' distribution

studies with radioisotopes

Does de Bye, J.A.W. van der 1956 Nucleonics 14 (11), 128 Analysis of the scintiscanning problem

Doust, C. and Simons, H.A.B. 1961 Phys. Med. Biol. 6, 271 The localisation of positron sources by coincidence counting

Ellett, W.H., Brownell, G.L., and Reddy, A.R. 1968 Phys. Med. Biol 13, 219. An assessment of Monte Carlo calculations to determine gamma ray dose from internal emitters

Ephraim, K.H. 1962 Amer. J. Roent. 87, 141 Detection of liver tumours with colloidal radiogold

Ephraim, K.H. 1964 Med. Radioisotope Scanning. Athens, I 291. Clinical photoscintillography, technique and applications

Francis, J.E., Harris, C.C. and Bell, P.R. 1962 J. Nucl. Med. 3, 10. A focusing collimator for research in scanning

Garrett, M.W. 1954 Rev. Sci. Instr. 25 (12), 1208. Solid angle subtended by a circular aperture

Gopala Rao, U.V. and Wagner, H.N. 1968 Radiology 90, 14 Plane spread-functions in radioisotope scanning

Griffith, M.A., Goland P.P. and Chamberlain, R.H. 1950 Nucleonics 6 (4), 37. Localisation of radioactive materials in the phantom brain

Harris, C.C., Bell, P.R., Francis, J.E., Satterfield, M.M., Jordan, J.C. and Murray, J.P. 1962. Progress in Med. Radioisotope Scanning, Oak Ridge, 25 Collimators for radioisotope scanning

Harris, C.C., Jordan, J.C., Satterfield, M.M., Goodrich, J.K., Stone, H.L. and Hill, R 1964. J. Nucl. Med. 5, 653. A collimator for scanning with low-energy photons

Haybittle, J.L. 1966 Phys. Med. Biol. 11, 474. The quantitative analysis of cerebral scintiscans

Hindel, R. and Gilson, A.J. 1967 Nucleonics 25 (3), 52 Multicrystal scanner is rapid and versatile

Hine, G.J. 1967 Int. J. appl. Radiat. Isotopes 18, 815 Evaluation of focused collimator performance II Digital recording of line-source response

Höfer, R. and Roszuczky, A. 1964 Med. Radioisotope Scanning, Athens, I, 233. Construction of a

high-efficiency low energy collimator

Horwitz, N.H., Lofstrom, J.E. and Forsaith, A.L. 1965 J. Nucl. Med. 6, 724. The Spintharicon: a new approach to radiation imaging

Kakehi, H. 1959 Med. Radioisotope Scanning, Vienna, 13 Problems of collimation

Keller, E.L. 1968 J. Nucl. Med. 9, 233. Optimum dimensions of parallel hole, multi-aperture collimators for gamma-ray cameras

Kellershohn, C., Desgrez, A. and Lansiart, A. 1964 Medical Radioisotope Scanning, Athens, I, 333 Deux nouveaux types de détecteur pour caméra a rayons X ou γ

Kibby, P.M. 1969 Br. J. Radiol. 42, 91. The design of multichannel collimators for radioisotope cameras

Kibby, P.M. To be published Int. J. appl. Radiat. Isotopes Single and double headed detector systems for scanning (Letter to Editor)

Kuhl, D.E. 1964 Med. Radioisotope Scanning, Athens, I, 273 A clinical radioisotope scanner for cylindrical and section scanning

Kuhl, D.E. 1965 Phys. Med. Biol. 10, 93. Influence of collimator design, photon energy and radiation dose on detection effectiveness in liver scanning

Libby, R.L. 1964 J. Nucl. Med., 5, 887. Statistical evaluation of ^{125}I versus ^{131}I for scanning of cold lesions

Love, W.D. and Smith, R.O. 1966 J. Nucl. Med., 7, 781 Focusing collimators for use with the hard gamma-emitters rubidium - 86 and potassium - 42

Mallard, J.R. and Myers, M.J. 1963, Phys.Med. Biol., 8, 165 The performance of a gamma-camera for the visualisation of radioactive isotopes 'in vivo'

Mallard, J.R. and Wilks, R.J. 1968. J. Nucl. Med., 9, 96 Characteristics of display systems in scanning and a simple phantom procedure to evaluate over-all scanner performance

Marvin, J.F. and Moore, G.E. 1948 Nucleonics, 3(4), 63 Localisation of brain tumours with radiodyes

Mather, R.L. 1957 J. Appl. Phys. 28, 1200. Gamma-ray collimator penetration and scattering effects

Matthews, C.M.E. 1965 J. Nucl. Med., 6, 155
Comparison of isotopes for scanning

Matthews, C.M.E. 1967 Acta Radiol. 6, 464
Collimators and counting systems for brain scanning

Matthews, C.M.E. 1968 Phys. Med. Biol. 13, 118
The use of "figure of merit" for collimators (Letter to Editor)

Matthews, C.M.E. and Kibby, P.M. 1968 Br. J. Radiol., 41, 580. The effect of collimator resolution on the detection of lesions in brain scanning

McAfee, J.G., Mozley, J.M., Natarajan, T.K., Fueger, G.F. and Wagner, H.N. 1966 J. Nucl. Med., 7, 521
Scintillation scanning with an eight-inch diameter sodium iodide (Tl) crystal

Myers, M.J. and Mallard, J.R. 1964 Int. J. appl. Radiat. Isotopes 15, 725. Some long focusing "depth independent" collimators for 'in vivo' radioisotope scanning

Myhill, J. 1961 Int. J. appl. Radiat. Isotopes 12, 10
Theory of multichannel collimated scintillation detectors

Newell, R.R., Saunders, W. and Miller, E. 1952 Nucleonics 10 (7), 36. Multichannel gamma-ray collimators

Peřinová, V. and Hušák, V. 1967 Phys. Med. Biol. 12, 333 Remarks on the concept 'resolution' in scintillation scanning

Popovic, S. and Mallard, J.R. 1968 Int. J. appl. Radiat. Isotopes 19, 303. The longitudinal and lateral responses of multichannel focusing collimators

Popovic, S. and Fowler, J.F. 1968 Int. J. appl. Radiat. Isotopes 19, 313. The response of double-head and single head collimators for scanning

Rotenberg, A.D. and Johns, H.E. 1965 Phys. Med. Biol. 10, 51 Collimator efficiency and design I Collimator efficiency

Siegbahn, K. 1965 α, β and γ ray spectroscopy, Vol. I, North Holland Publ. Co., Amsterdam

Simons, H.A.B. 1962 Phys. Med. Biol. 6, 561 The calculation of gamma ray penetration of the walls of cylindrical and conical collimating holes

Simons, H.A.B. and Bailey, J.M. 1967 Phys. Med. Biol. 12, 29. An investigation into the usefulness of "figure of merit" as a criterion of a collimating system

Ter-Pogossian, M.M. and Eichlung, J.O. 1964 Med. Radioisotope Scanning, I, 411. Autofluorography with an X-ray image amplifier

Ter-Pogossian, M.M., Niklas, W.F., Bell, J. and Eichlung, J.O. 1966 Radiology, 86, 463. An image-tube scintillation camera for use with radioactive isotopes emitting low-energy photons

West, J.B. 1966 Phys. Med. Biol. 11, 357. Distribution of blood and gas in lungs

Westerman, B.R. and Glass, H.I. 1968 J. Nucl. Med. 9, 24 Physical specification of a gamma camera

Williams, A. and Birdseye, R.A. 1967 Int. J. appl. Radiat. Isotopes 18, 202. Calibration factors for the type 1383A β-γ ionization chamber for low energy γ-emitters

Vetter, H.G. 1967 Int. J. appl. Radiat. Isotopes 18, 231. Characterization of geometric imaging properties

of gamma-ray detectors

Vetter, H.G. 1967 Int. J. appl. Radiat. Isotopes 18, 237

A simple method to predict the resolution of a focused collimator at any depth.

APPENDIX 1

COMPUTER PROGRAM TO CALCULATE POINT SOURCE EFFICIENCIES IN AIR

This program calculates the total geometrical efficiency for a point source situated in air at any position in front of a focusing collimator. The position of the source relative to each hole of the collimator is found from the equations given in section 3.3 and the geometrical efficiency for each hole is calculated using equation 3.9. The efficiencies for the individual holes are then summed.

The dimensions of the collimator are specified in the input data and also the positions of the source for which calculations are required. The source positions are specified by three coordinates; the distance of the source from the collimator in the direction of the collimator axis, the distance of the source from the collimator axis, and the angular displacement of the source from a diagonal of the hexagon of holes. The distance of the source from the collimator axis is increased in steps of DELRAD

until it is greater or equal to SETRAD and then the distance is increased by twice DELRAD. In most cases it is not necessary to run the program for different angular displacements of the source. Thus ANGMIN can be set to zero and DELANG can be set greater than ANGMAX.

The output from the program consists of the title as input under 'instring', the dimensions of the collimator, and a matrix of total point source efficiencies in air for each angular displacement. The rows of the matrix correspond to increasing distances of the source from the collimator and the columns correspond to increasing distances of the source from the collimator axis.

```
PAUSE.CLEAR;

"BEGIN" "REAL" HRAD,SEPT,ANGMIN,DELANG,ANGMAX,RADMIN,DELRAD,RADMAX,
        SEGRAD,DISMIN,DELDIS,DISMAX,LENGTH,FOCAL,DIAM,FRAD,SHAPE,HDIST,ROOT,
        AREA,REFIG,A,B,C,P,V,Z;
"INTEGER" N,BIGN,NUMBER,NO,M,PRING,RING,SRG,MAXSEG,QMAX,EMAX,DMAX,
        O,R,D,I,J;
"REAL" "ARRAY" ANG[0:5],RAD[0:10],DIST[0:20],SUMEFF[0:5,0:10,0:20],
        X[0:10],Y[0:10],H[0:20],E[0:20],RS[0:20],RD[0:20],R[0:20],IGH[0:20];
"INTEGER" "ARRAY" F[0:100];
"SWITCH" SS:=L1,L2,L3,L4,L5,L6,L7,L8,L9,L10,L11;

"READ" NUMBER;
"FOR" NO:=1 "STEP" 1 "UNTIL" NUMBER "DO"
"BEGIN" M:=1;  INSTRING (F,M);  M:=1;  OUTSTRING (F,M);
        "READ" N,HRAD,SEPT,LENGTH,FOCAL,RIGN,DIAM,FRAD,ANGMIN,DELANG,ANGMAX,
                RADMIN,DELRAD,RADMAX,SEGRAD,DISMIN,DELDIS,
                DISMAX;
        MRING:=(N-1)/2;  Y[5]:=HRAD↑2;  Y[6]:=4*Y[5]↑2;  Y[7]:=3.141593*Y[5];
        SHAPE:=.208*(DIAM↑2)/((FRAD+2*HRAD)↑2);
        ANG[1]:=ANGMIN;  Q:=1;
        "FOR" Q:=Q+1 "WHILE" ANG[Q-1] "LE" ANGMAX "DO" ANG[Q]:=ANG[Q-1]+DELANG;  RAD[1]:=RADMIN;  B:=1;
        "FOR" B:=B+1 "WHILE" RAD[B-1] "LE" RADMAX "DO" "BEGIN";
                "IF" RAD[B-1]<SEGRAD "THEN" RAD[B]:=RAD[B-1]+DELRAD "ELSE" RAD[B]:=RAD[B-1]+2*DELRAD;  "END";
        DIST[1]:=DISMIN;  D:=1;
        "FOR" D:=D+1 "WHILE" DIST[D-1] "LE" (DISMAX+.1+DELDIS) "DO" "BEGIN"
                DIST[D]:=DIST[D-1]+DELDIS;  H[D-1]:=LENGTH/DIST[D-1];  K[D-1]:=(1+H[D-1])/(1+LENGTH/FOCAL);
                KS[D-1]:=K[D-1]↑2;  R[D-1]:=LENGTH+DIST[D-1];  RD[D-1]:=R[D-1]↑2;  KH[D-1]:=Y[5]*KS[D-1];
                "END";
```

```
        "END";
    "END";
"END"
```

```
        "ELSE" "BEGIN" "IF" I > (ENTIER(RING/2+.1)-1) "THEN" "GO TO" L9;
        HDIST:=(2*HRAD+SEPT)*(.75*RING↑2+I↑2)↑.5;
        "IF" I=0 "THEN" P:=.523599 "ELSE"
        P:=.523599-ARCCOS((RING↑2/(RING↑2+1.333333*
                I↑2))↑.5);
        J:=CHECKI(J+2);  "IF" ANG[Q]<.0000001 "THEN" "BEGIN" MAXSEG:=3;  M:=2;  "END";  "GO TO" L11;
```

```
    "END"
L9:RING:=CHECKI(RING+1);  "IF" ANG[Q]<.0000001 "THEN" MAXSEG:=4 "ELSE" MAXSEG:=6;
"IF" RING="LE" MRING "THEN" "GO TO" L1;
    DMAX:=D-1;  EMAX:=E-1;
"PRINT" "1,255 NO S7 CRYSTAL S4 RESOLUTION S4 FOCAL S5 COLLIMATOR S5 HOLE S7 SEPTUM S6 SHAPE";
"PRINT" "1,153 NODES S6 DIAMETER S4 DIAMETER S5 LENGTH S6 RADIUS S4 THICKNESS S5 FACTOR";
"PRINT" "1,152",SAMELINE,DIGITS(3),BIGN,"S2",ALIGNED(2,2),PREFIX("S6"),DIAM,FRAD,FOCAL,LENGTH;
"PRINT" PREFIX("S6"),ALIGNED(1,3),HRAD,SEPT,ALIGNED(2,2),SHAPE;
"FOR" Q:=1 "STEP" 1 "UNTIL" QMAX "DO"
"BEGIN" "PRINT" "1,S10 ANGLE =",SAMELINE,ALIGNED(1,3),ANG[Q];
        "PRINT" "1,S3 XATAL S20 RADIAL 1,S DISTANCE S17 DISTANCES 1,S10";
    "FOR" E:=1 "STEP" 1 "UNTIL" EMAX "DO"
    "PRINT" PREFIX("S2"),ALIGNED(1,3),RAD[E];
    "FOR" D:=1 "STEP" 1 "UNTIL" DMAX "DO"
    "BEGIN" "PRINT" "1,S2",ALIGNED(2,3),DIST[D],"S3";
        "FOR" E:=1 "STEP" 1 "UNTIL" EMAX "DO"
        "PRINT" SAMELINE,ALIGNED(0,6),SUMEFF[Q,E,D];
    "END";
"END";
"END"
```

```
HDIST:=.5*(2*HRAD+SEPT)*(3*RING↑2+J↑2)↑.5;
P:=.523599-ARCCOS((3*RING↑2/(3*RING↑2+J↑2))↑.5);
J:=CHECKI(J+2);  "IF" ANG[Q]<.0000001 "THEN" "BEGIN" MAXSEG:=3;  M:=2;  "END";  "GO TO" L11;
"END"
"ELSE" "BEGIN" "IF" I > (ENTIER(RING/2+.1)-1) "THEN" "GO TO" L9;
    HDIST:=(2*HRAD+SEPT)*(.75*RING↑2+I↑2)↑.5;
    "IF" I=0 "THEN" P:=.523599 "ELSE"
    P:=.523599-ARCCOS((RING↑2/(RING↑2+1.333333*I↑2))↑.5);
I:=CHECKI(I+1);  "IF" ANG[Q]<.0000001 "THEN" "BEGIN" MAXSEG:=3;  M:=2;  "END";  "GO TO" L11;
"END"
    "END";
L9:RING:=CHECKI(RING+1);  "IF" ANG[Q]<.0000001 "THEN" MAXSEG:=4 "ELSE" MAXSEG:=6;
"IF" RING="LE" MRING "THEN" "GO TO" L1;
    DMAX:=D-1;  EMAX:=E-1;
"PRINT" "1,255 NO S7 CRYSTAL S4 RESOLUTION S4 FOCAL S5 COLLIMATOR S5 HOLE S7 SEPTUM S6 SHAPE";
"PRINT" "1,153 NODES S6 DIAMETER S4 DIAMETER S5 LENGTH S6 RADIUS S4 THICKNESS S5 FACTOR";
"PRINT" "1,152",SAMELINE,DIGITS(3),BIGN,"S2",ALIGNED(2,2),PREFIX("S6"),DIAM,FRAD,FOCAL,LENGTH;
"PRINT" PREFIX("S6"),ALIGNED(1,3),HRAD,SEPT,ALIGNED(2,2),SHAPE;
"FOR" Q:=1 "STEP" 1 "UNTIL" QMAX "DO"
"BEGIN" "PRINT" "1,S10 ANGLE =",SAMELINE,ALIGNED(1,3),ANG[Q];
        "PRINT" "1,S3 XATAL S20 RADIAL 1,S DISTANCE S17 DISTANCES 1,S10";
    "FOR" E:=1 "STEP" 1 "UNTIL" EMAX "DO"
    "PRINT" PREFIX("S2"),ALIGNED(1,3),RAD[E];
    "FOR" D:=1 "STEP" 1 "UNTIL" DMAX "DO"
    "BEGIN" "PRINT" "1,S2",ALIGNED(2,3),DIST[D],"S3";
        "FOR" E:=1 "STEP" 1 "UNTIL" EMAX "DO"
        "PRINT" SAMELINE,ALIGNED(0,6),SUMEFF[Q,E,D];
    "END";
"END";
"END"
```

```
RING:=0;  MAXSEG:=0;
I4:I:=0;  J:=1;  HDIST:=PING*(2*HRAD+SEPT);  P:=0;  M:=1;  Q:=1;
L11:C:=HDIST;
    L2:SEG:=0;
    L4:E:=1;
L5:V:=RAD[E]*COS(SEG*1.047198+P-ANG[Q]);
Z:=RAD[E]*SIN(SEG*1.047198+P-ANG[Q]);
    D:=1;
L6:"IF" RING=0 "THEN"  SUMEFF[Q,E,D]:=0;  A:=ABS(Z*H[D]);
B:=K[D]*HDIST-V*H[D];
V[3]:=A↑2+(B-C)↑2;
ROOT:=Y[6]*KS[D]-(Y[5]*(KS[D]+1)-Y[3])↑2;
"IF" ROOT="LE" 0 "OR" X[3]<.0000001 "THEN" "BEGIN" "IF" SQRT(Y[3]) "GE" (HRAD*(1+K[D])) "THEN" "GO TO" L8
        "ELSE" "IF" X[D]<1 "THEN" AREA:=CHECKR(Y[7]*KS[D]);
        "GO TO" L7;
    "END";
ROOT:=SQRT(ROOT);
X[1]:=(B+C)/2+(Y[5]*(KS[D]-1)*(C-B)+A*ROOT)/(2*Y[3]);
X[2]:=(B+C)/2+(Y[5]*(KS[D]-1)*(C-B)-A*ROOT)/(2*Y[3]);
Y[1]:=A/2-(A*Y[5]*(KS[D]-1)-(C-B)*ROOT)/(2*Y[3]);
Y[2]:=A/2-(A*Y[5]*(KS[D]-1)+(C-B)*ROOT)/(2*Y[3]);
X[3]:=(X[1]-C)/HRAD;
X[4]:=(X[1]-B)/(HRAD*K[D]);
X[5]:=(X[2]-C)/HRAD;
X[6]:=(X[2]-B)/(HRAD*K[D]);
X[7]:=ARCSIN(X[3]);
X[8]:=ARCSIN(X[4]);
X[9]:=ARCSIN(X[5]);
X[10]:=ARCSIN(X[6]);
AREA:=CHECKR(Y[5]/2*(X[3]*SQRT(1-X[3]↑2)+X[7]-X[5]*
        SQRT(1-X[5]↑2)-X[9])+RH[D]/2*(X[4]*
        SQRT(1-X[4]↑2)+X[8]*SQRT(1-X[6]↑2)-X[10])
        -A↑2*ROOT/Y[3]);
L10: "IF" A < Y[2] "THEN" AREA:=AREA+CHECKR(KH[D]*(1.570796
        +X[6]*SQRT(1-X[6]↑2)+X[10]))
    "PLUS" "IF" Y[2] < 0 "THEN" AREA:=AREA+CHECKR(Y[5]
```

Input of data

*NUMBER

instring
*N
HEAD
SEPT
LENGTH
FOCAL
BIGN
DIAM
FRAD
ANGMIN
DELANG
ANGMAX
RADMIN
DELRAD
RADMAX
SETRAD
DISMIN
DELDIS
DISMAX

Notes

instring	title and other details required
ANGMIN	usually 0
ANGMAX	unnecessary to be greater than $\pi/6$ radians
RADMIN	usually 0
RADMAX	approximately equal to radius of the field of view at DISMAX

An asterisk denotes an integer variable.

Variables

A	Location for calculations
AREA	Location for calculations
ANG	Angle to a diagonal of hexagonal array
ANGMAX	Maximum angle to diagonal for which calculations required
ANGMIN	Minimum angle to diagonal for which calculations required
B	Location for calculations
BIGN	Number of holes in collimator (N)
C	HDIST
* D	Counter for DIST
DELANG	Increment in angle to diagonal
DELDIS	Increment in distance from collimator
DELRAD	Increment in distance from collimator axis
DIAM	Crystal diameter (D)
DISMAX	Maximum distance from collimator for which calculations required
DISMIN	Minimum distance from collimator for which calculations required
DIST	Distance from collimator
* DMAX	Maximum value of counter D
* E	Counter for RAD
EFFIC	Efficiency of individual hole
* EMAX	Maximum value of counter E
* F	Location reservation for title
FOCAL	Focal length (f)
FRAD	Radius of field of view in focal plane (R_f)
HRAD	Hole radius (r) at crystal face
HDIST	Distance of centre of base of hole from collimator axis
H	Location for calculations

*I	Counter
*J	Counter
K	Location for calculations
KS	Location for calculations
KH	Location for calculations
LENGTH	Collimator length
* M	Counter for string
* MRING	Maximum number of rings of holes in collimator
* MAXSEG	Maximum number of segments in hexagon
* N	Small n where $N = (3n^2 + 1)/4$
* NUMBER	Number of sets of data to be run
* NO	Counter for NUMBER
P	Angular displacement of hole from diagonal of hexagon (ϕ)
* Q	Counter for ANG
* QMAX	Maximum value of Q
RADMIN	Minimum distance from collimator axis
RADMAX	Maximum distance from collimator axis
ROOT	Location for calculations
* RING	Number of collimator ring
RAD	Distance from collimator axis
RD	Location for calculations
R	Location for calculations
SEPT	Septum thickness (s)
SETRAD	Distance at which DELRAD is doubled
SHAPE	Shape factor
* SEG	Counter for segment of hexagon
SUMEFF	Total point source efficiency

V	Position co-ordinate of source
X	Location for calculations
Y	Location for calculations
Z	Position co-ordinate of source

A P P E N D I X 2

COMPUTER PROGRAM FOR FOCUSING COLLIMATOR DESIGN

Details of this program are given in section 4.1 and a flow chart is given in fig. 4.1.

The output from the program contains the title as input under 'instring' followed by the collimator dimensions, the shape factor and the penetration fraction. If these quantities are all within the specified limits a matrix is output otherwise the words DIMENSIONS TOO LARGE are printed. The rows of the matrix correspond to increasing distances of the source from the collimator. The first column gives the point source efficiencies in air, the second column the efficiencies corrected for attenuation using LAMBDA(1) and the third column the collimator figures of merit. When a double detector system is specified, the following two columns contain the summed attenuated efficiencies and the figures of merit for both detectors. If more than one value of LAMDA is input, the second and further columns are repeated for the new attenuation factors.

```
PAMELB
PAMELB KIBBY CYCLOTRON UNIT;


"BEGIN" "REAL" DIAM,H2,D2,H4,HS,K2,HD2,HD4,FRAD,DISTA,DISTB,DISTC,DELH,GAP,PHANT,LLAMDA,HRAD,LENGTH,FOCAL,MSEPT,MINFOC,DELFOC,MAXFOC,MAXSHAPE,MAXLENGTH,MAXP,SETP,TRANS,PENET,GRAD,SEPT,
SHAPE,PEFFIC,PLEFFIC
,HDIST,SHRAD,DISTD,DISTE,K,AREA,EFFIC,BEFF,MAX;
      "INTEGER" M,NUMBER,Q,NO,DESIGN,LMAX,COUNT,GRAPH,N,BIGN,ENERGY,NMIN,DELN,NMAX,TIMES,T,D,MRING,RING,I,J,DMAX,L,F,FF,DZ,Z;
      "REAL" "ARRAY" DIST[0:50],SUMEFF[0:50],LAMDA[0:3],PLMERIT[0:3],AEFF[0:50,0:3],AMERIT[0:50,0:3],BMERIT[0:50,0:3],MAXMER[0:3],KI[0:50],KS[0:50];
      "INTEGER" "ARRAY" A[0:100];
      "SWITCH" SS:=NEXTNUMBER,L1,L3,L4,L5,L6,START,INCD,AGAIN,NEXTFOCAL,HIGHENERGY,DIMENSIONS,TEST,CONTINUE,NEXTDISTANCE,NEXTRING,CALCULATION,NEXTHOLE,TOTAL,INCREMENT,FINISH;

      "READ" NUMBER;
      "FOR" NO:=1 "STEP" 1 "UNTIL" NUMBER "DO"
      "BEGIN" M:=1;   INSTRING (A,M);   M:=1;   OUTSTRING (A,M);
            "READ" DESIGN,DIAM,FRAD,MSEPT,DISTA,DISTB,DISTC,GAP,PHANT,LLAMDA,LMAX,COUNT,GRAPH;
            "FOR" L:=1 "STEP" 1 "UNTIL" LMAX "DO" "READ" LAMDA[L];
      "IF" DESIGN=0 "THEN" "BEGIN" "COMMENT" DESIGN NOT REQUIRED;
                                          "READ" N,BIGN,HRAD,LENGTH,FOCAL;
                        "PRINT" ´´L1`COLLIMATOR DESIGN NOT NEEDED`;
                        ENERGY:=0;

                        "GO TO" DIMENSIONS;
                        "END";

      "COMMENT" DESIGN PROCEDURES;
      "READ" ENERGY,NMIN,DELN,NMAX,MINFOC,DELFOC,MAXFOC,MAXSHAPE,MAXLENGTH,MAXP;
      "IF" ENERGY=1 "THEN" "BEGIN" "READ" TIMES,SETP;
                           "PRINT" ´´L1`HIGH ENERGY DESIGN`;
                           "END"
                 "ELSE" "PRINT" ´´L1`LOW ENERGY DESIGN`;
     N:=NMIN;
NEXTNUMBER:BIGN:=(3*N↑2+1)/4;      FOCAL:=MINFOC;
NEXTFOCAL: T:=0;   HRAD:=FRAD*.5*(DIAM-MSEPT*(N-1))/(N*FRAD+MSEPT*(N-1));  Q:=0;
HIGHENERGY: LENGTH:=2*FOCAL*HRAD/FRAD;   DELH:=.5*DELH;
DIMENSIONS: H2:=HRAD↑2;  D2:=DIAM↑2;  H4:=H2↑2;   TRANS:=4*H2*BIGN/D2;
      PENET:=6*BIGN/(LLAMDA↑3*LENGTH↑3*(2+TRANS)*(1-TRANS)↑2*TRANS↑2);
      "IF" ENERGY=1 "THEN" "BEGIN" "IF" T=0 "THEN" "BEGIN"
TRANS:=.653;        LENGTH:=FOCAL*DIAM/FRAD*(TRANS/BIGN)↑.5;
      PENET:=6*BIGN/(LLAMDA↑3*LENGTH↑3*(2+TRANS)*(1-TRANS)↑2*TRANS↑2);  SHRAD:=FRAD*LENGTH/(FOCAL*2);
      "IF" PENET>SETP "THEN" "BEGIN" HRAD:=SHRAD;  H2:=HRAD↑2;  H4:=H2↑2;  "GO TO" CONTINUE;  "END";
      "IF" SHRAD>HRAD "THEN" "GO TO" L3 "ELSE" "GO TO " L4;  "END";
      "IF" Q=1 "THEN" "GO TO" L5 "ELSE" "GO TO" L6;
L4:DELH:=.5*(HRAD-SHRAD);  HRAD:=SHRAD;  Q:=1;  T:=0;
L5:T:=T+1;  "IF" T>TIMES "THEN" "GO TO" CONTINUE;
"IF" PENET>SETP "THEN" HRAD:=HRAD-DELH "ELSE" HRAD:=HRAD+DELH;
"GO TO" HIGHENERGY;
L3:DELH:=.5*SHRAD;  HRAD:=SHRAD;  T:=0;  Q:=0;  PENET:=.5*SETP;
L6:T:=T+1;  "IF" T>TIMES "THEN" "GO TO" CONTINUE;
"IF" PENET>SETP "THEN" HRAD:=HRAD+DELH "ELSE" HRAD:=HRAD-DELH;
"GO TO" HIGHENERGY;
                        "END";
CONTINUE: SEPT:=(DIAM-2*HRAD*N)/(N-1);      HS:=2*HRAD+SEPT;
      SHAPE:=.208*(D2)/((FRAD+2*HRAD)↑2);
      PEFFIC:=BIGN*(H2)/(4*(LENGTH+FOCAL)↑2);
      PLEFFIC:=(3.142*BIGN*FRAD↑4*H2)/(16*FOCAL↑2*(FRAD+2*HRAD)↑2);


      "PRINT" ´´L2S5`NO´S7`CRYSTAL´S4`RESOLUTION´S4`FOCAL´S5`COLLIMATOR´S5`HOLE´S7`SEPTUM´S6`SHAPE´S4`TRANSMISSION´S3`POINT´S7`PLANE´S5`PENETRATION´S2`NON-TARGET`;
      "PRINT" ´´L1S3`HOLES´S6`DIAMETER´S4`DIAMETER´S5`LENGTH´S6`LENGTH´S6`RADIUS´S4`THICKNESS´S5`FACTOR´S6`RATIO´S5`EFFICIENCY´S2`EFFICIENCY´S3`FRACTION´S3`EFFICIENCY`;
      "PRINT" ´´L1S2``,SAMELINE,DIGITS(3),BIGN,´´S2``,ALIGNED(2,2),PREFIX(´´S6``),DIAM,FRAD,FOCAL,LENGTH;
      "PRINT" PREFIX(´´S6``),ALIGNED(1,3),HRAD,SEPT,ALIGNED(2,2),SHAPE,ALIGNED (0,4),TRANS;
      "PRINT" PREFIX(´´S4``),ALIGNED(0,6),PEFFIC,PLEFFIC,PENET;

      "IF" DESIGN=1 "THEN" "BEGIN" "IF" SHAPE > MAXSHAPE "OR" LENGTH > MAXLENGTH "OR" PENET > MAXP "THEN" "BEGIN" "PRINT" ´´L1`DIMENSIONS TOO LARGE`;
                                    "GO TO" INCREMENT;
                                    "END";
                        "END";

      "COMMENT" CALCULATION OF EFFICIENCIES;
      D:=1;   DIST[D]:=DISTA;
L1: KI[D]:=(1+LENGTH/DIST[D])/(1+LENGTH/FOCAL);  KS[D]:=KI[D]↑2;
"IF" DIST[D]<FOCAL "THEN" SUMEFF[D]:=.25*H2/(LENGTH+DIST[D])↑2
  "ELSE" SUMEFF[D]:=.25*H2*KS[D]/(LENGTH+DIST[D])↑2;
D:=D+1;  DIST[D]:=DIST[D-1]+DISTB;
"IF" DISTC "GE" DIST[D] "THEN" "GO TO" L1;
   MRING:=(N-1) "DIV" 2;      RING:=0;
NEXTRING: RING:=RING+1;   "IF" RING > MRING "THEN" "GO TO" TOTAL;
      I:=0;   J:=1;   HDIST:=RING*HS;
START:D:=1;  HD2:=HDIST↑2;  HD4:=HD2↑2;
TEST:"IF" FOCAL > DIST[D] "THEN" "BEGIN" DISTD:=LENGTH*(HDIST-HRAD)/((HDIST+HRAD)*(1+LENGTH/FOCAL)-(HDIST-HRAD));
                                    "IF" DIST[D] < DISTD "THEN" "GO TO" INCD "ELSE" "GO TO" CALCULATION;
                              "END";
 DISTE:= LENGTH*(HDIST+HRAD)/((HDIST-HRAD)*(1+LENGTH/FOCAL)-(HDIST+HRAD));
                                    "IF" DISTE "GE" 0 "AND" DIST[D] > DISTE "THEN" "GO TO"INCD;

CALCULATION: K:=KI[D];  K2:=KS[D];
      AREA:=(2*HD2*H2*(1+K2)-HD4*(1-K)↑2-H4*(1+K)↑2)↑.5;
      "IF" DIST[D] < FOCAL "THEN" AREA:=1.571*H2*(1+K2)-(K-1)*AREA*.5-H2*CHECKR(ARCTAN((HD2*(K-1)-H2*(1+K))/AREA))-K2*H2*CHECKR(ARCTAN((HD2*(K-1)+H2*(1+
K))/ARAA))
                        "ELSE" AREA:=1.571*H2*(1+K2)-(1-K)*AREA*.5-H2*CHECKR(ARCTAN((HD2*(1-K)+H2*(1+K))/AREA))-K2*H2*CHECKR(ARCTAN((HD2*(1-K)-H2*(1+K))/AREA));
     EFFIC:=AREA*(DIST[D]+LENGTH)/((HDIST↑2+(DIST[D]+LENGTH)↑2)↑1.5*12.568);
      EFFIC:="IF" I "LE" 1 "AND" J=1 "THEN" (6*EFFIC) "ELSE" (12*EFFIC);
      SUMEFF[D]:=EFFIC+SUMEFF[D];
INCD:D:=D+1;  "IF" DISTC "GE" DIST[D] "THEN" "GO TO" TEST;

NEXTHOLE: "IF" RING > 1 "THEN" "BEGIN" "IF" (RING/2-RING "DIV" 2) > .1 "THEN"
"BEGIN" "IF" J > (RING-2) "THEN" "GO TO" NEXTRING;
      HDIST:=.5*HS*(3*RING↑2+J↑2)↑.5;
      J:=J+2;   "GO TO" START;
"END"
"ELSE" "BEGIN" "IF" I > (RING "DIV" 2-1) "THEN" "GO TO" NEXTRING;
          HDIST:=HS*(.75*RING↑2+I↑2)↑.5;
          I:=I+1;   "GO TO" START;
     "END";
                        "END";
      "GO TO" NEXTRING;



     "COMMENT" CALCULATION OF ATTENUATION;
TOTAL:DMAX:=D-1;         "FOR" L:=1 "STEP" 1 "UNTIL" LMAX "DO"
     "BEGIN"
           PLMERIT[L]:=PLEFFIC*(1-1/EXP(LAMDA[L]*PHANT))/LAMDA[L];
           "PRINT" SAMELINE,´´S4``,ALIGNED(0,6),PLMERIT[L];
           "FOR" D:=1 "STEP" 1 "UNTIL" DMAX "DO"
           "BEGIN" "IF" DIST[D] "LE" GAP "THEN" AEFF[D,L]:=SUMEFF[D]
      "ELSE" "IF" DIST[D] < (GAP+PHANT) "THEN" AEFF[D,L]:=SUMEFF[D]/EXP((DIST[D]-GAP)*LAMDA[L])
      "ELSE" AEFF[D,L]:=SUMEFF[D]/EXP(LAMDA[L]*PHANT);
       "END";
       "END";


       "COMMENT" PRINT OUT;
       "PRINT" ´´L2S28`ATTENUATED IN WATER PHANTOM  *  *  *  *  *´L1S17``;
       "FOR" L:=1 "STEP" 1 "UNTIL" LMAX "DO"
       "BEGIN" "PRINT" ´´S18`ONE COUNTER`;   MAXMER[L]:=0;
            "IF" COUNT=2 "THEN" "PRINT" ´´S18`TWO COUNTERS`;
       "END";
       "PRINT" ´´L1S1`DISTANCE´S4`EFFICIENCY´S1``;
       "FOR" L:=1 "STEP" 1 "UNTIL" (COUNT*LMAX) "DO" "PRINT" ´´S4`EFFICIENCY´S4`FIGURE MERIT`;
       "FOR" D:=1 "STEP" 1 "UNTIL" DMAX "DO"
       "BEGIN" "PRINT" ´´S2``,ALIGNED(2,2),DIST[D],SAMELINE,´´S7``,ALIGNED(0,6),SUMEFF[D];
            "FOR" L:=1 "STEP" 1 "UNTIL" LMAX "DO"
            "BEGIN" AMERIT[D,L]:=AEFF[D,L]/PLMERIT[L]↑.5;
                 "IF" AMERIT[D,L] > MAXMER[L] "THEN" MAXMER[L]:=AMERIT[D,L];
                 "PRINT" PREFIX(´´S7``),ALIGNED(0,6),AEFF[D,L],AMERIT[D,L];
                 "IF" COUNT=2 "THEN" "BEGIN" BEFF:=AEFF[D,L]+AEFF[(DMAX-D+1),L];
                                        BMERIT[D,L]:=BEFF/(2*PLMERIT[L])↑.5;
                 "IF" BMERIT[D,L] > MAXMER[L] "THEN" MAXMER[L]:=BMERIT[D,L];
"PRINT" PREFIX(´´S7``),ALIGNED(0,6),BEFF,BMERIT[D,L];
            "END" "ELSE" BMERIT[D,L]:=0;
     "END";
     "END";


     "COMMENT" GRAPH PLOTTING PROCEDURE;
     "IF" GRAPH=0 "THEN" "GO TO" INCREMENT;
     F:="IF" DMAX > 30 "THEN" 1 "ELSE" "IF" DMAX > 20 "THEN" 2 "ELSE" "IF" DMAX > 10 "THEN" 3 "ELSE" 6;
     "IF" DMAX > 60 "THEN" "BEGIN" "PRINT" ´´L1`GRAPH DIMENSIONS TOO LARGE`;
                              "GO TO" INCREMENT;
                         "END";
     "FOR" L:=1 "STEP" 1 "UNTIL" LMAX "DO"
     "BEGIN" "PRINT" ´´L2`LAMDA=`,SAMELINE,ALIGNED(2,2),LAMDA[L],´´L2``;
          MAX:=(ENTIER(MAXMER[L]*1000)+1)*10;
          DZ:="IF" MAX > 100 "THEN" 5 "ELSE" "IF" MAX > 50 "THEN" 2 "ELSE" 1;
          "FOR" Z:=MAX "STEP" -DZ "UNTIL" 0 "DO"
          "BEGIN" "IF" (Z/10-Z "DIV" 10) > .001 "THEN" "PRINT" ´´L1S8`+`
                        "ELSE" "PRINT" ALIGNED(0,6),Z/10000,´+`;
          "IF" Z=0 "THEN" "FOR" D:=1 "STEP" 1 "UNTIL" (F*DMAX) "DO" "PRINT" ´´S2`+`;
          "IF" Z=0  "THEN" "GO TO" AGAIN;
          T:=1;

          "FOR" D:=1 "STEP" 1 "UNTIL" DMAX "DO"
        "BEGIN" "IF" AMERIT[D,L] > Z/10000 "AND" AMERIT[D,L] < (Z+DZ)/10000 "OR" BMERIT[D,L] > Z/10000 "AND" BMERIT[D,L] < (Z+DZ)/10000 "THEN" "BEGIN" "FOR" FF:=T "STEP" 1 "UNTIL"
 (D*F) "DO"
          "BEGIN" "IF" FF=(D*F) "THEN" "PRINT" ´ ` "ELSE" "PRINT" ´  `;
          "END";
          "PRINT" ´*`;   T:=D*F+1;
          "END";
        "END";
AGAIN: "END";
     "PRINT" ´´L1S6``;
  T:=1;   "FOR" FF:=T "STEP" 1 "UNTIL" F "DO"
     "BEGIN" "IF" FF=F "THEN" "PRINT"´  `;
     "END";

   "FOR" D:=1 "STEP" 6 "DIV" F "UNTIL" DMAX "DO" "PRINT" SAMELINE,ALIGNED(2,1),DIST[D],´´S13``;
      "END";
INCREMENT: "IF" DESIGN=0 "THEN" "GO TO" FINISH;
"IF" Q=1 "THEN" "GO TO" L3;
FOCAL:=FOCAL+DELFOC;
"IF" FOCAL "LE" MAXFOC "THEN" "GO TO" NEXTFOCAL;
"IF" ENERGY=1 "AND" PENET > MAXP "THEN" "GO TO" FINISH;
N:=N+DELN;
"IF" N "LE" NMAX "THEN" "GO TO" NEXTNUMBER;
FINISH: "END";
"END";
```

Input of data

↓

*NUMBER

↓

instring
*DESIGN
DIAM
FRAD
MSEPT
DISTA
DISTB
DISTC
GAP
PHANT
LLAMDA
*LMAX
*COUNT
*GRAPH
LAMDA(1)
LAMDA(2)
"

either

or

for no design

*N
*BIGN
HRAD
LENGTH
FOCAL

for design procedures

*ENERGY
*NMIN
*DELN
*NMAX
MINFOC
DELFOC
MAXFOC
MAXSHAPE
MAXLENGTH
MAXP

↓ if

penetration to be considered

*TIMES
SETP

Notes

An asterisk denotes an integer variable.

NUMBER	-	no sets of collimator data
instring	-	title and details
DESIGN	-	0 for no design, 1 for high or low energy design
MSEPT	-	usually set by casting techniques (approx. 0.1 cm?)
DISTA, DISTB, DISTC	-	Distances at which figure of merit is to be determined (see index). For two counters, dista and distc must be equal distances from centre of phantom.
LMAX	-	no. values of λ for water
COUNT	-	no. detectors
GRAPH	-	0 for no graph, otherwise integer
LAMDA	-	no. values of λ must correspond to LMAX
ENERGY	-	0 for low energy, 1 when penetration must be considered ($>$ 150 keV)
NMIN	-	odd integer, 3 correspond to 7-holes, 5 to 19-holes, etc.
DELN	-	usually 2
NMAX	-	odd integer (see NMIN)
MINFOC, DELFOC, MAXFOC	-	range of focal lengths to try

MAXSHAPE	-	determined by organ, avoids unnecessary computation if collimator is unsuitable
MAXLENGTH	-	set by practicability, avoids unnecessary computation as above
MAXP	-	0.05 or less, also avoids unnecessary computation
TIMES	-	depends on accuracy required, 10 usually suitable
SETP	-	optimum penetration, about 0.02 or 0.01. If set too low gives low efficiency

Locations

*A	Location reservation for title
AEFF	Attenuated efficiency for one detector
AMERIT	Collimator figure of merit for one detector
AREA	Location for calculations
*BIGN	Number of holes in collimator (N)
BMERIT	Collimator figure of merit for two detectors
BEFF	Attenuated efficiency for two detectors
*COUNT	Number of detectors
DIAM	Crystal diameter (D)
D2	D^2
DISTA	Minimum distance from collimator face at which efficiency required
DISTB	Increment in DISTA
DISTC	Maximum distance from collimator face
DELH	Increment in HRAD, required for high energy designs only
DELFOC	Increment in focal length
DISTD	Limiting distance at which radiation incident on detector
DISTE	Limiting distance for points beyond focus
*DESIGN	Indicates whether design required or calculations for existing collimator
*DELN	Increment in n
*D	Counter for distance
*DMAX	Maximum number of distances
*DZ	Counter for graph plotting routine
DIST	Location for distances
EFFIC	Efficiency of individual holes
*ENERGY	Indicates whether design requires penetration routine
FRAD	Radius of field of view in focal plane (R_f)
FOCAL	Focal length (f)
*F	Counter for graph plotting routine
*FF	Counter for graph plotting routine

GAP	Air gap between external collimator face and phantom
GRAD	dP/dr
* GRAPH	Indicates whether graph plotting routine required
H2	r^2
H4	r^4
HS	2r + s
HD2	Location for calculations
HD4	Location for calculations
HRAD	Hole radius (r) at crystal face
HDIST	Ring number times HS
* I	Counter
* J	Counter
K2	Location for calculations
K	Location for calculations
KI	Location for calculations
KS	Location for calculations
LLAMDA	Linear absorption coefficient for lead
LENGTH	Collimator length (t)
* LMAX	Maximum number of linear absorption coefficients for water required
* L	Counter for LAMDA
LAMDA	Linear absorption coefficient for water
MSEPT	Minimum possible septum thickness at external face
MINFOC	Minimum focal length for which design required
MAXFOC	Maximum focal length for which design required
MAXSHAPE	Maximum tolerable shape factor
MAXLENGTH	Maximum tolerable collimator length
MAXP	Maximum tolerable penetration fraction
MAX	Location for calculations
* M	Counter
* MRING	Maximum number rings of holes in collimator
MAXMER	Location for graph plotting routine

*NUMBER	Number of times program to be run
*NO	Counter for NUMBER
*N	Small n where N = $(3n^2 + 1)/4$
*NMIN	Minimum value of n required
*NMAX	Maximum value of n required
PENET	Penetration fraction (P)
PEFFIC	Point source efficiency at focus (Beck's equation)
PLEFFIC	Plane source efficiency
PHANT	Depth of phantom
PLMERIT	Non-target efficiency
*Q	Counter
*RING	Number of collimator ring
SETP	Penetration fraction required
SEPT	Septum thickness (s)
SHAPE	Shape factor (K)
SHRAD	Location for calculations
SUMEFFIC	Total point source efficiency
TRANS	Transmission ratio (τ)
*TIMES	Number of times penetration routine carried out
*T	Counter
Z	Counter

APPENDIX 3

Letter to editor, accepted for publication in Int. J. applied Radiat. Isotopes.

SINGLE AND DOUBLE HEADED DETECTOR SYSTEMS FOR SCANNING

Popovic and Fowler (1968) in a comparison of single and double headed detector systems show that the target/non-target ratio for one particular double headed system is greater than that for a particular single detector system at all depths. I should like to point out the circumstances under which the probability of detection of a lesion is higher for single than for double headed systems.

Consider two equally collimated detectors, one on each side of the body, and a target region of increased activity close to one side of the body. The target count rate for the double detector system consists of the sum of the response of the detector closest to the target (E_{T_1}) and the response of the detector furthest from the target (E_{T_2}) which is relatively low because of the decrease of response with depth. The non-target response from the body volume is the same for both detectors and is double that of one detector (E_{NT}). Therefore, the target/non-target ratio for the

double headed system (R_2) is given by the expression:

$$R_2 = \frac{E_{T_1} + E_{T_2}}{2E_{NT}}$$

For the single detector closest to the target, the target/non-target ratio (R_S) is given by the expression:

$$R_S = \frac{E_{T_1}}{E_{NT}}$$

Since $E_{T_1} \gg E_{T_2}$, $R_S > R_2$ and therefore the target/non-target ratio is higher for the single detector. This occurs because the detector furthest from the target contributes little to the target count rate but gives a large increase to the non-target count rate, thus decreasing the signal to noise ratio.

For a target at the centre of the body, $E_{T_1} = E_{T_2}$ and the target/non-target ratios are the same for both systems. The probability of detecting the target must however be greater for the double headed system because the responses are doubled and a difference in count rate is more statistically significant. This difference between the detector systems can be demonstrated using a figure of merit (B)

based on a statistical test of the difference in count rates, which was introduced by Dewey and Sinclair (1961) and has been developed by Matthews (1965, 1967). For the double headed system:

$$B_2 = \frac{E_{T_1} + E_{T_2}}{\sqrt{2E_{NT}}}$$

and for a single detector:

$$B_S = \frac{E_{T_1}}{\sqrt{E_{NT}}}$$

Therefore, for a target close to the body surface, the probability of detection is higher for the single detector than for the double headed system, but for a target at the centre of the body, since $B_2/B_s = \sqrt{2}$, the double headed system gives a higher probability for detection.

Therefore, using the same crystals and collimators, a single detector is more efficient for detecting superficial lesions and a double headed system is more efficient for detecting deeply-lying lesions. The sensitivity of a single detector for deeply-lying lesions may be fractionally

increased by using a collimator with a longer focal length (Myers and Mallard, 1964), but this does not necessarily lead to a significant increase in the probability of detection (Kibby). Collimators with longer focal lengths also give a relatively large decrease in the sensitivity and the probability of detection for superficial lesions. Since there are relatively few applications for which it is advantageous to have a more uniform variation of sensitivity with depth at the expense of decreased sensitivity over a large region, it is doubtful whether such collimators give superior results in practice. In order to compare single and double headed systems it may therefore be more constructive to consider a collimator for the single detector with a slightly shorter focal length than that chosen by Popovic and Fowler. It may then be possible to design a collimator for a single 5" detector system with a similar variation of resolution with depth, but giving a higher probability of detecting a lesion up to the mid-line of the body than a double headed system using 3½" detectors.

A double headed system undoubtedly gives a more uniform sensitivity throughout the body and generally gives a higher probability for the detection of deeplying-lying lesions. The superiority of a single detector for the detection of

superficial lesions should not however be neglected and it is suggested that where a double headed system is in use, the best results would be obtained by recording the scan on paper or magnetic tape and playing back each detector response separately for visualisation of superficial lesions and then the combined detector response for visualisation of mid-line lesions. The simple considerations presented here also show the importance of using a figure of merit based on a statistical test rather than the target/non-target ratio which may give a misleading result.

Pamela M. Kibby,
M.R.C. Cyclotron Unit,
Hammersmith Hospital,
Ducane Road, London, W.12.

References

Popovic, S. and Fowler, J.F. The response of double-head and single-head collimators for scanning. Int. J. appl. Radiat. Isotopes, 19, 313 (1968)

Dewey, W.C. and Sinclair, W.K. Criteria for evaluating collimators used in 'in vivo' distribution studies with radioisotopes. Int. J. appl. Radiat. Isotopes, 10, 1 (1961)

Kibby, P.N. In preparation.

Matthews, C.M.E. Comparison of isotopes for scanning. J. Nucl. Med. 6, 155 (1965)

Matthews, C.M.E. Collimators and counting systems for brain scanning. Acta Radiol., 6, 464 (1967).

Myers, M.J. and Mallard, J.R. Some long-focusing "depth-independent" collimators for "in-vivo" radioisotope scanning. Int. J. appl. Radiat. Isotopes, 15, 725 (1964)

1968, *Br. J. Radiol.*, *41*, 580–585

The effect of collimator resolution on the detection of lesions in brain scanning

By C. M. E. Matthews, B.A., B.Sc., Ph.D., and P. M. Kibby, B.A.

M.R.C. Cyclotron Unit, Hammersmith Hospital, Ducane Road, London, W.12

(*Received October, 1967*)

The purpose of this study is to illustrate with photoscans some theoretical conclusions on the choice of collimator resolution in brain scanning. Calculations based on theoretical and experimental figures of merit (Matthews, 1964, 1965, 1967) give the minimum tumour size detectable with a given collimator for a given dose of a specific radionuclide; for example, after administration of 10 mCi of ^{99m}Tc pertechnetate a 1·2 cm diameter tumour at the centre of the head may just be detectable using a single detector and a typical collimator with a resolution of about 2 cm in the focal plane. The same calculations also indicate that collimators with coarser resolution, that is with larger resolution diameters, are better than fine resolution collimators for detection of small tumours. The increased efficiency of coarse resolution collimators results in a higher counting rate, thus reducing the statistical fluctuations in the background and making a small increase in counting rate over a tumour more significant. In order to demonstrate this point, ^{99m}Tc photoscans of head phantoms with simulated tumours of different sizes have been carried out with two collimators having different resolution diameters. The collimators were both designed to have uniform resolution with depth.

Collimators and detector

A single detector head was used, with a 3×1 in. sodium iodide crystal. The dimensions of the two collimators are given in Table I; the 50 per cent resolution in the focal plane for the 37-hole collimator is approximately double that for the seven-hole collimator. The shape factors of these collimators are also given; this quantity has been defined by Beck (1964) as the ratio of the area of the field of view at the collimator face to that at the focal plane. It is therefore a measure of the uniformity of the field of view with depth and gives an approximate indication of the variation of resolution with depth in front of the focal plane; beyond the focal plane the field of view always diverges. The relationship between shape factor, efficiency and resolution has been discussed by Beck (1964) and by Matthews (1967). As the shape factor is increased, the collimator efficiency increases but there is a greater variation of resolution with depth. A collimator designed with a fine resolution in the focal plane but with a large shape factor has a large increase in resolution diameter in front of and beyond the focal plane. A higher efficiency and the same average resolution over an appreciable depth may be obtained with a collimator with coarser resolution and with a smaller shape factor. The collimators used in this study have been designed for uniform resolution with depth by selecting shape factors of about 1. However, this gives rather low efficiency and in practice it would probably be better to use collimators with shape factors of about 2 for which the non-uniformity of resolution is not too serious and for which the efficiency is much higher. The collimator efficiencies, shown in Fig. 1 have been calculated theoretically for a point source at different distances on the axes of the collimators (P. M. Kibby, to be published). The attenuation of radiation in a head phantom of 15 cm width has been taken into account, but any scattered radiation incident on the crystal has been neglected. The 37-hole collimator is from three to five times more efficient than the seven-hole collimator.

Phantom

The head phantom consisted of a Perspex tank 15×20×20 cm high filled with approximately 5 l. of a radioactive solution of ^{99m}Tc. The tumours were represented by spherical glass bulbs filled with a more concentrated solution of ^{99m}Tc. The tank and bulb concentrations were 0·043 μCi/ml. and 0·43 μCi/ml. respectively; values similar to those expected for normal brain and tumour after injection of 10 mCi ^{99m}Tc (Matthews and Mallard, 1965). The head phantom was positioned so that the centre lay in the focal plane of the collimator leaving an air gap of 2·5 cm, and scans were carried out with the bulbs either at the centre of the tank or touching the front edge of the tank nearest to the collimator.

Scans

Scans were recorded on magnetic tape and later

TABLE I

DIMENSIONS OF COLLIMATORS (CM)

No. of holes	Collimator length	Hole radius*	Septum thickness*	Radius of field of view†	Focal length	Shape factor
7	20·0	1·17	0·36	1·24	10·6	0·94
37	3·7	0·47	0·17	2·52	10·0	1·01

*Crystal end. †In focal plane, ≃ 50 per cent resolution diameter.

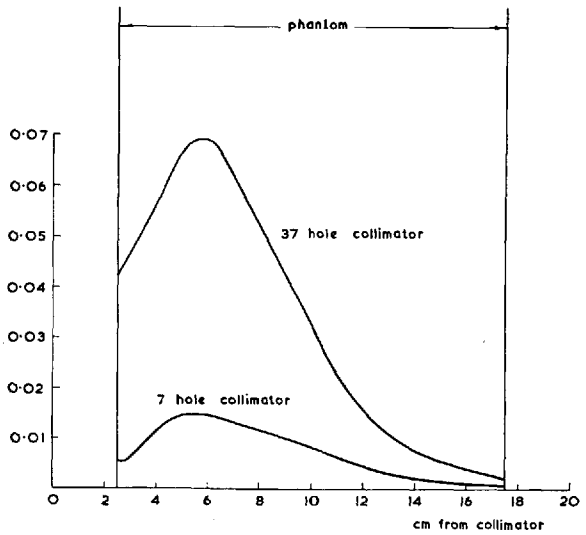

FIG. 1.

Variation of point source efficiencies with depth in water phantom. $\epsilon 0 \alpha 0$ = ratio of number of photons striking crystal per unit time to number of photons emitted from point source per unit time.

played back into a Picker Magnascanner. To avoid scalloping effects each scan line was carried out in the same direction. The line spacing was 0·5 cm for the first series of scans (Figs. 2–5) and 0·4 cm for the second series (Figs. 6–9); the scan speed was 30 cm/minute. During replay into the Picker scanner, a ratemeter time constant of one second was used and the maximum light source voltage, range differential and density settings were adjusted to give the full range of film blackening (optical density 0·3–2) over the range of count rate from the tank background to the peak count over the bulbs. Theoretically the ratemeter time constant should be related to the 80 per cent resolution diameter of the collimator (Matthews, 1964, 1967), giving values of 0·35 and 0·85 second for the seven-hole and 37-hole collimators respectively. For the 37-hole collimator the nearest available time constant was one second. For the seven-hole collimator, scans were also carried out with a time constant of 0·4 second, but these are not shown since they differed little from those with a one second time constant. The pulse height analyser window was set to include the whole photo-electric peak in the first series of scans. In the second series a narrow window was used with the lower bias set at 126 keV (90 per cent of the peak energy).

Statistical test

The level of significance of change in count rate for detection of bulbs of different sizes in different positions was calculated theoretically in a manner similar to that described by Matthews (1965, 1967) by calculating n where

$$n = \frac{\text{increase in count rate over bulb}}{\text{standard error of difference in count rate over bulb and over tank}}$$

If the value of n is greater than 3 the increase in count rate is statistically significant. It can be shown that

$$n = \text{constant} \times \sqrt{t} \times B \times V_T$$

where the constant depends on concentrations of radioactivity in the bulb and the tank and on the number of photons per disintegration.

t = time in which counts accumulate

B = a factor which can be calculated from the collimator and crystal dimensions and the position and volume of the source

V_T = bulb volume

The value of t was taken as the time to scan an area equal to the 80 per cent resolution distance squared. The choice of this value has already been discussed (Matthews, 1967). If t were much greater than this, the peak count rate would be reduced and if t were too small, statistical fluctuations would be increased.

With the wide window this calculation only gives an approximate estimate of the actual level of significance in these scans, since scattered radiation which enters the crystal has not been included and the background count rate has been neglected.

However, with the narrow window the contribution of scattered radiation is very small.

The values of n calculated from the collimator dimensions and radioactive concentrations for each bulb size used with the wide window are given in Table II, and corrected values are also shown which allow for the measured effect of scattered radiation from the tank. The effect of background has been included for the seven-hole fine collimator, but this correction was negligible for the 37-hole coarse collimator. In Table III the corresponding values for the narrow window (126–200 keV) are given; in this

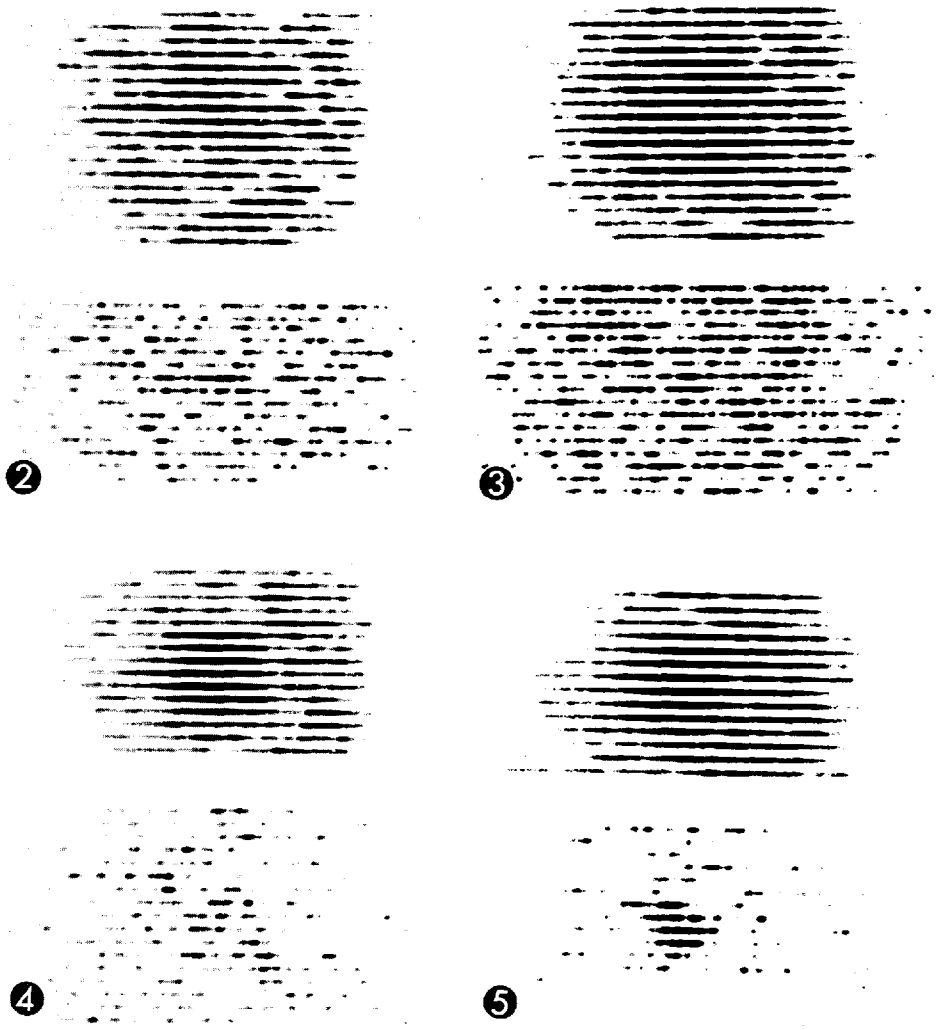

FIG. 2. Photoscans of 0·93 cm diameter bulb at the edge of the tank with wide window.
Below: seven-hole fine collimator, $n=1·3$.
Above: 37-hole coarse collimator, $n=3·2$.

FIG. 3. Photoscans of 1·33 cm diameter bulb at the centre of the tank, with wide window.
Below: seven-hole fine collimator, $n=1·0$.
Above: 37-hole coarse collimator, $n=2·1$.

FIG. 4. Photoscans of 1·94 cm diameter bulb at the centre of the tank, with wide window.
Below: seven-hole fine collimator, $n=2·0$.
Above: 37-hole coarse collimator, $n=5·2$.

FIG. 5. Photoscans of 2·68 cm diameter bulb at the centre of the tank, with wide window.
Below: seven-hole fine collimator, $n=3·4$.
Above: 37-hole coarse collimator, $n=11·0$.
On the original scans the diameter of the tank and the centre of the scan are marked.

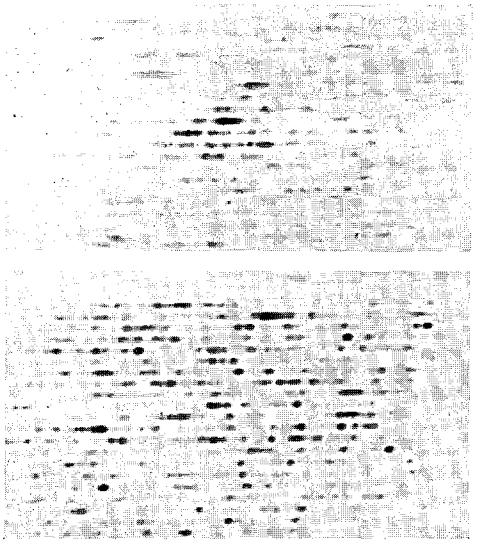

FIG. 6.

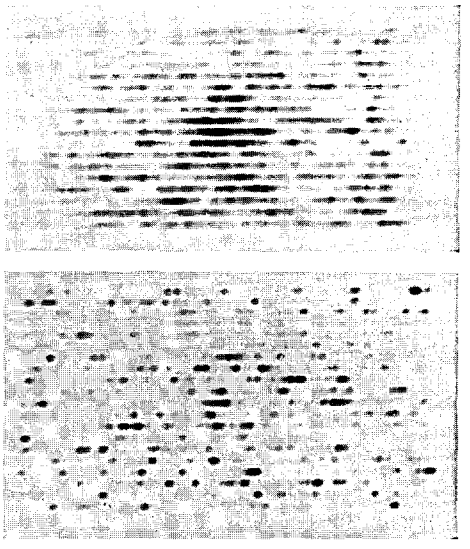

FIG. 7.

FIG. 6. Photoscans of 0·96 cm diameter bulb at the edge of the tank, with narrow window to reduce scatter.
Below: seven-hole fine collimator, $n=1{\cdot}5$.
Above: 37-hole coarse collimator, $n=3{\cdot}5$.

FIG. 7. Photoscans of 1·33 cm diameter bulb at the centre of the tank, with narrow window to reduce scatter.
Below: seven-hole fine collimator, $n=1{\cdot}2$.
Above: 37-hole coarse collimator, $n=2{\cdot}3$.
On the original scans the diameter of the tank and the centre of the scan are marked.

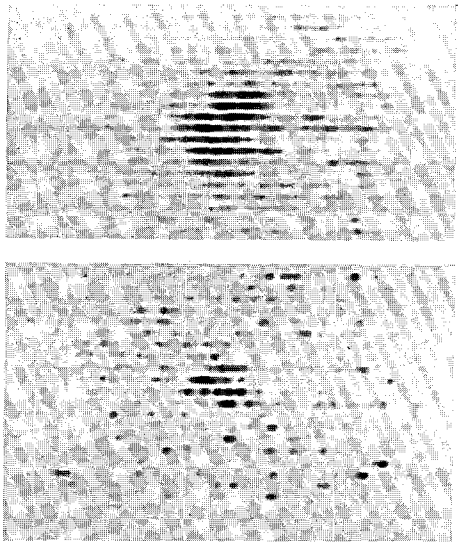

FIG. 8.

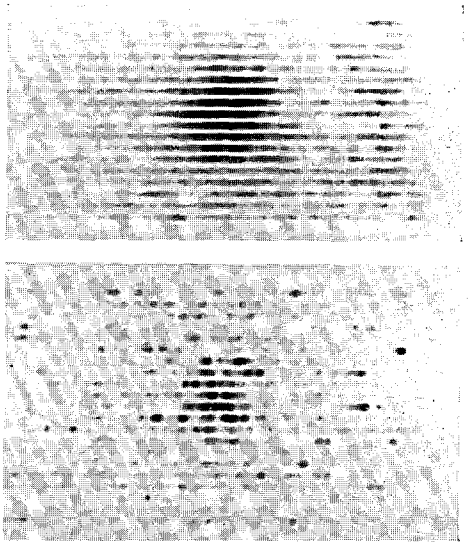

FIG. 9.

FIG. 8. Photoscans of 2·06 cm diameter bulb at the centre of the tank, with narrow window to reduce scatter.
Below: seven-hole fine collimator, $n=2{\cdot}6$.
Above: 37-hole coarse collimator, $n=6{\cdot}8$.

FIG. 9. Photoscans of 2·68 cm diameter bulb at the centre of the tank, with narrow window to reduce scatter.
Below: seven-hole fine collimator, $n=4{\cdot}0$.
Above: 37-hole coarse collimator, $n=12{\cdot}0$.
On the original scans the diameter of the tank and the centre of the scan are marked.

TABLE II

Bulb diameter cm	Position	*n* (calculated)			
		7-hole		37-hole	
		Uncorrected	Corrected for scatter and background	Uncorrected	Corrected for scatter
0·93	Edge	1·7	1·3	3·9	3·2
1·33	Centre	1·3	1·0	2·5	2·1
1·94	Centre	2·6	2·0	6·3	5·2
2·65	Centre	4·5	3·4	13·3	11·0

Wide analyser window set to include the whole photoelectric peak.

TABLE III

Bulb diameter	Position	*n* (calculated)	
		7-hole	37-hole
0·96	Edge	1·75	4·02
1·33	Centre	1·17	2·25
2·06	Centre	2·64	6·76
2·65	Centre	4·05	12·0

Narrow analyser window (126–200 keV).

case the contribution from scattered radiation is very small and the efficiency for unscattered radiation is slightly reduced.

RESULTS

The photoscans obtained with the two collimators for four bulb sizes, one at the front edge and the others at the centre of the tank are shown in Figs. 2–5 for the wide window and in Figs. 6–9 for the narrow window. The smallest bulbs (0·93, 0·96 and 1·33 cm diameter, Figs. 2, 3, 6 and 7) cannot be seen with the seven-hole fine resolution collimator but are visible with the 37-hole coarse collimator as predicted theoretically.

The 1·33 cm diameter bulb is just visible when the narrow window is used, when the value of *n* is 2·3 (Fig. 7). These results show that the coarse resolution collimator is better for the detection of small bulbs, even when the bulb diameter is smaller than the 50 per cent resolution diameter of either collimator.

A bulb of about 2 cm diameter (Figs. 4 and 8) is clearly seen with the 37-hole coarse collimator but is only seen with the seven-hole fine collimator when the narrow window which eliminates most of the scattered radiation is used. The largest bulb (Figs. 5 and 9) is clearly seen with both collimators even when the wide window is used. These results are in agreement with theoretical predictions (Tables II and III).

When bulbs are visible with both collimators, the 37-hole coarse collimator and seven-hole collimator appear to give equally good indications of shape; the greater statistical fluctuation with the less efficient fine collimator tends to obscure the outline of the bulb despite the improved resolution.

DISCUSSION AND CONCLUSIONS

The results illustrate that the high sensitivity of coarse resolution collimators enables smaller bulbs to be detected than with fine resolution collimators, even when the bulb diameter is less than the 50 per cent resolution diameter of the collimator. The resolution diameters used in this study were 1·24 and 2·52 cm and bulbs of 0·93, 0·96 and 1·33 cm diameter were seen better with the coarse resolution collimator. With the coarse collimator it appears possible to detect a tumour at about 1·5 cm at the centre of the head and one of about 1 cm diameter near the skull. With a collimator with a larger shape factor of about 2 these diameters could be reduced by about 11 per cent.

Furthermore, the results show that the calculation of *n* gives a reasonable indication of whether a bulb will be detected. The value of *n* for which bulbs are just visible appears to be about 2.5 but the exact value which is taken to indicate the presence of a tumour depends on the relative importance of not missing tumours and not obtaining false positives. For low γ-ray energies collimators may there-

fore be evaluated for a particular purpose by an entirely theoretical calculation, independent of experimental measurements of collimator efficiency. Scattered radiation can be almost eliminated by using a narrow window, but when the whole photoelectric peak is included for measurements a correction must, however, be applied. The narrow window which we have used is the same as that which Beck (1966) found to be optimum, using a figure of merit calculation.

In practice there will be other considerations, such as the variation of brain background due to radioactivity in blood sinuses and other regions. This may tend to give the finer collimator more advantage in showing the shape of these structures, which must be differentiated from the presence of a tumour. However, this detailed visualisation of anatomic structures with a fine collimator is obtained at the expense of the ability to detect small tumours. It is no use trying to show sharp outlines with a fine collimator if this prevents the detection of small tumours in regions of the brain where this detail is not necessary. With a coarser collimator small tumours may at least be detected in regions of the brain where they are not obscured by the sinuses. Probably the optimum brain scanning procedure is to use a coarse resolution collimator for a preliminary scan, and then to scan small areas where a tumour is suspected more slowly, using a fine resolution collimator to show the detailed structure.

ACKNOWLEDGMENTS

We are very grateful to Dr. J. Ambrose and Miss A. Boss for the use of their Picker Magnascanner and to Mr. S. Gunasekera and Mr. A. Ranicar for technical assistance.

ABSTRACT

Photoscans are shown of phantoms representing tumours in brain. The phantoms consist of a 5 l. tank containing 0·043 μCi/ml. of ^{99m}Tc with spherical glass bulbs containing 0·43 μCi/ml. of ^{99m}Tc representing the tumours. Bulbs of diameters from 0·9 to 2·7 cm were scanned with two collimators with 50 per cent resolution diameters of about 1·2 cm and 2·5 cm, both collimators being designed for uniform resolution with depth. It is shown that, in agreement with theoretical predictions, smaller bulbs can be detected with the coarser resolution collimator than with the finer resolution one. The statistical test of significance of increase in count rate used in the theoretical calculation correctly predicts whether a bulb of a given size will be detected; this calculation uses only the physical dimensions of the collimator, the crystal efficiency, the radioactivity in the bulb and tank, the tank thickness and the bulb volume. The scans are much improved if most of the scattered radiation is cut out by setting the bottom of the analyser window at 90 per cent of the photopeak energy.

REFERENCES

BECK, R. N., 1964, in *Medical Radioisotope Scanning*, Vol. I, 211 (I.A.E.A., Vienna); 1966, personal communication.

MATTHEWS, C. M. E., 1964, *Br. J. Radiol.*, *37*, 531; 1965, *J. nucl. Med.*, *6*, 155; 1967, *Acta radiol.*, in press.

MATTHEWS, C. M. E., and MALLARD, J. R., 1965, *J. nucl. Med.*, *6*, 404.

1969, *Br. J. Radiol.*, *42*, 91–101 FEBRUARY 1969

The design of multichannel collimators for radioisotope cameras

By Pamela M. Kibby, B.A.

M.R.C. Cyclotron Unit, Hammersmith Hospital, Ducane Road, London, W.12

(*Received March, 1968*)

The resolution and sensitivity of a radioisotope camera depends upon the design of the collimator and also on the properties of the image-converting system, as reviewed by Anger (1966). The collimating system of the pin-hole camera (Anger, 1958; Mallard and Myers, 1963) consists of a small aperture in a lead shield. These collimators are only suitable for small objects which can be placed close to the pin-hole, since they give low sensitivity and poor localisation for larger subjects (Anger, 1963; 1966). Under such conditions, multichannel collimators, as used with scintillation cameras (Anger, 1964), image-converters (Ter-Pogossian, Niklas, Bell and Eichlung, 1966) and spark chambers (Lansiart and Kellershohn, 1966; Horwitz, Lofstrom and Firsaith, 1965) give improved performance. They normally consist of a large number of parallel cylindrical holes through the collimator material, although a modified design, with holes focusing in a plane parallel to the collimator face, has been used with the autofluoroscope (Bender and Blau, 1962).

The performance of pin-hole collimators has been investigated theoretically by Mallard and Myers (1963) and by Paix (1967). Anger (1964) has derived approximate theoretical expressions relating the resolution and the sensitivity of a multi-cylindrical-channel collimator to the collimator parameters. In the present work, the theory of these collimators has been developed more accurately. In addition, since there are a large number of possible combinations of collimator parameters which give collimators suitable for a particular γ-ray energy, those designs which give the highest sensitivity for a specified resolution have been found.

Method

It has been assumed that the channels are circular in cross-section and that they are arranged in a hexagonal array (Fig. 1). A digital computer (Elliott 4100) has been used in the calculations.

Septum penetration

One basic requirement of a collimator is that the septa should be of sufficient thickness to prevent significant penetration. Some rays will inevitably penetrate the top and bottom corners of the septa (Figs. 1A and 1B); others may penetrate one or more septa and lead to a more serious loss of resolution as they may originate from a larger volume of the subject (Figs. 1C, 1D and 1E).

The minimum path length through one septum may be expressed geometrically as (Fig. 1):

$$w = s\sqrt{1+\frac{t^2}{(4r+s)^2}} \quad . \quad . \quad . \quad . \quad (1)$$

where s is the septum thickness, r is the hole radius and t is the collimator length. In these collimator designs, the following criterion has been adopted, namely, that the minimum path length through septa should be equal to five mean free paths through the collimator material at the specified energy; this restricts the number of γ rays penetrating the septa to less than 1 per cent of those incident in this direction, *i.e.*

$$w = \frac{5}{\mu} \quad . \quad . \quad . \quad . \quad . \quad (2)$$

where μ is the total linear absorption coefficient in the collimator material at the specified energy.

Combining equations (1) and (2):

$$\frac{5}{\mu} = s\sqrt{1+\frac{t^2}{(4r+s)^2}}$$

Therefore, when $t >> 4r+s$, $\frac{5}{\mu} = \frac{st}{(4r+s)}$ . . (3)

This approximation leads to an underestimate of the path length and an overestimate of the required septum thickness, but the error is generally small.

Mather (1957) has shown that for a single cylindrical channel collimator, penetration of the top and bottom corners of the septa may be allowed for approximately, by effectively shortening the collimator length by two mean free paths at the specified energy. The approximation was considered adequate

Present address: X-ray Physics Department, Churchill Hospital, Oxford.

for this theoretical work since, in general, a distance of two mean free paths is small compared with the collimator length.

Point source efficiency

The collimator efficiency for a point source of radiation, at a stated distance from the collimator face, was defined as the fraction of the photons emitted from the source which is incident on the detector; it is therefore equal to the sum of the efficiencies of all those channels which contribute to the detector response. To simplify the calculations, it was assumed that the point source was situated on the axis of one collimator channel, referred to as the source channel.

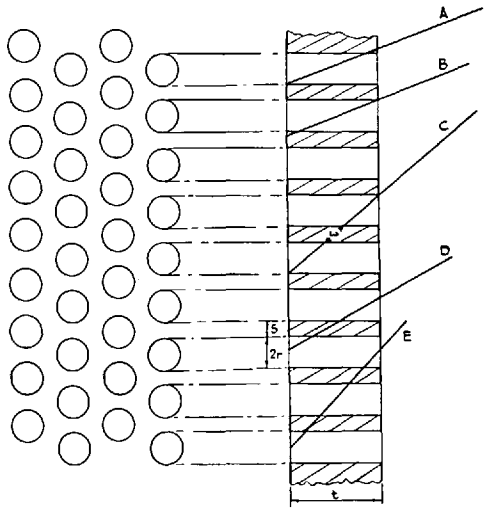

FIG. 1.
Multichannel collimator in cross-sections perpendicular and parallel to the channel axes.

Consider the channel whose axis is a perpendicular distance h ($h>r$) from the axis of the channel on which the source is situated (Fig. 2). Radiation from the source at P is incident on the area of intersection of the base of the channel with the projection of the top of the channel on the base plane. The accurate calculation of the solid angle subtended by this area at point P, and hence of the channel efficiency, involves integration over each element of area, requiring the solution of incomplete elliptic integrals. However, provided the area is small it may be considered as a whole without a significant loss in accuracy. Let the projected circle have radius r and let its centre lie a perpendicular distance h from the source channel axis.

Then $r'=kr$ and $h'=kh$

where $k=1+\frac{t'}{d'}$

t' is the effective collimator length, and d' is the effective distance of the source P from the collimator face, *i.e.*

$$t'=t-\frac{2}{\mu} \text{ and } d'=d+\frac{2}{\mu}.$$

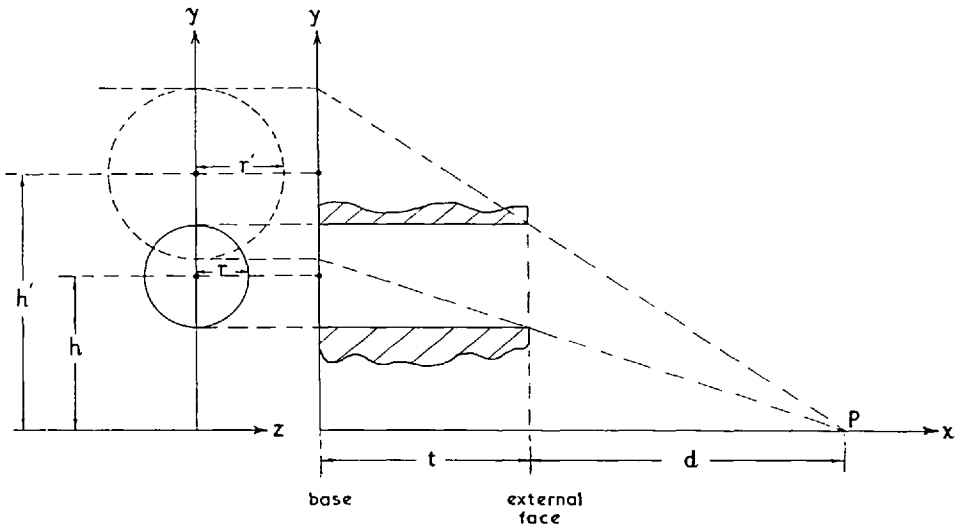

FIG. 2.
One collimator channel in cross-section showing the method of calculation of channel efficiency.

Then, since the radii of the projected circle and that forming the base of the channel are known and also the distance apart of the centres of the circles (h'-h), the area of intersection (A) may be calculated and is given by

$$A=\frac{\pi r^2(k^2+1)}{2}$$
$$-\frac{(k-1)}{2}\sqrt{2r^2h^2(k^2+1)-h^4(k-1)^2-r^4(k+1)^2}$$
$$-r^2\sin^{-1}\left[\frac{h^2(k-1)-r^2(k+1)}{2hr}\right]$$
$$-k^2r^2\sin^{-1}\left[\frac{h^2(k-1)+r^2(k+1)}{2hkr}\right] \quad . \quad (4)$$

The centre of the projected area is a distance H along the y-axis, given by:

$$H=h+\frac{(h-r)(k-1)}{2} \quad . \quad . \quad . \quad (5)$$

Hence, the solid angle subtended by the area at the point P is given by:

$$\Omega=A(t+d)/\left[\left(h+\frac{(h-r)(k-1)}{2}\right)^2+(t+d)^2\right]^{3/2}$$
$$. \quad . \quad . \quad . \quad . \quad . \quad . \quad . \quad . \quad (6)$$

and the efficiency of the channel may then be calculated from the equation:

$$\epsilon_T=\frac{\Omega}{4\pi}$$

Equations (4) and (6) are not valid when $h<r$ because the projected circle does not then overlap with the circle forming the base of the channel. The only such case which need be considered for these calculations is when the source is situated on the channel axis, *i.e.* $h=0$,

Then, $$\epsilon_T=r^2/4(t+d)^2$$

This method of approach to the calculation of collimator efficiencies was first outlined by Brownell (1958) for single cylindrical channels.

The total point source efficiency may be calculated by summing the efficiencies of those channels in the array which contribute to the detector response. In order that radiation from a point source, a distance d from the collimator face, should be incident on the detector at the base of the channel which is a distance h from the source axis, the following condition must hold:

$$h<r\left(1+\frac{2d'}{t'}\right) \quad . \quad . \quad . \quad . \quad (7)$$

Values of h for channels in a hexagonal array may be readily calculated. Let the channel on the axis of which the source is situated be designated by $g=0$; the surrounding hexagon of six channels by $g=1$; the surrounding hexagon of 12 channels by $g=2$, etc. When $g=0$, there is one channel at distance $h=0$, and for each surrounding hexagon ($g=1,2,3\ldots$) there are six channels at distances:

$$h=g(2r+s) \quad . \quad . \quad . \quad . \quad . \quad (8)$$

In addition, when g is an even integer, there are six channels at distances: $h=g(2r+s)\sqrt{\frac{3}{2}}$ and 12 channels at distances: $h=(2r+s)\sqrt{\frac{3g^2}{4}+i^2}$ for each value of i given by 1,2,3 . . . for which $i\leqslant(g/2-1)$. When g is an odd integer, there are twelve channels at distances: $h=\frac{(2r+s)}{2}\sqrt{3g^2+i^2}$ for each value of i given by 1,3,5 . . . for which $i\leqslant(g-2)$. All those channels which have values of h satisfying condition (7) therefore contribute to the detector response.

Resolution. Consider a point source situated at a specified distance along the axis of one collimator channel A (Fig. 3); the resolution may be defined as twice the distance between the axes of channel A and another channel, the efficiency of which is 50 per cent of the efficiency of channel A; this is analogous to the full width at half-height. In the general case, the point source efficiencies of consecutive channels may be plotted against the distance of the centre of the channel from some specified point and the resolution defined as the full width at half-maximum of the resulting curve. In practice, the centre of the area on which radiation is incident is farther from the source than the centre of the channel (Equation (5)) and this leads to a broadening of the resolution curve. The error is usually small, although it may become significant when the source is imaged in only a few channels. The validity of this definition will depend on the inherent resolution of the image transfer system of the particular camera device; when the collimator septa are comparable with or larger than the inherent resolution, the resultant camera image may display undulations in intensity due to individual channels. This is unlikely to occur with the γ-camera of the kind devised by Anger (1964), for which the inherent resolution is relatively large, but some difficulty may be encountered with other systems. When the source is imaged mainly in one channel, the definition of resolution becomes more complex as discussed in a later section.

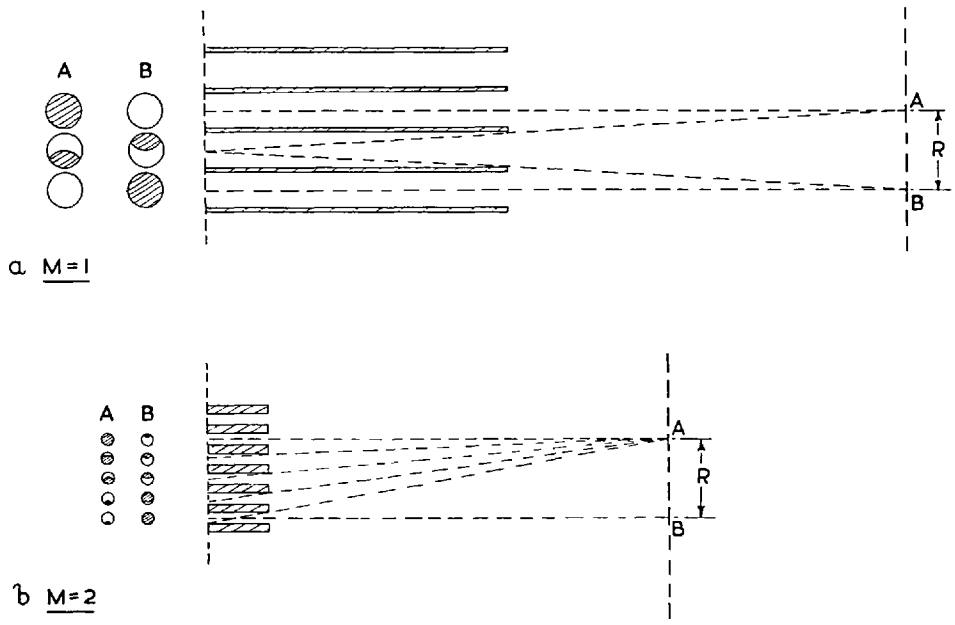

FIG. 3.
Collimators in cross-section illustrating the first method of design.

COLLIMATOR DESIGN

There are an infinite number of possible combinations of channel radius, septum thickness and collimator length which give the required resolution at a specified distance, and which limit penetration of septa at the specified energy. The optimum values of the parameters, those fulfilling the requirements and giving the maximum collimator efficiency, were selected by two methods.

Method (1)—photon energies up to 0·3 MeV

In general, it is difficult to find those combinations of parameters which give a specified resolution, since the resolution is not known prior to the calculation of all the channel efficiencies. There are, however, several cases for which the resolution may be set to a chosen value in a relatively simple way; in this method, the efficiencies of these particular collimators were calculated and the collimator of highest efficiency for the specified energy was then found by interpolation.

Consider the situation shown in Fig. 3a and let values of channel radius and septum thickness be related to the required resolution R, by the expression:

$$R=2(2r+s) \quad . \quad . \quad . \quad . \quad (9)$$

If values of channel radius, septum thickness and collimator length are found which satisfy Equation (9), the penetration limitation condition obtained by rearranging Equation (3):

$$\frac{r}{s}=\frac{\mu t-5}{20} \quad . \quad . \quad . \quad . \quad (10)$$

and the condition that the efficiency of a neighbouring channel is 50 per cent of the efficiency of the source channel, then the resulting collimator has the required resolution R at the specified distance ($d=F$).

Similarly, consider the situation shown in Fig. 3b and let values of channel radius and septum thickness be related by the expression:

$$R=4\ (2r+s).$$

If the collimator parameters are then adjusted so that the efficiency of the second channel to A is 50 per cent of the efficiency of the channel on the axis of which A is situated, this collimator will also have the required resolution at distance F. It should therefore be possible to design collimators for which:

$$R=2M(2r+s) \quad . \quad . \quad . \quad . \quad (11)$$

where M takes the values 1,2,3 . . .

For a given value of M, there are an infinite number of collimators which satisfy Equations (10) and (11), but not all of these also satisfy the condition that the efficiency of the Mth channel from the source is 50 per cent of the efficiency of the source channel. Those collimators satisfying the condition

were found by taking an arbitrary collimator length and calculating values of r and s from Equations (10) and (11). The efficiencies of the source and Mth channels were then found. This procedure was repeated ten times taking progressively smaller increments or decrements in the collimator length as the efficiency condition was approached. This process, which was carried out by computer, was then repeated for all possible values of M over a range of energies and resolutions.

The efficiencies of the resulting collimators were plotted against the ratio of channel radius to septum thickness (r/s) for different resolutions at each energy. At a specified energy, the total point source efficiency was found to be a maximum at one value of the ratio r/s; in addition, the optimum ratios were found to be independent of the resolution specified for a given distance from the collimator face. The maximum occurs due to two opposing effects: (i) as the ratio of hole radius to septum thickness is made smaller, the collimator may be made shorter, resulting in higher efficiency owing to the inverse square law; however, (ii) as the collimator is made shorter, thicker septa are required to limit penetration and a larger fraction of the detector area becomes covered, resulting in a decrease in efficiency.

At each energy, the optimum value of the collimator length was obtained from Equation (10). The optimum values of r and s were found by plotting the collimator efficiencies against the channel radii and septum thickness for different resolutions at each energy and finding those values corresponding to maximum efficiency.

The total efficiencies and channel efficiencies of the optimum designs for each energy were calculated at different distances from the collimator face.

Method 2—photon energies between 0·3 and 0·5 MeV

The first method requires that the efficiency of a neighbouring channel is equal to or greater than 50 per cent of the efficiency of the source channel. As the energy increases (*i.e.* as μ decreases), in order to limit penetration it becomes necessary to increase the collimator length, to decrease the ratio of channel radius to septum thickness or to combine the two (Equation (10)). These requirements tend to reduce the efficiencies of neighbouring channels and above 0·3 MeV it becomes impossible to fulfil the efficiency condition of the first method.

There are many possible collimator designs for which the efficiency of a neighbouring channel is less than 50 per cent of the efficiency of the source channel, but in these cases a slightly different definition of resolution is required. Although the efficiencies of consecutive channels could be plotted, there may be a considerable error in determining the full width at half-maximum of the resulting curve, since the shape of the resolution curve is undefined.

Consider the circumstances under which two point sources are most likely to be resolved, that is, when they are at equal distances from one channel axis (Fig. 4a), referred to as the central channel axis. At one particular distance from the axis, the efficiency of the central channel for one source will be 50 per cent of the efficiency of the neighbouring channel. Therefore, if this condition is fulfilled at a separation $2(r+x)$, the sources wlll be resolved at greater distances of separation and the resolution may be defined as:

$$R_1=2\ (r+x).$$

Consider now the circumstances under which two point sources are least likely to be resolved, that is, when they are at equal distances from the central axis of one septum when shown in cross-section (Fig. 4b). Since a point source may be moved up to a distance r from one channel axis without a significant reduction in the channel efficiency, provided $2r<<(t+d)$, the sources C and D (Fig. 4b) may be moved a distance $(4r+s)$ apart without a significant difference in the efficiencies of the channels nearest to the septum axis for which the efficiencies are the same; it has been assumed that under these conditions the sources are not resolved as discussed later. When the source separation is increased to a distance $(4r+2s)$, the efficiencies of the channels second to the septum axis increase until they are equal to the efficiencies of the channels nearest to the septum axis, which decrease simultaneously. At greater separations the sources may be resolved, and therefore under these conditions the resolution may be defined as:

$$R_2=4r+2s.$$

An estimate of the resolution may therefore be obtained from the average of R_1 and R_2 given by the equation:

$$R=3r+s+x \qquad . \ . \ . \ . \ (13)$$

For this method of design, collimators were found which satisfied Equations (10) and (13) and the efficiency condition stated above, and the most efficient collimators were found by interpolation.

A value for collimator length was taken and x was set at some arbitrary value. The channel radius and septum thickness were calculated from Equations (10) and (13) and the channel efficiencies were then found. The calculations were repeated ten times taking progressively smaller increments or decrements

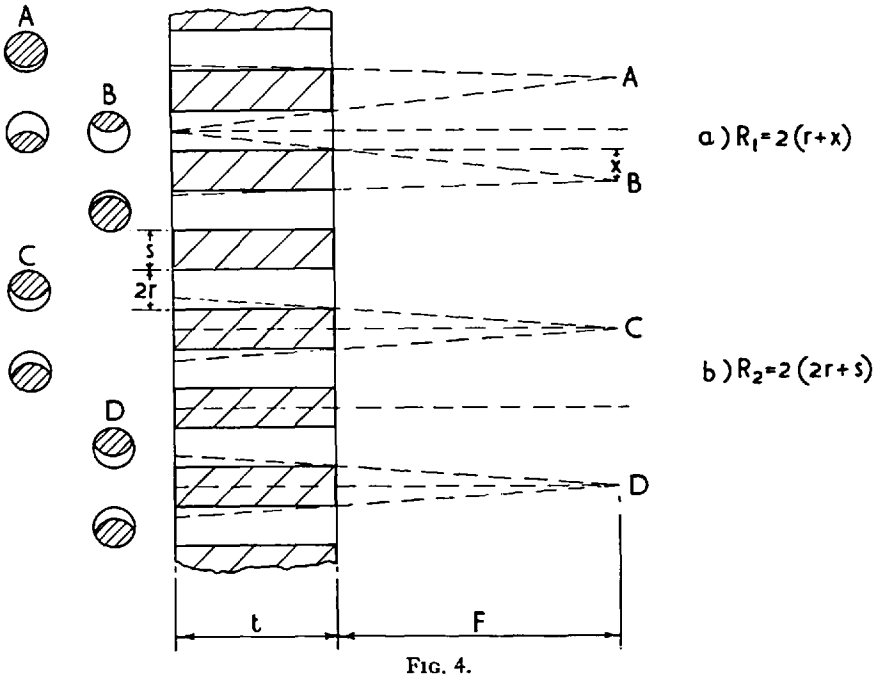

FIG. 4.

Collimator in cross-section illustrating the second method of design.

in the distance x, in order closely to approximate the condition that the central channel efficiency is 50 per cent of the efficiency of a neighbouring channel.

The complete process was carried out over a range of collimator lengths at several energies and resolutions.

The total efficiencies, calculated for a point source on one channel axis, were plotted against collimator length for different resolutions; it was found that at each energy the efficiency was a maximum at one value of the collimator length which was independent of resolution. Although the contribution of neighbouring channels decreases as the collimator length is increased, thinner septa may be used to reduce penetration to the same amount and hence the channel radii may be increased, leading to an increase in efficiency of the source channel. The total efficiency, therefore reaches a maximum in between the extremes of a large contribution from neighbouring channels and a large contribution from the source channel alone.

When the collimator lengths corresponding to maximum efficiency had been found for each energy, the corresponding values of x were obtained from graphs of x against t for different resolutions. Values of channel radius and septum thickness for a specified resolution were then calculated from Equations (10) and (13). The total efficiencies and channel efficiencies of these collimators were calculated at different distances from the collimator face.

RESULTS

Optimum collimators for photon energies below 0·3 MeV

A summary of the optimum designs obtained by method 1 is given in Fig. 5. In general, as the γ-ray energy decreases, the optimum collimator lengths, which like the ratios r/s are independent of resolution (Equation (10)), become smaller (Fig. 5a). The optimum channel radii and septum thicknesses are also smaller at lower energies. These parameters are given in Figs. 5b and 5d for a resolution of 1 cm at 10 cm from the collimator face, but since they are directly proportional to the collimator resolution (Equation (11)) values may be found from Fig. 5 for any specified resolution. The total point source efficiencies of the optimum designs (Fig. 5c) increase for lower energies and were found to be proportional to the square of the resolution to within ± 5 per cent. The dimensions of some optimum designs over a range of energies are given in Table I.

In general, the point source efficiency in air is relatively independent of the distance of the source from the collimator face, the variation being less than 4 per cent. Close to the collimator, however, the source is imaged in only one channel, and over this region the collimator efficiency varies according to the inverse square law. A typical example of the variation of resolution diameter with distance for an optimum collimator is shown in Fig. 6; since the

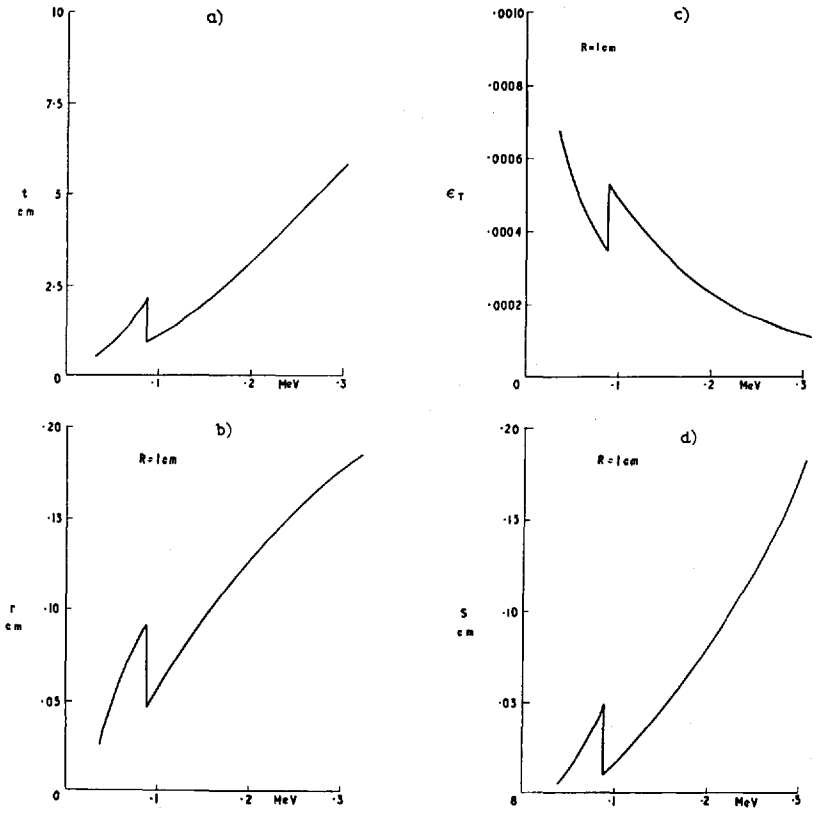

FIG. 5.

Maximum efficiency lead collimator designs for photon energies below 0·3 MeV. The hole radii (r), septum thickness (s) and point source efficiencies (ϵ_T) are given for a resolution of 1 cm at 10 cm from the collimator face. The discontinuity at 0·088 MeV is due to the K-absorption edge for lead.

TABLE I

LEAD COLLIMATORS WITH RESOLUTIONS OF 1 CM FOR SOURCES AT 10 CM FROM THE COLLIMATOR FACE

Energy MeV	Collimator length cm	Channel radius cm	Septum thickness cm	Point source efficiency* in air; source at 10 cm from collimator face
0·05	0·80	0·048	0·012	0·000538
0·075	1·65	0·080	0·038	0·000394
0·10	1·10	0·056	0·016	0·000487
0·15	2·00	0·094	0·046	0·000337
0·20	3·15	0·127	0·080	0·000232
0·25	4·45	0·154	0·121	0·000160
0·30	5·75	0·177	0·175	0·000115

* $\frac{\text{photons emitted}}{\text{photons incident on crystal}}$

efficiency is constant with distance the volumes of revolution of the curves are similar. This rapid increase of resolution with distance is also illustrated in Fig. 7 for the optimum collimators for 0·1, 0·2 and 0·3 MeV, showing that the increase is larger at lower energies. It was found that the variation could only be improved with a considerable reduction in the collimator efficiency. The change in resolution with distance is independent of the value specified at a given distance. Hence, these lines may be applied to any optimum collimator designs.

Optimum collimators for photon energies above 0·3 MeV

A summary of the optimum designs obtained by the second method is shown in Fig. 8. These collimators show an increase in length with increase in

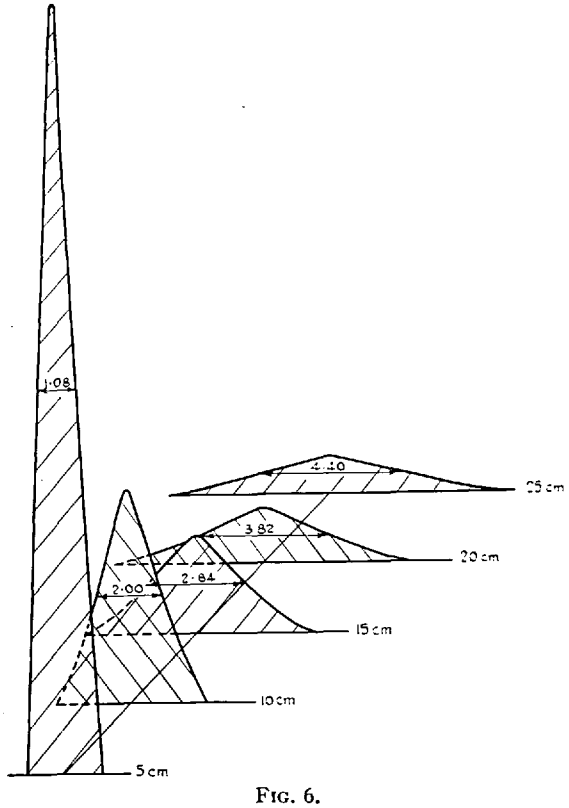

FIG. 6.

Typical theoretical resolution curves for a multichannel collimator for distances of 5, 10, 15, 20 and 25 cm from the collimator face.

γ-ray energy (Fig. 8a) and also an increase in septum thickness (Fig. 8d); the channel radii show a very slight decrease with increase in energy (Fig. 8b). The values of x, septum thickness and channel radius are all directly proportional to resolution and although they are shown here for a resolution of 1 cm at 10 cm from the collimator face, values may be obtained from Fig. 8 for any resolution. The collimator length is independent of resolution and the efficiency is approximately proportional to the square of the resolution as was true for the previous designs. Examples of collimators designed by the second method are shown in Table II.

TABLE II

LEAD COLLIMATORS WITH RESOLUTIONS OF 1 CM FOR SOURCES AT 10 CM FROM THE COLLIMATOR FACE

Energy MeV	Collimator length cm	Channel radius cm	Septum thickness cm	Point source efficiency in air source at 10 cm from collimator face
0·3	5·6	0·173	0·174	0·000110
0·35	6·1	0·167	0·217	0·000078
0·4	6·8	0·164	0·252	0·000051
0·45	7·8	0·163	0·274	0·000031
0·5	9·0	0·163	0·286	0·000019

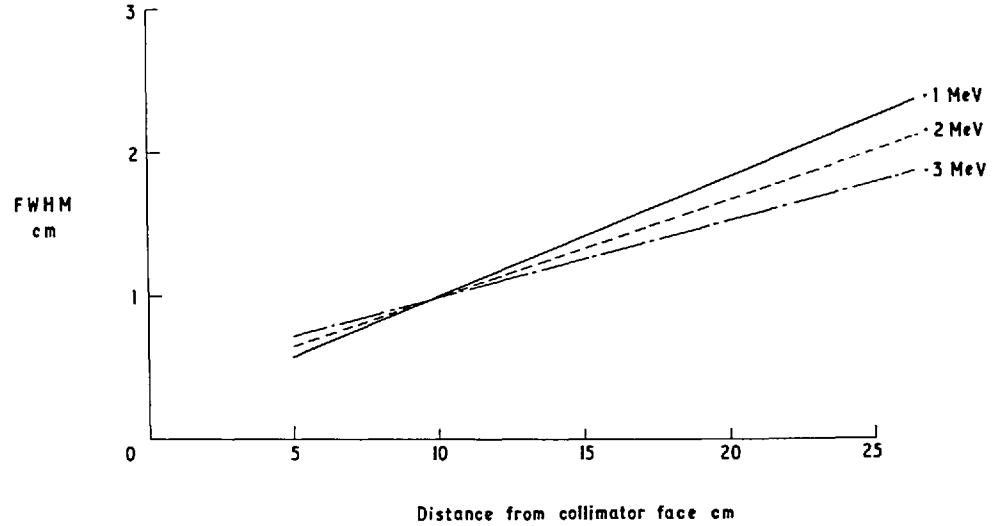

FIG. 7.

The variation of the full width at half-maximum of the resolution curve with distance from the collimator face, for the optimum collimators for 0·1, 0·2 and 0·3 MeV.

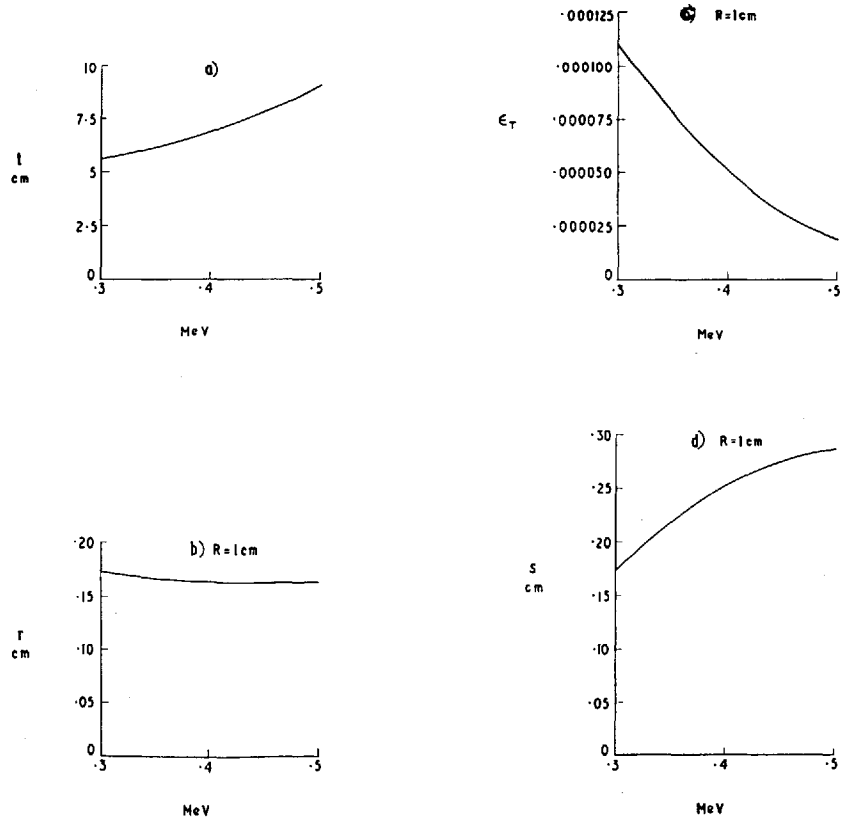

FIG. 8.

Maximum efficiency lead collimator designs for photon energies between 0·3 and 0·5 MeV. The hole radii (r), septum thicknesses (s) and point source efficiencies (ϵ_T) are given for a resolution of 1 cm at 10 cm from the collimator face.

The total point source efficiency in air only becomes constant at distances greater than 10 cm for these designs, because the source is mainly imaged in a single channel at smaller distances.

When the source is mainly imaged in one channel, it may be assumed that the resolution is reasonably constant at the value specified for 10 cm; at greater distances the resolution was found to increase in a similar manner to that of collimators below 0·3 MeV.

DISCUSSION

Application of results

The results shown in Fig. 5 and Fig. 8 enable lead collimators to be designed for energies below 0·5 MeV for any specified resolution, using the relationships between the resolution and the collimator parameters stated above. For example, a lead collimator with a resolution of 2 cm at 10 cm from the collimator face which is suitable for 0·08 MeV radiation has the following dimensions:

length, t=1·85 cm

channel radius, r=(0·084×2) cm=0·168 cm

and septum thickness, s=(0·038×2)cm=0·076 cm

giving a total point source efficiency: =0·000373×2^2

=0·00148.

The factors which determine the maximum efficiency depend only on the values of collimator length and on the ratio of channel radius to septum thickness and are independent of the values of these latter parameters which determine the resolution. Hence, smaller resolution collimators are obtained by maintaining the same collimator length and decreasing the channel radius and septum thickness, thus increasing the number of channels. Decreasing the septum thickness under these conditions does not increase septum penetration because, owing to the smaller channel radii, γ rays of minimum path length pass more obliquely through the septum material.

At the upper limit of application of the first method, 0·3 MeV, the optimum collimator is similar to that obtained for 0·3 MeV by the second

method. However, the first method only takes into account the case when two sources are most likely to be resolved, that is, when they are symmetrically placed about one channel axis. This collimator therefore has a slightly larger resolution in practice than that designed by the second method, and hence a slightly higher efficiency. Calculations show that the variation of resolution with source position in a plane parallel to the collimator face increases with γ-ray energy from ± 4 per cent at 0·3 MeV to ± 23 per cent at 0·5 MeV. The error introduced in the first method by ignoring this variation below 0·3 MeV is less than 4 per cent.

It has been assumed that two sources which are imaged in neighbouring channels with the same efficiency are not resolved. However, if the septum thickness is greater than the inherent resolution of the image-converting system, then two point sources on the axes of neighbouring channels will give a two-peaked response. The same type of response will also be obtained with an extended source and therefore this type of collimator is undesirable. At higher energies, particularly for large resolutions, it may be possible to overcome this difficulty by using tungsten instead of lead, in order to be able to reduce the septum thickness.

Penetration criterion

The criterion that the minimum path length through one septum should be equal to five mean free paths through the collimator material, is open to question. The $1\frac{1}{2}$ in. long collimator ($\frac{1}{4}$ in. diameter hole) for the Nuclear-Chicago scintillation camera is similar to the optimum collimator for 0·23 MeV radiation. This is the energy at which in practice the collimator starts to show significant penetration effects (Westerman, 1967) and suggests that the criterion for limitation of septum penetration is valid. However, Anger (1966) has suggested that a minimum path length through septa of three mean free paths may be sufficient. It may be possible to tolerate thinner septa, especially when the radioactivity in the subject is distributed throughout a comparatively small volume. The optimum collimator under these circumstances may also be obtained from Fig. 5; a minimum path length of three mean free paths is equivalent to one of five mean free paths at a lower energy for which the linear absorption coefficient is 5/3 of the original energy. Collimators of materials other than lead may be designed by a similar method using an equivalent energy.

General remarks

The formula for collimator efficiency derived by Anger (1964):

$$\epsilon_T = \left[\frac{0{\cdot}952\, r^2}{\left(t - \frac{2}{\mu}\right)(2r+s)} \right]^2$$

agrees to within ± 5 per cent with these calculations when the source is imaged in more than one channel. Anger's expression does not, however, take into account variations in efficiency close to the collimator face. The formula for resolution derived by Anger (1964):

$$R = 2r \frac{(t+F)}{\left(t - \frac{2}{\mu}\right)}$$

tends to overestimate by up to 15 per cent the values obtained in these calculations when the source is imaged in more than one channel; this is probably owing to his assumption that the resolution curve is triangular in shape. When the source is mainly imaged in one channel the equation is no longer applicable. Keller (1968) has derived a simple method of multi-channel collimator design based on Anger's equations; the method is subject to the limitations of the equations described above.

The suggested collimators have the disadvantage of a large variation of resolution with depth, and this can only be improved with a significant reduction in efficiency. In addition, since the efficiency in air is reasonably independent of distance from the collimator, the efficiency in tissue decreases with depth due to attenuation of radiation; this is particularly evident at low energies. These disadvantages may, however, be possibly overcome by the use of multichannel collimators with channels focusing in a plane parallel to the collimator face.

CONCLUSIONS

The results presented here enable the design of the optimum efficiency multichannel collimator for a particular resolution to be rapidly determined for any photon energy below 0·5 MeV. All the suggested collimators show a significant variation in resolution with distance from the collimator face and, in addition, those designed for energies higher than 0·3 MeV show a significant variation in resolution in a plane parallel to the collimator face. These disadvantages may only be overcome with a considerable reduction in the collimator efficiency.

ACKNOWLEDGMENTS

The author is most grateful to Dr. Christine M. E. Matthews for many helpful discussions and to Dr. D. K. Bewley and Mr. D. D. Vonberg for their encouragement and interest in this work.

The design of multichannel collimators for radioisotope cameras

ABSTRACT

Two methods of design of multi-cylindrical-channel collimators for radioisotope cameras are described; the first method was used to design collimators for photon energies below 0·3 MeV and the second method for energies between 0·3 and 0·5 MeV. Of the many possible collimators fulfilling a set of specifications the one giving the highest efficiency for a given resolution at a given distance from the collimator face was considered the optimum design. The dimensions and efficiencies of some optimum lead collimators have been calculated and the results enable collimators of any material to be designed for any resolution. The sensitivities and resolutions at different distances from the collimators have been calculated theoretically. The results indicate that, although the efficiency is reasonably constant, the resolution increases approximately linearly with distance.

REFERENCES

ANGER, H. O., 1958; *Rev. sci. Instrum.*, *29*, 27; 1963, *Nucleonics*, *21* (10), 56; 1964, *J. nucl. Med.*, *5*, 515; 1966, *ISA Transactions*, *5*, 311.

BENDER, M. A., and BLAU, M., 1962, in *Progress in Medical Radioisotope Scanning*, Eds. R. M. Kniseley, G. A. Andrews, and C. C. Harris, 151 (Institute of Nuclear Studies, Oak Ridge, Tennessee).

BROWNELL, G. L., 1958, *Int. J. appl. Radiat. Isotopes*, *3*, 181.

HORWITZ, N. H., LOFSTROM, J. E., and FIRSAITH, A. L., 1965, *J. nucl. Med.*, *6*, 724.

KELLER, E. L., 1968, *J. nucl. Med.*, *9*, 233.

LANSIART, A. J., and KELLERSHOHN, C., 1966, *Nucleonics*, *24*(3), 56.

MALLARD, J. R., and MYERS, M. J., 1963, *Phys. Med. Biol.*, *8*, 165.

MATHER, R. L., 1957, *J. appl. Phys.*, *28*, 1200.

PAIX, D., 1967, *Phys. Med. Biol.*, *12*, 489.

TER-POGOSSIAN, M. M., NIKLAS, W. F., BALL, J., and EICHLUNG, J. O., 1966, *Radiology*, *86*, 463.

WESTERMAN, B., 1967, personal communication.